UNIVERSITY OF CALIFORNIA
RIVERSIDE

An Exploration of Peptide-Based Cancer Therapeutics

A Dissertation submitted in partial satisfaction
of the requirements for the degree of

Doctor of Philosophy

in

Chemistry

by

Nicole Guadalupe Perkins

September 2021

Dissertation Committee:
Dr. Min Xue, Chairperson
Dr. Quan Jason Cheng
Dr. Wenwan Zhong

The Dissertation of Nicole Guadalupe Perkins is approved:

_____

_____

_____

Committee Chairperson

University of California, Riverside

Acknowledgements

I must begin by thanking God for the opportunity and blessings He has graciously given me. Through His strength I was able to overcome many trials and tests. I could not have completed this work without my savior, Jesus Christ's guidance. I thank my most cherished family who are my parents, Patricia and Timothy Perkins. Dad, you have protected me, guided me, you keep me on the straight and narrow path, you remind me to enjoy life, and you're truly my hero. I'm proud to be your daughter. Mom, you are my best friend. We laugh together, we cry together, you've taught me so much, and youre always there for me. I always wanted to grow up to be like you; I hope I got halfway there! I'm blessed to have such loving parents whom I am so extremely close to. I want to thank my brother, Tim Perkins. You always make me laugh, keep my spirits up, and inspire me. I always miss you and the good old days playing our silly games. No matter what happens in life, you will always be my bud and my rock. Thank you three for being my support, for giving me confidence, for believing in me, for sending me love, and for your prayers every day. God truly blessed me with the best family in the world.

I also thank mi tío favorito, Tío Ray, my Tía Soralla, my Tía Wendy, my cousin, Jessica, and my cousin, Alyssa for believing in me. I also thank my extended family and home friends for all of your support and love. I want to thank all my friends I have made at UC Riverside for all their help and support. Thank you especially Priyanka Sarkar, Siwen Wang, Rohit Chaudhuri, and Zhonghan Li.

I want to give a special thanks to my first research professor, Dr. Gregory Barding. Thank you for your confidence in me and for encouraging me to reach greater heights. I remember being told I would be a shoo-in for grad school, and at first, I didn't believe it. However, thanks to your counsel, I was able to confidently take on the task. You are an example what it means to be a great professor: which is one who educates, who inspires, and who encourages students to achieve more than what they believed they were capable of. Thank you.

Finally, thank you Dr. Min Xue for all your wisdom, guidance, advice, and teaching. No one could ask for a better boss, for a more friendly advisor, or for a more dedicated professor. You showed care in our research, for our well-being, and for our progress as both scientists and as growing people. You are another true example of great professor: you have a brilliant mind filled with ideas, yet are open to suggestions. You are intellectual, but humble. Despite your busy life, you still made time for each of your students. You have made great strides in your research with us, but you have also shown us you truly care about where we go moving forward into the future. You have truly gone above and beyond for all of us in the lab. I am proud to be one of your first graduate students. Thank you so much for everything and I wish you and your family all the best.

Dedication

First, this dedication for the thesis goes to God, I could not be where I am today without His grace. I dedicate this thesis to my Mom and Dad. I could not have done this without you. I love you both so much! I also dedicate this to Timehy! Love you, my brother.

Finally, I also want to dedicate this thesis to my grandparents: Guelita (Guadalupe Cisneros), Guelito (Rigoberto Cisneros), Nana (Gwendolyn Perkins), and Papa (Gregory Perkins). I also want to dedicate this to my Tía Carito and to my Tío Vico. I miss you all dearly. I hope I made you proud.

ABSTRACT OF THE DISSERTATION

An Exploration of Peptide-Based Cancer Therapeutics

by

Nicole Guadalupe Perkins

Doctor of Philosophy, Graduate Program in Chemistry
University of California, Riverside, September 2021
Dr. Min Xue, Chairperson

Tumor heterogeneity poses a great challenge for current therapeutics. The ability of cancer cells to adapt and resist drug treatment provides a particular difficulty in two areas: having a full understanding of the mechanisms in which they adapt and a full understanding of how to overcome those mechanisms. Peptide-based therapeutics show great potential in confronting these challenges as they are known to aid in targeting drug targets previously deemed "undruggable." To date, many peptide drugs are commercially available. With this in mind, our studies focused on the utilization of peptides for therapeutic purposes and investigating how cancer cell heterogenous characteristics respond to peptide drug treatment. In our first study, we treated cancer cells of known low mutational load with an immunogenic peptide. This treatment ultimately flagged the cancer cells as "pathogen-infected," and we aimed to elicit an immune response. The second study incorporated a cyclic peptide into a proteolysis targeting chimera (PROTAC) structure to aid in the degradation of a commonly hyperactive protein in cancers known as AKT. This study also shed some light on the adaptation mechanisms cells can use in response to this drug treatment. In our final study, we used another cyclic

peptide and other metabolic inhibitors to examine how varying types of inhibition affect the heterogeneity of cellular movement in cancer cells. Each study showcases how peptide-based drugs serve as a valuable tool for treating and further understanding the complexities of cancer.

TABLE OF CONTENTS

LIST OF FIGURES

LIST OF TABLES

Chapter 1: Introduction

1.1 Tumor Heterogeneity

Heterogeneity within cancer cells is one major key in resisting therapeutic treatments. The existence of both intratumoral and intertumoral heterogeneity makes finding a cure for cancers a daunting challenge (Figure 1.1).[1] Intertumoral heterogeneity refers to the characteristic differences between tumors of the same histological kind within different patients, while intratumoral heterogeneity refers to differences among individual or groups of cancer cells within the same patient. Another challenge added to this is that intratumoral heterogeneity has been shown to manifest itself in two forms, spatial heterogeneity, and temporal heterogeneity. In spatial heterogeneity, there are genetically diverse groups or subpopulations of cancer cells in different parts of the same tumor or in between disease sites (such as cancers that have metastasized). Temporal diversity is defined as genetic differences and variations of cancer cells within a tumor as time passes.[1]

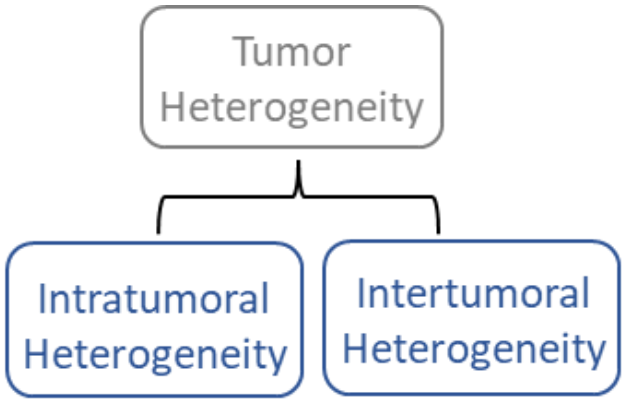

Figure 1.1. Tumoral heterogeneity and its subcatergories.

It has been suggested that intratumoral heterogeneity is the critical component that leads to cell proliferation, invasion, and drug resistance. Genetic instability, epigenetics, behavioral, and immunological factors have shown to play a role in influencing the dynamics of intratumoral heterogeneity. Such clonal cell diversity allows cancers to acquire characteristics such as high tumor mutational burden (TMB), immunogenicity, plasticity, ability to bypass or upregulate signaling pathways, and having metabolic flexibility under varying microenvironments to aid in invasion.[2] With all of this in mind, it is of no surprise that many therapeutics have limited success against the most aggressive and dynamic cancer types. There is still an urgent need for investigating alternative or newer methods to effectively treat and investigate the cellular dynamics of cancers.

1.2 Current Therapeutics that Tackle Various Parts of Tumor Heterogeneity

Fortunately, many studies have afforded more therapeutic routes that have shown successful progress in eradicating tumors. In studying the TMB of cancers, researchers have discovered that the number of somatic mutations within a specific cancer type correlates to the production of tumor-specific neoantigens. Researchers can also use this information to predict how responsive a tumor may be to certain immunotherapeutic drugs that target these neoantigens.[3] With cancer types of high TMB, neoantigen sequences can be predicted and specifically targeted using adoptive cell transfer or CAR-T cell therapy (Figure1.2). Other advancements in immunotherapy include immune checkpoint inhibitors or oncolytic virotherapy. [4-6] However, these therapies are dependent

on high TMB cancers and may not yield successful treatment of cancers with lower TMB. In addition, intratumoral heterogeneity implies the possibility of various cancer cells producing different neoantigens (or some cells may lack the production of neoantigens altogether),[2,14-15] thus posing another challenge for current immunotherapies to address.

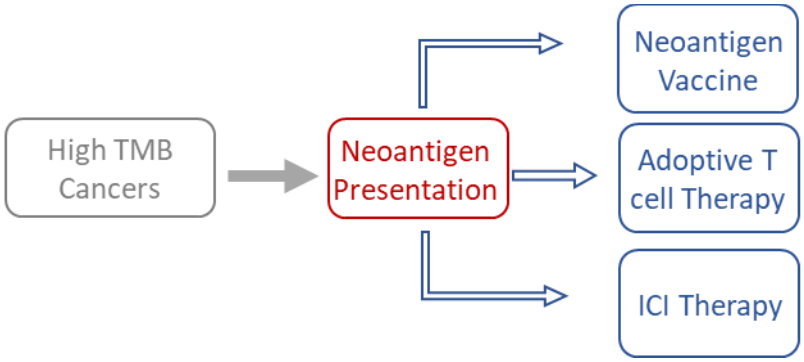

Figure 1.2. A list of current of immunotherapies for targeting high TMB cancers.

In terms of cell signaling and metabolism, heterogeneity is responsible for the upregulation/downregulation of various pathways, hyperactivation of proteins, and changing the processing of specific metabolites. For example, the PI3K/AKT/mTOR pathway is upregulated in many cancers due to genetic alterations.[7] In addition, many cancers increase their uptake of glucose and glutamine as they serve as essential metabolites.[6] Current therapeutics to target these mechanisms to further inhibit cell proliferation and invasion involve small molecule inhibitors. [6, 8] The drawback of inhibitors is that some lack selectivity/specificity.[8-9] Inhibitors are also reported to be occupancy-driven, meaning higher concentrations are needed in order to achieve

maximal effect. [9] As it is seen, there is a need for a more selective and more potent method of targeted therapeutics.

1.3 Peptide-Based Therapeutics

Peptide-based therapeutics was first introduced in the early 20th century with the isolation of insulin from animal sources to treat diabetes. Many decades later, synthetic peptides and naturally occurring peptides have been successful in clinical use.[10-11] Peptide drugs have been shown to be an attractive therapeutic modality due to their many advantages such as improved selectivity, lowered toxicity, and enhanced potency (Figure 1.3).[11] They also have shown advantages over traditional small molecule drugs as they are not limited to binding to "hot spot" binding pockets/areas on proteins; therefore, they can engage targets that were previously deemed "undruggable."[10, 12]

To date, peptide therapeutics have shown efficacy in inhibiting protein-protein interactions, binding to intracellular targets, inhibiting cellular functions, and more.[10, 13] In recent years, there has been work on the development/improvement of personalized peptide-based cancer vaccines against high TMB cancer types, commonly referred to as neoantigen vaccines. These neoantigens can be predicted, synthesized, and introduced into patients. Some studies have showcased that these vaccines exhibited quite high immunogenicity.[14-15] Therefore, peptide-based drugs show great potential as they have found their way into the realm of cancer immunotherapy.

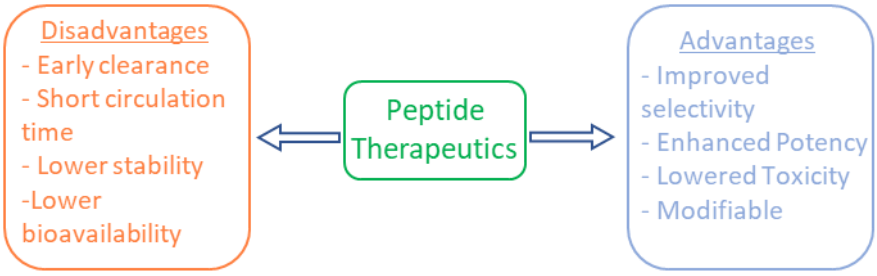

Figure 1.3. Advantanges and disadvantages of peptide-based therapeutics.

Peptide therapeutics has certainly gained the attention of the pharmaceutical industry, as there are currently around 100 peptide drugs available commercially and more than 600 are currently under clinical investigation.[10] The introduction of this therapeutic method shows great promise, but some disadvantages do arise such as early renal clearance, lower oral bioavailability, shorter circulation times, and lowered stability in plasma. However, these disadvantages can be overcome through chemical modifications such as PEGylation or conjugations to larger molecules. [11-12] Another possible way to overcome these obstacles is the use of delivery platforms such as lipid nanoparticles, which can aid in the protection of the peptide until it is released into the area of interest.[10] Changing the overall structure of short peptides is another route. It has been established that cyclic peptides have a better advantage compared to linear peptides. Cyclic peptides have reduced conformational flexibility, thus giving them improved biological activity and higher cell permeability. They also are resistant to enzymatic degradation due to their rigidity and lack of N or C termini.[16]

Despite the challenges presented, peptide-based drugs appear to show great flexibility in terms of modification and design for effective drug treatment. Due to their ability to target and treat numerous areas of interest, peptide-based therapeutics show promise in the field of cancer medicine as well as other areas of disease. The potential of peptide-based drugs has led us to pursue further study using peptides for immunotherapeutic treatment, targeted-protein degradation, and inhibition of cell movement in cancer cells.

1.4 Motivations and Contents of the Studies in this Thesis

Current cancer therapies have made great strides for aiding in tumor regression and prolonging patient life. However, each new therapy still has one or more drawbacks and clinical/safety concerns. Peptide-based drugs serve many advantages and have shown clinical successes in many areas. In our work, we have looked towards the utilization of peptides for the design of novel therapeutic methodologies to tackle difficult cancer cell lines. We specifically investigated the following areas that help in confronting heterogeneity: creating an immunotherapeutic approach for dealing with low-TMB cancers using a public antigen-based peptide, attempting to inhibit upregulated signaling pathways by using a peptide-based proteolysis targeting chimera (PROTAC), and trying to inhibit cell migration through a combination of using a cyclic peptide inhibitor for migration and inhibiting metabolic uptake.

One of the challenges tumor heterogeneity poses is that due to the TMB status, tumor cells can have variation in or completely lack neoantigen presentation. For

example, cancers of high TMB can increase the immunogenicity of the tumor through the larger number of somatic mutations producing more neoantigens.[2] Therefore, the opposite is true with cancers of lower TMB status. The previously mentioned therapies lack efficacy in treating multiple cancer types because of their mutational load. Our first study answers this challenge through the delivery of an immunogenic peptide derived from a public antigen (such as from human papilloma virus or cytomegalovirus) (Figure 1.4). The introduction of this peptide which is ultimately presented by the cells allows for eliciting an immune response against cancer cells that are recognized as pathogen-infected, regardless of their TMB status.

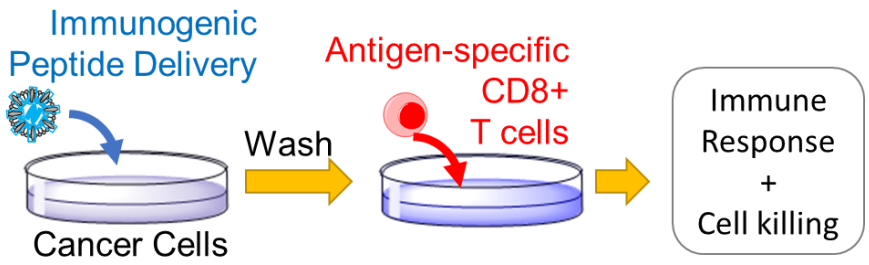

Figure 1.4. Experimental flow of immunogenic peptide delivery.

Another challenge previously raised by tumor heterogeneity is the hyperactivation of proteins commonly relied on for typical cell survival. One such protein is AKT and our second study focuses on attempting to remove AKT without the use of inhibitors. We designed a peptide-based PROTAC whose purpose is to serve in specifically degrading AKT (Figure 1.5). In addition, our goal was also to study possible resistance mechanisms many of the cancer cells may have against the PROTAC method. As PROTACS are

becoming a recent area of interest in protein degradation studies, it would be useful to discover how cancer cells can adapt to such a therapy due to their heterogeneity.

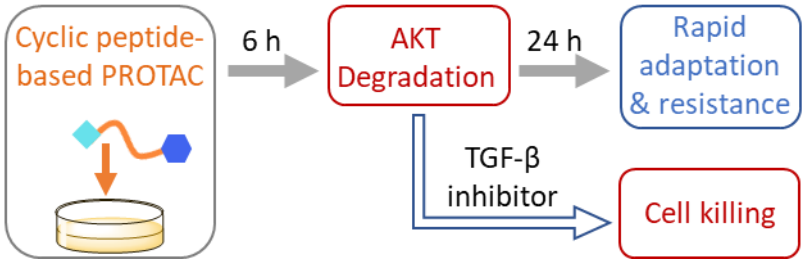

Figure 1.5. Experimental flow of the PROTAC study.

Lastly, there are many unknowns regarding how heterogeneity affects cell movement and migration at the single-cell level. Our final study is much more exploratory as we sought to monitor how different essential metabolites affect the overall heterogeneity of the migration patterns of single cells (Figure 1.6). After investigating which essential metabolite was critical for migration, we decided to explore how migration can be modulated by introducing both a peptide-based inhibitor and small molecule inhibitors to cancer cells. This investigation highlights the importance of studying how the heterogeneity single-cell movement is affected with peptide inhibitors and other drugs has direct therapeutic implications.

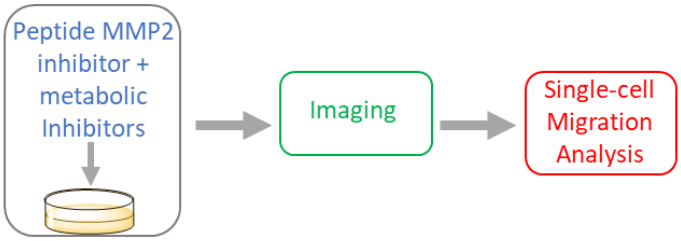

Figure 1.6. Experimental flow of the cell migration analysis.

Overall, our three studies provide several investigations concerning the following: finding ways to overcome challenges imposed by heterogeneity, how heterogeneity can adapt to novel therapeutic strategies, and how heterogeneity is reflective of cellular behavior. Each study introduces the use of a peptide drug to answer our questions. As it will be further explained, peptide-based drugs have served well in providing more information on therapeutic potential and cancer cell's biological mechanisms.

1.5 References

1. Dagogo-Jack, I.; Shaw, A. T., Tumour heterogeneity and resistance to cancer therapies. *Nat Rev Clin Oncol* **2018,** *15* (2), 81-94.

2. Vitale, I.; Shema, E.; Loi, S.; Galluzzi, L., Intratumoral heterogeneity in cancer progression and response to immunotherapy. *Nat Med* **2021,** *27* (2), 212-224.

3. Sha, D.; Jin, Z.; Budczies, J.; Kluck, K.; Stenzinger, A.; Sinicrope, F. A., Tumor Mutational Burden as a Predictive Biomarker in Solid Tumors. *Cancer Discov* **2020,** *10* (12), 1808-1825.

4. Morotti, M.; Albukhari, A.; Alsaadi, A.; Artibani, M.; Brenton, J. D.; Curbishley, S. M.; Dong, T.; Dustin, M. L.; Hu, Z.; McGranahan, N.; Miller, M. L.; Santana-Gonzalez, L.; Seymour, L. W.; Shi, T.; Van Loo, P.; Yau, C.; White, H.; Wietek, N.; Church, D. N.; Wedge, D. C.; Ahmed, A. A., Promises and challenges of adoptive T-cell therapies for solid tumours. *Br J Cancer* **2021,** *124* (11), 1759-1776.

5. Rezaei, R.; Esmaeili Gouvarchin Ghaleh, H.; Farzanehpour, M.; Dorostkar, R.; Ranjbar, R.; Bolandian, M.; Mirzaei Nodooshan, M.; Ghorbani Alvanegh, A.,

Combination therapy with CAR T cells and oncolytic viruses: a new era in cancer immunotherapy. *Cancer Gene Ther* **2021**.

6. Hahn, W. C.; Bader, J. S.; Braun, T. P.; Califano, A.; Clemons, P. A.; Druker, B. J.; Ewald, A. J.; Fu, H.; Jagu, S.; Kemp, C. J.; Kim, W.; Kuo, C. J.; McManus, M.; G, B. M.; Mo, X.; Sahni, N.; Schreiber, S. L.; Talamas, J. A.; Tamayo, P.; Tyner, J. W.; Wagner, B. K.; Weiss, W. A.; Gerhard, D. S.; Cancer Target, D.; Development, N., An expanded universe of cancer targets. *Cell* **2021,** *184* (5), 1142-1155.

7. Cintas, C.; Guillermet-Guibert, J., Heterogeneity of Phosphatidylinositol-3-Kinase (PI3K)/AKT/Mammalian Target of Rapamycin Activation in Cancer: Is PI3K Isoform Specificity Important? *Front Oncol* **2017,** *7*, 330.

8. Landel, I.; Quambusch, L.; Depta, L.; Rauh, D., Spotlight on AKT: Current Therapeutic Challenges. *ACS Med Chem Lett* **2020,** *11* (3), 225-227.

9. Konstantinidou, M.; Li, J.; Zhang, B.; Wang, Z.; Shaabani, S.; Ter Brake, F.; Essa, K.; Domling, A., PROTACs- a game-changing technology. *Expert Opin Drug Discov* **2019,** *14* (12), 1255-1268.

10. Acar, H.; Ting, J. M.; Srivastava, S.; LaBelle, J. L.; Tirrell, M. V., Molecular engineering solutions for therapeutic peptide delivery. *Chem Soc Rev* **2017,** *46* (21), 6553-6569.

11. Muttenthaler, M.; King, G. F.; Adams, D. J.; Alewood, P. F., Trends in peptide drug discovery. *Nat Rev Drug Discov* **2021,** *20* (4), 309-325.

12. Cooper, B. M.; Iegre, J.; DH, O. D.; Olwegard Halvarsson, M.; Spring, D. R., Peptides as a platform for targeted therapeutics for cancer: peptide-drug conjugates (PDCs). *Chem Soc Rev* **2021,** *50* (3), 1480-1494.

13. Lee, A. C.; Harris, J. L.; Khanna, K. K.; Hong, J. H., A Comprehensive Review on Current Advances in Peptide Drug Development and Design. *Int J Mol Sci* **2019,** *20* (10).

14. Li, W. H.; Li, Y. M., Chemical Strategies to Boost Cancer Vaccines. *Chem Rev* **2020,** *120* (20), 11420-11478.

15. Saxena, M.; van der Burg, S. H.; Melief, C. J. M.; Bhardwaj, N., Therapeutic cancer vaccines. *Nat Rev Cancer* **2021,** *21* (6), 360-378.

16. Abdalla, M. A.; McGaw, L. J., Natural Cyclic Peptides as an Attractive Modality for Therapeutics: A Mini Review. *Molecules* **2018,** *23* (8).

Chapter 2: Liposomal delivery of pathogen-derived peptides flags cancer cells for eliciting anti-tumor immunity

2.1 Introduction

Therapeutics targeting immune checkpoints have demonstrated astonishing success and brought new hope to patients with previously untreatable metastatic cancers.[1-4] The premise of those therapies requires existing immune recognition of cancer neoantigens. Tumor mutational burden (TMB) has, therefore, become an emerging biomarker for selecting patients for those immunotherapies[5]. Low TMB tumors often lack sufficient immunogenic neoantigens, and consequently have inadequate endogenous immunity to be unleashed by immune checkpoint inhibitors (ICIs). How to adapt immunotherapy to patients with low TMB tumors remains an open challenge.[6, 7]

Neoantigen vaccination holds great promise to stimulate tumor immunity and turn immunologically "cold" tumors (such as many low TMB tumors) into "hot" ones. Numerous clinical trials are ongoing to test their safety and efficacy. Unfortunately, most of the neoantigens are private antigens not shared between patients. Therefore, long lead time and high cost for on-demand production of this truly personalized vaccine is a critical challenge for broad clinical application. Additionally, the immunogenicity of neoantigens is difficult to predict. Therefore, normally multiple predicted neoepitopes need to be co-targeted in the vaccine manufacturing.

Emerging evidence[8-13] shows that infecting and killing tumor cells with infectious agents (such as oncolytic viruses or certain strains of bacteria) can change the local microenvironment and mediate anti-tumor immune response. They can turn immunologically cold tumors into hot ones. Several preclinical and clinical studies

showed promising efficacy of those infectious agents, either as monotherapies or in combination with checkpoint inhibitors[8-11]. However, those infectious agents can be recognized as pathogens and consequently cleared by the immune system prematurely before target tumor infection, leading to compromised therapeutic effects.[13] In addition, these infectious agents require complex manufacturing process, and their replication-competency poses potential safety concerns, especially for vulnerable patients.[5, 13]

With the goal to develop a simple, safe, and scalable therapeutic agent that can induce strong anti-tumor immunity, we hypothesized that we could leverage the pre-existing adaptive T-cell immunity against public antigens to elicit anti-tumoral immune responses[14-17]. As shown in Figure 2.1, we select pathogen-derived immunogenic peptide fragments and deliver them to the tumors using liposome vesicles.[18] These exogenous peptides (immunoflags) are derived from the viruses that infect large cohorts of people, and are proven immunogenic. Once inside the cells, these peptides can participate in the antigen presentation pathway and be presented by the major histocompatibility complex (MHC) class I molecules.[19] This process will promote immune recognition and trigger anti-tumor immunity, independent of the neoantigen level or TMB status. Herein, we demonstrate the feasibility of this proposed strategy *in vitro* and *in vivo*.

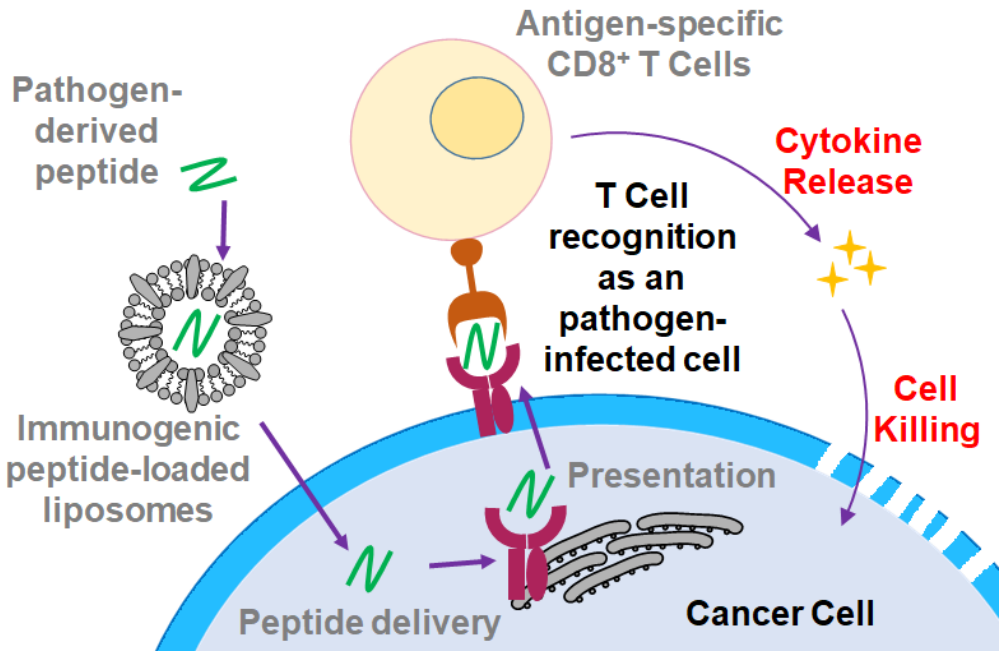

Figure 2.1. The proposed immunoflagging strategy.

2.2 Experimental

Reagents

The following lipids, 1,2-dioleoyl-3-trimethylammonium-propane (chloride salt) (DOTAP) and 1,2-dioleoyl-sn-glycero-3-phosphoethanolamine (DOPE), were purchased from Avanti Polar Lipids, Inc. Absolute methanol, HPLC grade Acetonitrile (ACN), chloroform (with 0.75% ethanol), HEPES, and Dimethyl Sulfoxide (DMSO) were all purchased from Fischer Scientific. Trifluoroacetic acid (TFA) was purchased from Oakwood Chemical. All protected amino acids were purchased from AAPPTEC. Resazurin sodium salt and glutaraldehyde solution (70% in water) were purchased from Sigma-Aldrich. Crystal Violet and paraformaldehyde were purchased from Acros Organics. Triisopropylsilane (TIPS) was purchased from TCI.

Cell materials

The human glioblastoma U87 cell line and the human colorectal SW620 cancer cell line used in this study were both purchased from ATCC. Anti-HPV $E7_{11-20}$ T cells, CMV-Specific T cells, and Peripheral Blood Mononuclear Cells (PBMCs) were purchased from Astarte Biologics. Dulbecco's Modified Eagle Medium (DMEM), heat-inactivated Fetal Bovine Serum (FBS), normal Roswell Park Memorial Institute (RPMI) 1640 Medium, and 0.25% Trypsin (with 2.21mM EDTA) were all purchased from Corning Cellgro. RPMI 1640 medium (supplemented with 25 mM HEPES and 2 mM L-glutamine) and 100 mM sodium pyruvate were purchased from GIBCO. Penicillin-Streptomycin (PS) was purchased from Sigma-Aldrich. 2-mercaptoethanol was purchased from FisherBiotech. Human Interleukin-2 (IL-2) was purchased from Stem Cell Technologies. Heat-inactivated Human AB Serum (HS) was purchased from Fischer Scientific. An anti-CD3-Alexa Fluor 647 antibody was purchased from BioLegend.

Peptide synthesis

The HPV $E7_{11-20}$ peptide sequence (YMLDLQPETT), the scrambled $E7_{11-20}$ sequence (YEQPMLTLDT), and the CMV-pp65 peptide sequence (NLVPMVATV) were synthesized on a peptide synthesizer (CS Bio Co.) using 2-chlorotrityl chloride resin (AAPPTEC). Synthesis was done using standard Fmoc-SPPS. The peptides were cleaved from the resin (in a 95% TFA, 2.5% H_2O, 2.5% TIPS solution) and purified through reversed-phase HPLC (using a Dionex UltiMate 3000 UHPLC from Thermo Fisher Scientific). The elution gradient for the preparative column used was 0-100% ACN/H_2O

(containing 0.1% TFA). The identities of the peptides were confirmed through matrix-assisted laser desorption ionization, MALDI TOF/TOF (AB Sciex).

Liposome preparation

A 10 mg/mL stock solution of DOTAP and a 10 mg/mL stock of DOPE, were separately prepared in chloroform. 0.2 mL were taken from both lipid stocks and mixed together (0.4 mL total) in a 1:1 ratio. The mixture was dried via rotary evaporation for 1 hour to fully remove the chloroform. The obtained film was rehydrated with 1 mL of either 20 mM HEPES (for an empty liposome control), or with a 100 μM peptide solution in 20 mM HEPES. This gave the total lipid/liposome concentration of 4 mg/mL. The mixture was sonicated 3 times for 1 minute each at room temperature to assist the rehydration process. The liposomes were extruded 20 times through a 19 mm polycarbonate membrane with a pore size of 0.2 μm on a mini-extruder block, which was heated to a temperature of 60 °C (Avanti Polar Lipids, Inc.). The liposome solution was then dialyzed overnight against a 20 mM HEPES solution using a Tube-O-Dialyzer (G-Biosciences). After liposome preparation, a volume of 200 μL of the peptide-loaded liposome solution was dried under vacuum and extracted with 50 μL of DMSO. The sample was centrifuged, and the supernatant was analyzed using reversed-phase HPLC. The elution gradient for the analytical column used was also 0-100% ACN/H_2O (containing 0.1% TFA). The amount of loaded peptide from the liposome sample was then determined by comparing the peak area to that of a standard 100 μM solution. The loading capacities were calculated accordingly.

Cell culture

All cancer cells were cultured in DMEM media containing 10% FBS and 1% PS, at 37°C with 5% CO_2 in a Hera Cell incubator (BioSurplus). PBMCs were cultured and primed over a period of ~15 days in the RPMI 1640 medium supplemented with 25 mM HEPES and 2 mM L-glutamine; it was additionally supplemented with 10% FBS, 1% sodium pyruvate, 0.05 mM 2-mercaptoethanol, and 1% PS. Upon co-culturing the cancer cells with immune cells for immunoflagging tests (T cells or PBMCs), DMEM was replaced with normal RPMI 1640 media supplemented only with 10% HS and 1% PS.

Immunoflagging with antigen-specific T cells

To conduct the immunoflagging experiments, 10 k cancer cells were seeded in a 96-well plate and allowed to incubate overnight. A solution of peptide-loaded liposomes was added to the cancer cells at the final concentrations of 1 μg/mL (low concentration) and 100 μg/mL (high concentration). Controls such as an empty liposome treatment and lone immunogenic peptides were also implemented. After ~24 h incubation of the cancer cells with the liposomes, the DMEM media was replaced with RPMI media containing 10% HS and 1% PS. 10 k antigen-specific T cells were added into each well and incubated with the cancer cells for either 24 hours (in which the RPMI was collected for cytokine analysis) or 72 hours (for cell viability assays). Cells were also later fixed and stained for imaging.

Cytokine quantification

The harvested media (after T cell treatment) were tested using a Human TNF-α ELISA kit (DuoSet, R&D Systems DY210) following manufacturer-supplied protocols.

Cell viability test

40 µL of resazurin solution (60 µg/mL in complete media) was added to each well containing 200 µL of media. The cells were incubated for 4 hours at 37 °C. The resulting fluorescence in each well was recorded every hour using a plate-reader (excitation 530 nm, emission 590 nm, Biotek).

Crystal violet blue staining

After cell viability testing, the cells were fixed with a crystal violet blue solution (0.5% in 10 mM PBS) containing either 1% glutaraldehyde (HPV $E7_{11-20}$ peptide-liposome test) or 4% paraformaldehyde (CMV-pp6 peptide-liposome test) for 30 minutes. The cells were later washed with 10 mM PBS or water to remove the free dye. The stained cell colonies were imaged with a digital scanner.

Immunofluorescence imaging

Crystal-violet blue was rinsed away from the fixed cells with 10% acetic acid in water. The fixed cells were then blocked with human AB serum (1% in PBS) to minimize the background. Blocked cells were treated with propidium iodide (10 µg/mL in PBS) to stain the nuclei, and anti-CD3-Alexa Fluor 647 antibody to stain the T cells. The stained cells were imaged using a Zeiss 880 confocal microscope.

Immunoflagging with PBMCs

For day 1 of PBMC culture and stimulation, ~80M PBMCs were counted and resuspended in 4 mL of RPMI which was also supplemented with 50 µg/ mL of CMV-

pp65 peptide. The cells were incubated at 37°C for 2 hours within a conical tube. The PBMCs were then resuspended to 40 mL with RMPI supplemented with 25 units/mL of IL-2 with the final peptide concentration being at 4.23 µg/mL. On Day 3, IL-2 was added to the PBMCs to obtain the final concentration of 50 units/mL. On Day 5, DNase was added to remove any clumping of the PBMCs, which were then later centrifuged for 5 min at 300-400G, recounted, and resuspended in 40 mL of fresh RPMI containing 4.23 µg/mL of peptide and 100 units/mL of IL-2. On Day 8, 5mL of RPMI containing 100 units/ml IL-2 was added to the cells. On Day 11, another 5 mL of RPMI containing 100 units/mL IL-2 was added. On Day 13, the PBMCs were again centrifuged, counted, and resuspended in 40 mL of fresh RPMI containing 4.23 µg/mL peptide and 100 units/mL of IL-2. Day 16 was the final day in which the PBMCs were centrifuged, counted, and added to SW620 cancer cells for the immunoflagging experiment.

Prior to adding the PBMCs to the SW620 cells, the SW620 cells were treated in a procedure similar to that of the first immunoflagging experiment. SW620 cells were seeded in a 96-well plate (10k cells/well) and allowed to settle overnight. The following day, both empty and peptide-loaded liposomes were added to the SW620 cells at either a final low concentration (1 µg/mL liposome) or a final high concentration (100 µg/mL liposome). The cells were incubated overnight ~24 hours. After 24 hours, the liposome/media was removed, and the cells were rinsed once with normal RPMI (containing 10% HS and 1% PS). Then 100 µL of the normal RPMI was added to the cells. Another 100 µL of normal RPMI containing ~200,000 PBMCs was added to each well, giving a total volume 200 µL/well. The 96-well plates were then left to co-culture

for 3 days. After incubation, the RPMI media was replaced with 200 μL of DMEM and were ready for cell viability testing.

Animals

All animal studies were approved by the UW Institutional Animal Care and Use Committee (IACUC) and performed in the UW vivarium. NOD scid gamma (NSG) mice were purchased from the Jackson Laboratory and housed in a BSL-2 room.

Influence of PBMCs on tumor growth and body weight

Five-week-old female NSG mice were inoculated with SW620 cells (3 million cells per mouse) via subcutaneous (s.c.) injection to the right flank. When the average tumor size reached ~200 mm^3, the mice were randomized into two groups (n = 2 per group), and intravenously (IV) administrated with 100 uL of PBS or PBMCs suspension (10 million per mouse), respectively. Tumor size and body weight were monitored every three days. Tumor volume (mm^3) was calculated using the formula V (mm^3) = L (mm) × W $(mm)^2$ × 0.5, where L and W were the longest and widest diameters of a tumor. At the end of the experiment, mice were sacrificed according to the IACUC protocol.

Tumor inhibitory experiment in vivo

Five-week-old female NSG mice were inoculated with SW620 cells (3 million cells per mouse) via s.c. injection to the right flank. When the average tumor size reached ~200 mm^3, the mice were randomized into three groups (namely peptide, PBMC, and peptide + PBMC; n = 3 per group), and I.V. administrated with 100 uL of PBS or PBMC (10 million per mouse) accordingly. One hundred microliters of liposomal peptide (2.5 mg/kg) or PBS was injected intratumorally using 33-gauge needles once every day.

Tumor size and body weight were monitored before each injection. At the end of the experiment, mice were sacrificed according to the IACUC protocol.

2.3 Results and Discussion

We first selected the $E7_{11-20}$ epitope (YMLDLQPETT) from the human papillomavirus, type 16 (HPV16) as the immunogenic peptide. This epitope is a well-known HLA-A*0201-restricted public antigen and is involved in the adaptive immunity against HPV16 in a large population.[20, 21] Here we chose the U87 cell line as our model system. U87 is a human glioblastoma cell line that has an HLA allele type of A*0201.[22] It has the necessary machinery to present the E7 antigen that could potentially be recognized by corresponding T cells.

The $E7_{11-20}$ peptide was synthesized through standard solid-phase protocols and purified through reversed-phase HPLC (Figure 2.2). We also synthesized a scrambled version of the epitope (YEQPMLTLDT) as a control. This sequence is predicted to be incompatible with the HLA-A*0201 allele type and should not be presented by the MHC complex. Therefore, no immune response is expected (Figure 2.3).

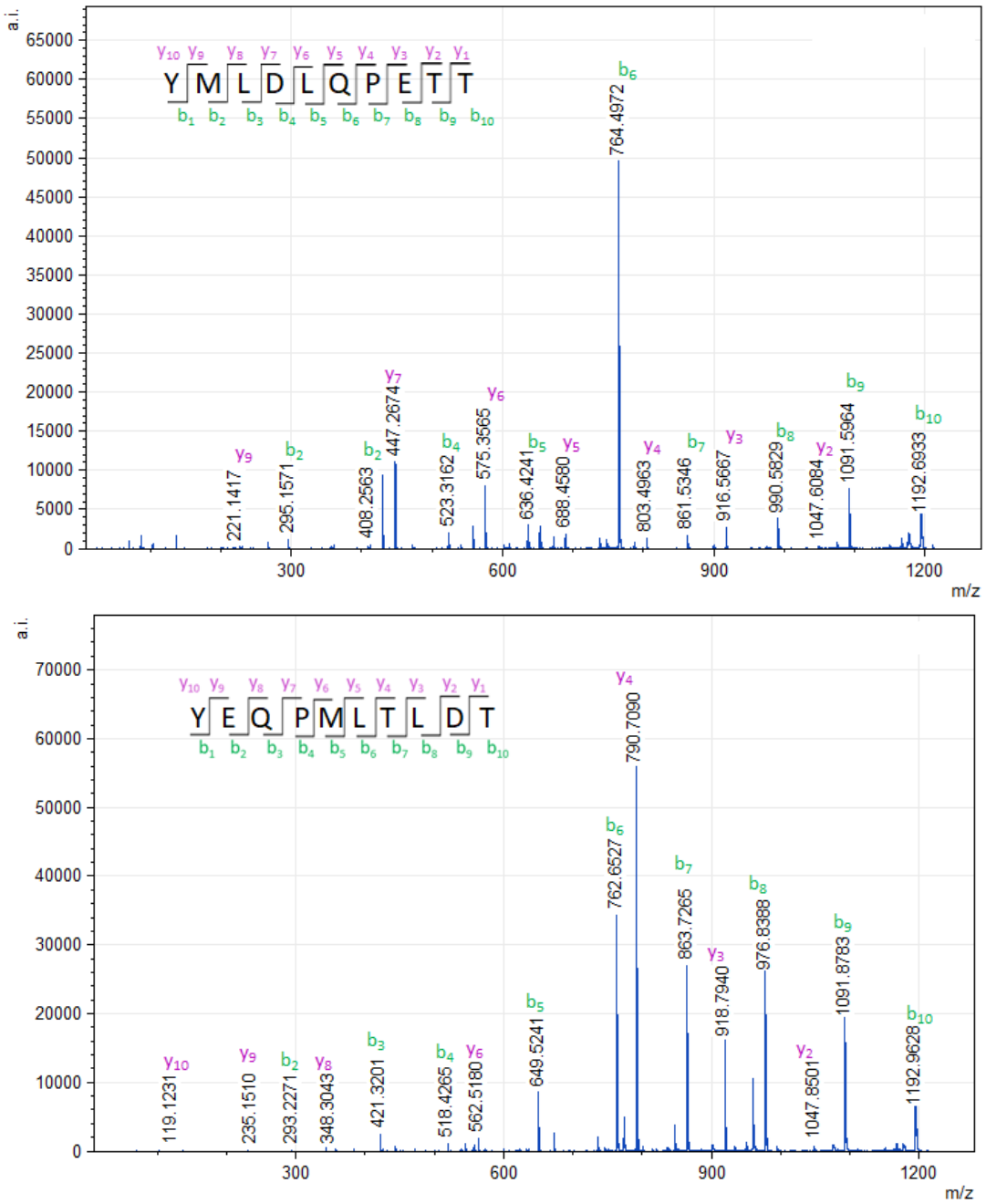

Figure 2.2. MS/MS spectra of the synthesized HPV peptides.

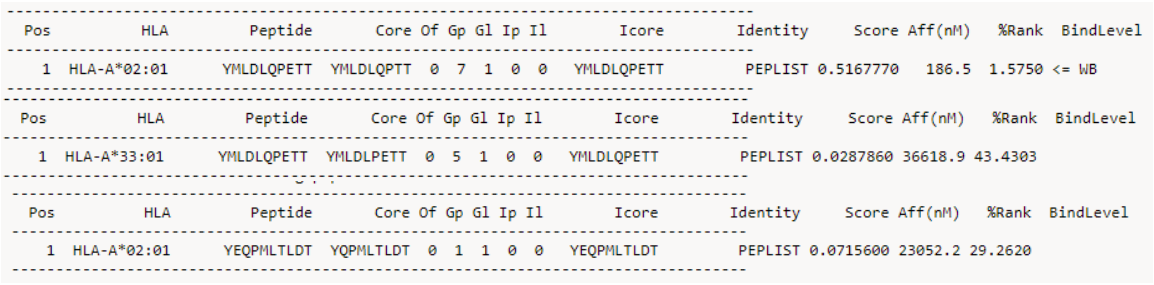

Pos	HLA	Peptide	Core	Of	Gp	Gl	Ip	Il	Icore	Identity	Score	Aff(nM)	%Rank	BindLevel
1	HLA-A*02:01	YMLDLQPETT	YMLDLQPTT	0	7	1	0	0	YMLDLQPETT	PEPLIST	0.5167770	186.5	1.5750	<= WB

Pos	HLA	Peptide	Core	Of	Gp	Gl	Ip	Il	Icore	Identity	Score	Aff(nM)	%Rank	BindLevel
1	HLA-A*33:01	YMLDLQPETT	YMLDLPETT	0	5	1	0	0	YMLDLQPETT	PEPLIST	0.0287860	36618.9	43.4303	

Pos	HLA	Peptide	Core	Of	Gp	Gl	Ip	Il	Icore	Identity	Score	Aff(nM)	%Rank	BindLevel
1	HLA-A*02:01	YEQPMLTLDT	YQPMLTLDT	0	1	1	0	0	YEQPMLTLDT	PEPLIST	0.0715600	23052.2	29.2620	

Figure 2.3. Binding affinities between the chosen peptide sequence and the HLA allele, as predicted by the NetMHCPan software (Jurtz, *et al.*, *The Journal of Immunology*, **2017**).

We chose liposomes to deliver the hydrophilic peptides across the cell membranes. The well-developed liposome field provides numerous types of formulations for various drug delivery applications.[23, 24] We chose a fusogenic liposome formulation: DOTAP/DOPE.[25] We followed the established procedures to load the E7 peptide into liposomes.[24, 25] The fully-assembled liposomes exhibited hydrodynamic diameters around 122 nm, as determined by dynamic light scattering experiments (Figure 2.4). Using HPLC, we determined that the peptide loading capacities for each liposome formulation were 2% and 0.5% (w/w, peptide to liposome) for the E7 and scrambled peptides, respectively.

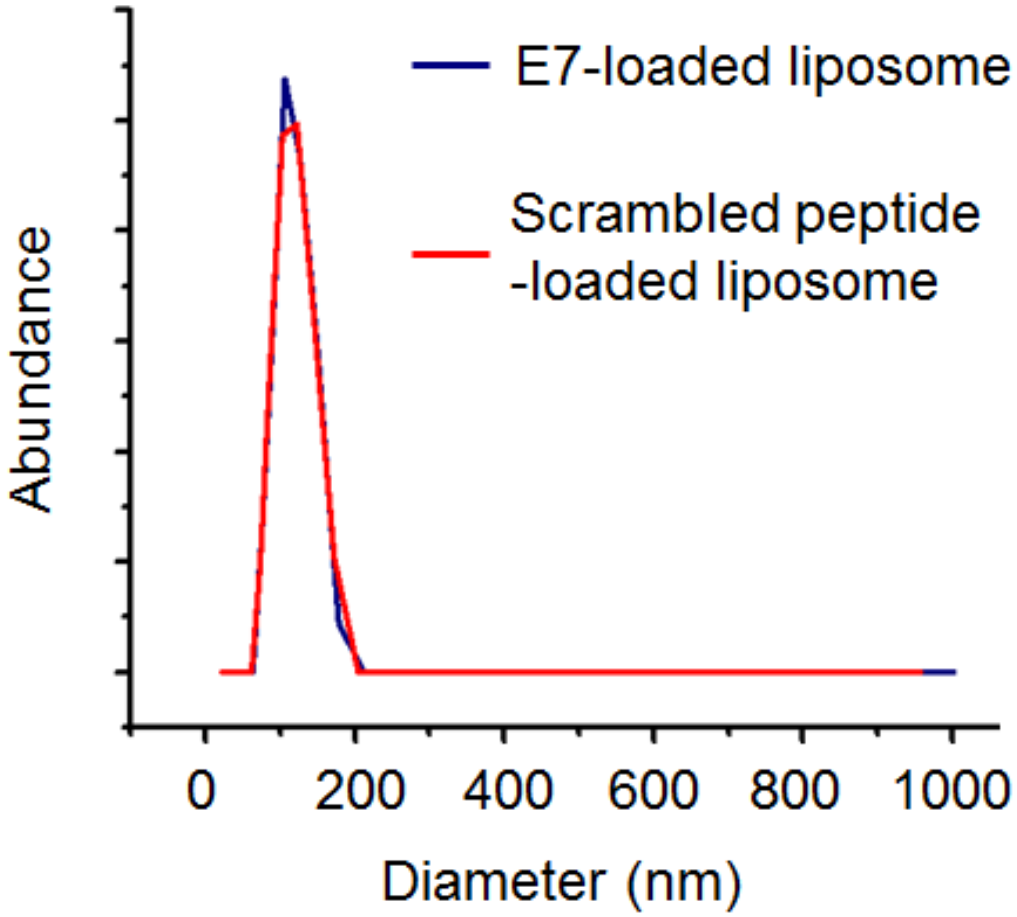

Figure 2.4. Dynamic light scattering results of the liposomes.

In order to ensure that the chosen liposome formulation can successfully perform cytosolic delivery, we employed propidium iodide (PI)-loaded liposomes to validate the cytosolic delivery. PI is a fluorescent dye that intercalates in the double-stranded DNA structure and stains the cell nucleus. Since PI is membrane-impermeable, the staining only takes place when PI is delivered into the cytoplasm.[26] Indeed, we observed effective nuclear staining after incubating the cells with the PI-loaded liposome (Figure 2.5). This result proved that the liposomes could effectively deliver cargo molecules into the cytoplasm, without being trapped in the endosomal/lysosomal compartments.

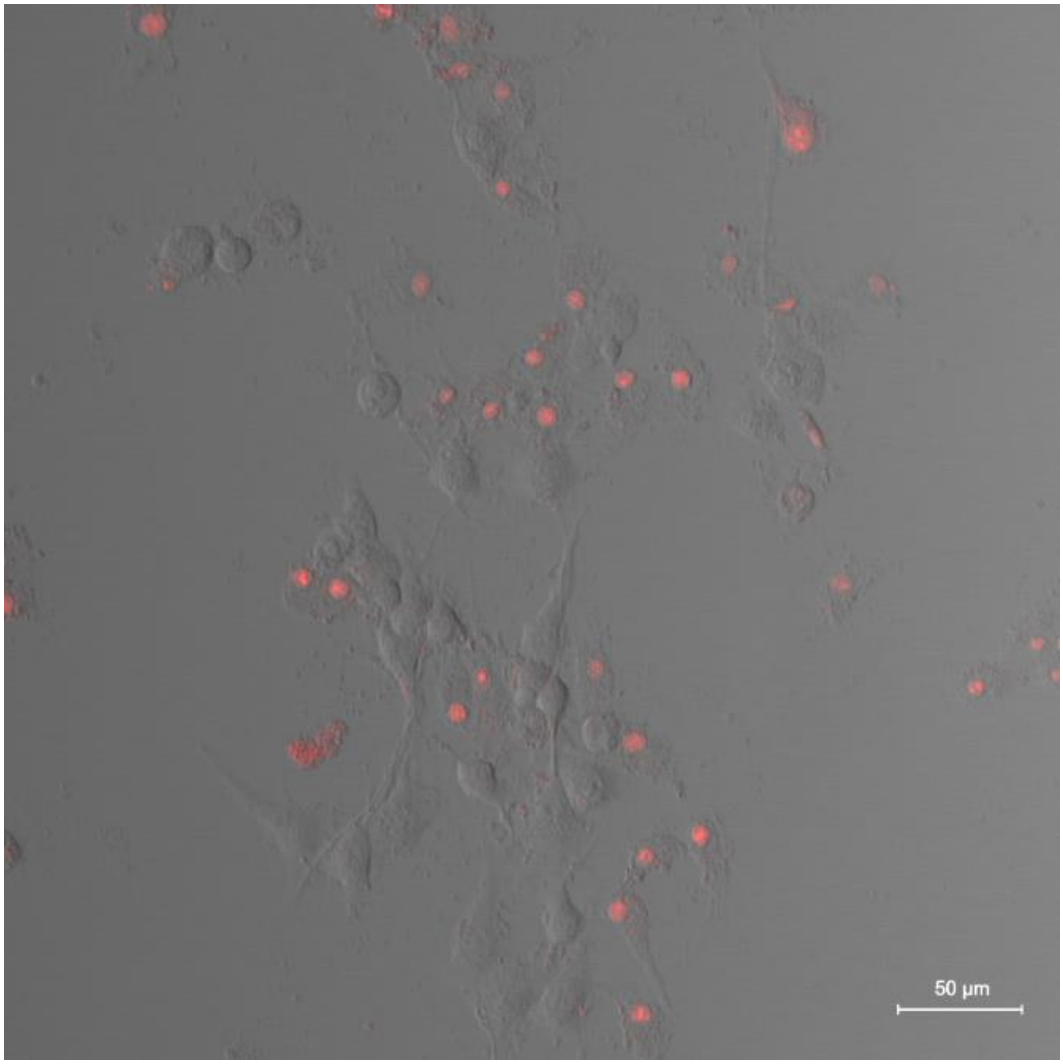

Figure 2.5. Confocal image of the cells treated with propidium iodide-laded liposomes. The liposome concentration was 1 µg/mL, and cells were incubated for 30 minutes.

We tested the proposed immunoflagging mechanism on these peptide-loaded cells by incubating them with pre-enriched $E7_{11-20}$ antigen-specific CD8+ T cells (Figures 2.6a, 2.7). In principle, only cells presenting the correct $E7_{11-20}$ antigen would be recognized by the T cells, thereby inducing an immune response; which is characterized by cytokine secretion from the T cells. After 24 hours of incubation, a prominent amount of tumor necrosis factor (TNF-α) was detected in samples containing U87 cells that were incubated with the $E7_{11-20}$ liposome (Figure 2.6b). In addition, higher amounts of liposomes led to increased cytokine levels. By comparison, U87 cells that were loaded with the scrambled peptide did not mount any immune response and negligible TNF-α was detected. As expected, cells treated with empty liposomes did not induce cytokine release. To further confirm the immunoflagging mechanism, we performed control experiments on another cell line, T47D (Figure 2.6b). These cells are human breast cancer cells that do no exhibit the HLA-A*02:01 allele type.[22, 27] Due to the allele type mismatch, the E7 peptide cannot be presented. Consequently, the antigen-specific T cells would not recognize the cancer cells, and therefore no immune response would be expected. Indeed, no TNF-α secretion was detected in these experiments.

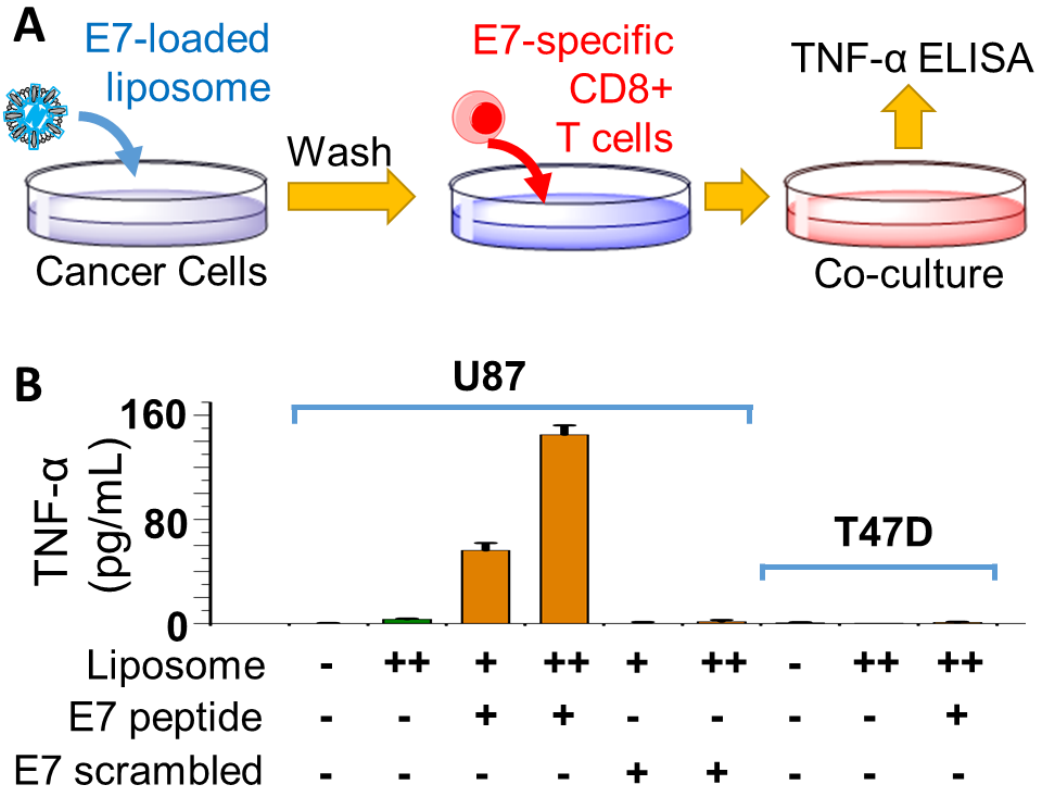

Figure 2.6. (a) The experimental scheme. (b) TNF-α release after various treatment conditions. Cells were treated with liposomes for 24 hours followed by thorough washing and T cell incubation for 24 hours. Liposome concentrations: +, 1 μg/mL; ++, 100 μg/mL.

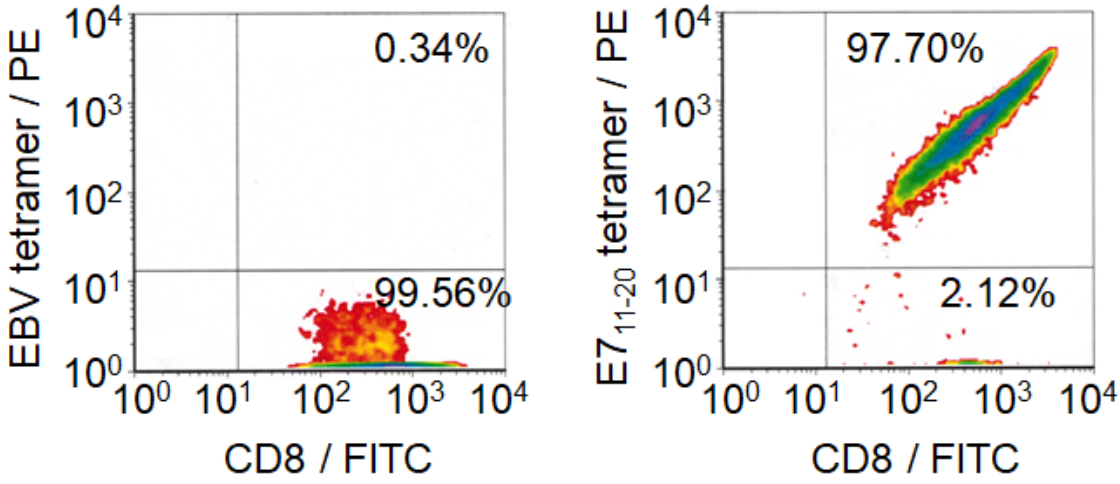

Figure 2.7. Specificity of the anti-HPV $E7_{11-20}$ T cells (obtained from Astarte Biologics).

We then sought to evaluate the growth inhibition efficacy of the T cells after 72 hours of incubation (Figure 2.8a). As shown in Figure 2.8b, the proliferation of the $E7_{11-20}$ antigen-loaded U87 cells was severely inhibited, while cells loaded with scrambled peptides were not affected. The inhibitory effect was further validated through crystal violet staining on the attached cells after 72 hours of incubation with the T cells (Figure 2.8c). Almost no colony was observed in the $E7_{11-20}$ antigen-loaded sample. As expected, no inhibitory effect was observed on T47D cells. These results are consistent with the TNF-α profile and demonstrate the selective and effective immune recognition.

Successful immune recognition can also be characterized by T cell adhesion. With proper TCR-MHC recognition, the T cells would interact with and adhere to the target cells. In our system, the U87 cells were attached to the surface while T cells were introduced in suspension. After 24 hours, we removed the cell media and fixed the attached cells. As shown in Figure 2.9, E7 antigen-loaded U87 cells successfully triggered T cell adhesion, proving the immune recognition.

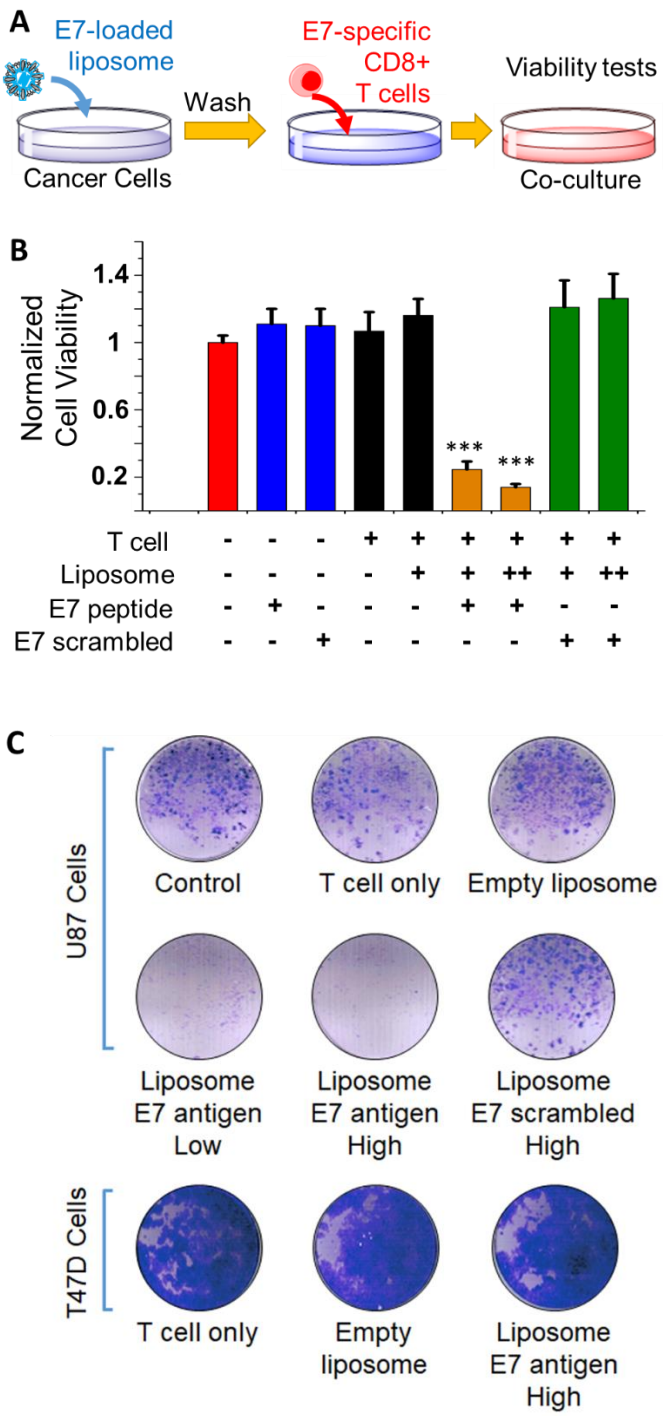

Figure 2.8. (a) Experiment process. (b) U87 cell viability after 72 hours of T cell incubation, as quantified through a resazurin assay. For peptide-only treatments, the peptide concentration was 100 μM. (c) Crystal violet staining of the attached cells after 72 hours of T cell incubation.

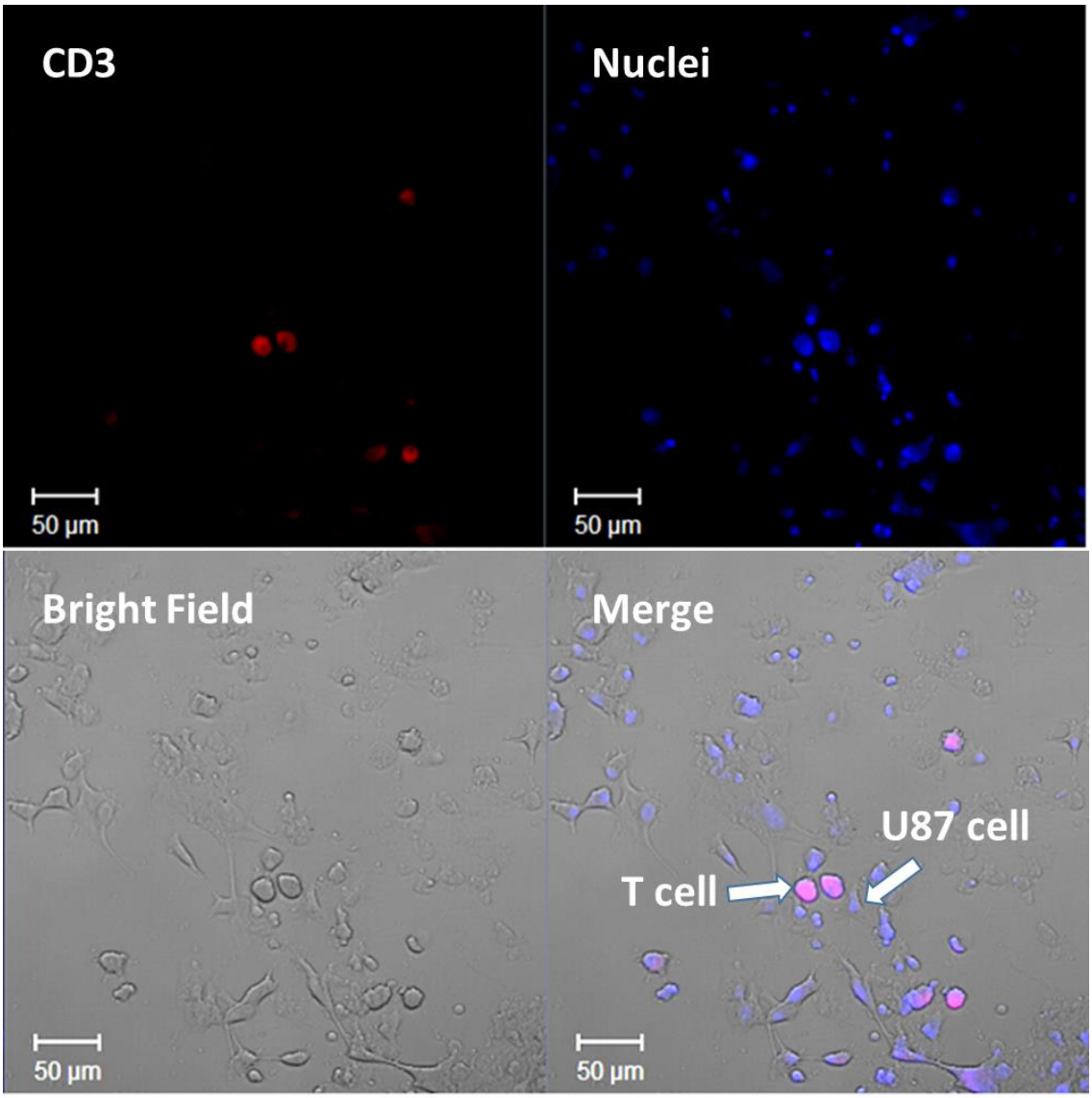

Figure 2.9. Confocal fluorescence microscopy images of T cells recognizing E7 peptide-loaded U87 cells. Cells were washed thoroughly to remove non-adhering T cells and subsequently fixed using glutaraldehyde. T cells were identified through CD3 staining, and the cell nuclei were stained using propidium iodide.

Encouraged by the positive results above, we moved on to test the immunoflagging approach in a more clinically relevant model. Here, we chose the cytomegalovirus CMV-pp65 peptide (NLVPMVATV)[28] and SW620 cells (human colorectal cancer with a low mutational load). Compared with HPV, CMV is far more prevalent in the population. The estimated seroprevalence is >50% in the general population.[29] Therefore, our immunoflagging method will be more generalizable if it can function with a CMV-derived peptide. On the other hand, SW620 is a representative low-TMB cell line with an HLA -A*0201 allele type, which is compatible with the pp65 peptide sequence.

We carried out liposomal encapsulation of the CMV-pp65 peptide (synthesized and purified in the same procedure as the previous peptides), (Figure 2.10) and achieved a loading capacity of 1.2%. The liposomes also obtained a hydrodynamic diameter of 108 nm (Figure 2.11). We then performed the immunoflagging experiment using the liposomes on SW620 cells (Figure 2.12a). Here, we used the CMV-specific CD8+ T cells (Figures 2.13, 2.14). Our results showed that treating the SW620 cells with pp65-loaded liposomes led to successful immunorecognition by the pp65-specific T cells (Figure 2.12b). In addition, this killing activity was consistent with the TNF-α levels in the samples. Taken together, these results demonstrated that the immunoflagging approach could extend to the CMV-pp65 peptide and low-TMB cells such as the SW620 cells.

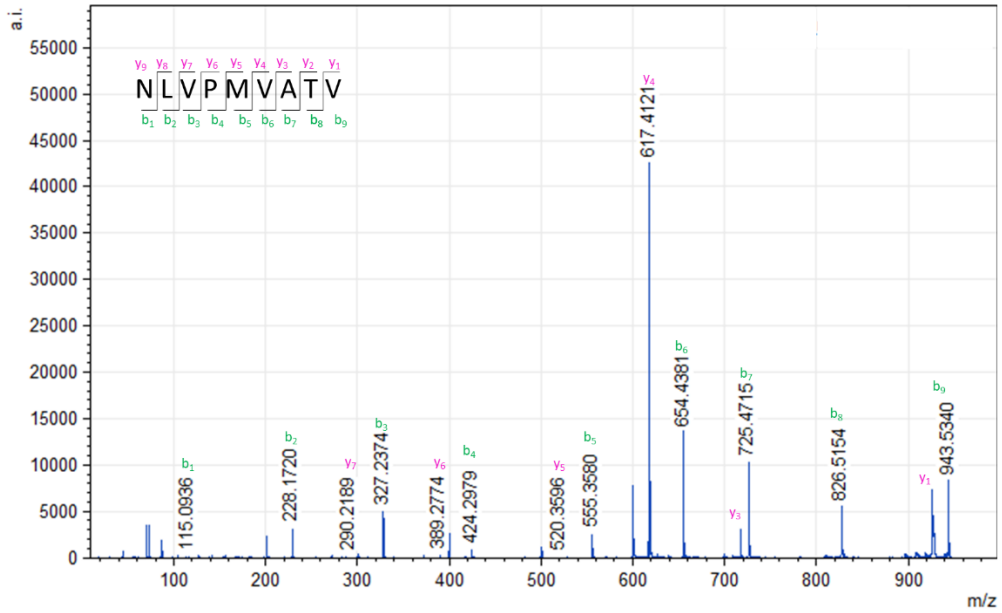

Figure 2.10. MS/MS spectra of the synthesized CMV-pp65 peptide.

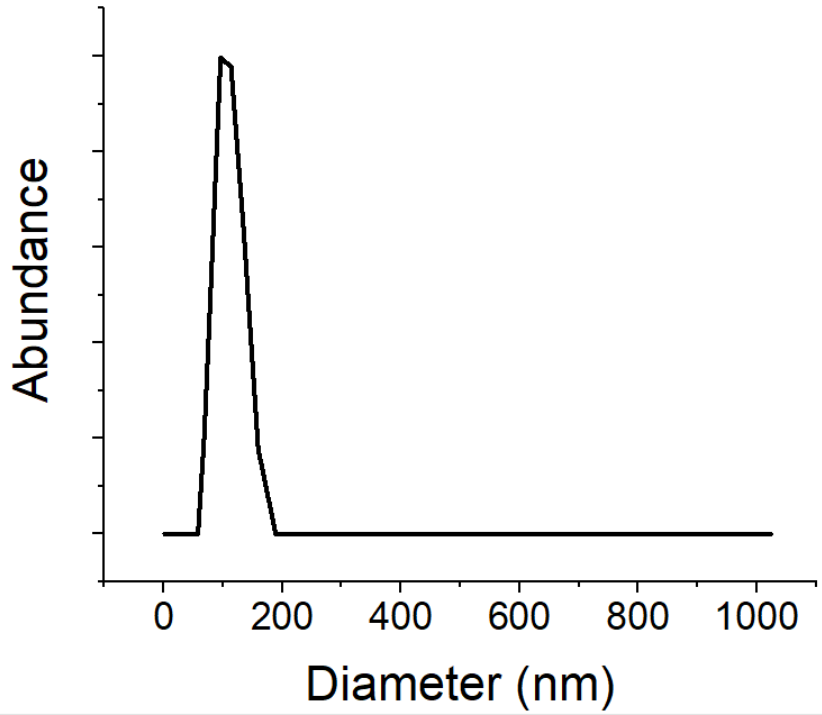

Figure 2.11. Dynamic light scattering results of the CMV pp65-loaded liposomes.

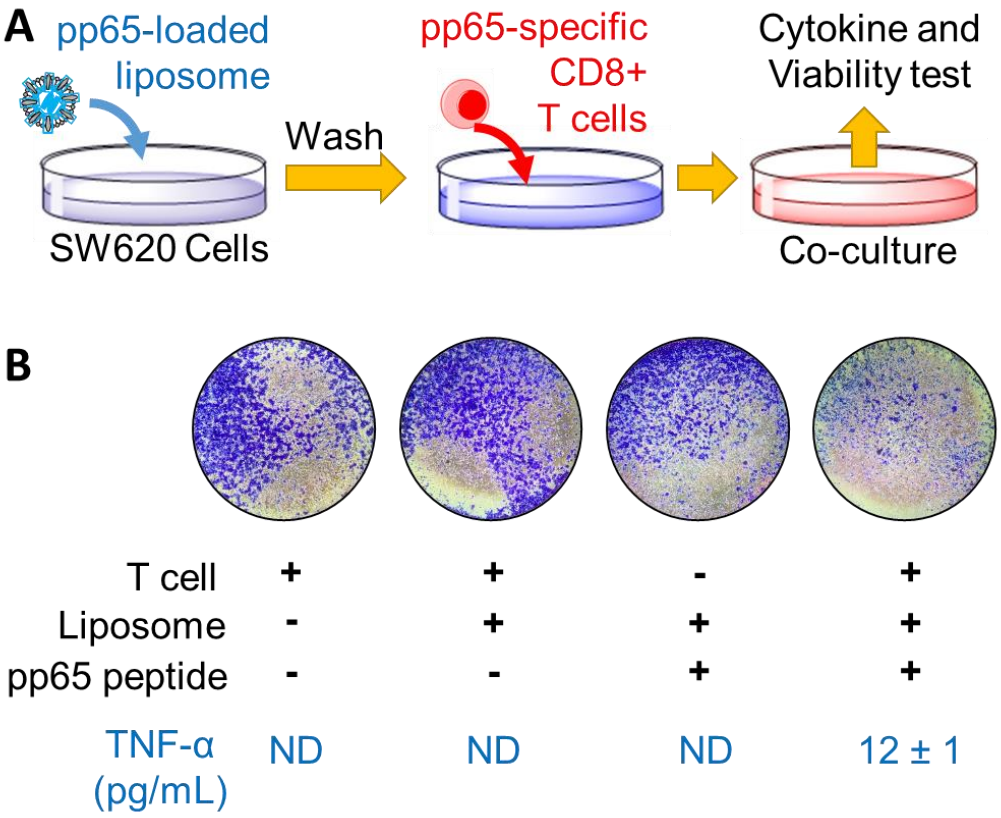

Figure 2.12. (a) Immunoflagging experiment using CMV-pp65-loaded liposomes and SW620 cells. (b) Crystal violet staining of culture plate at the end of the experiment, and the corresponding TNF-α levels in each sample.

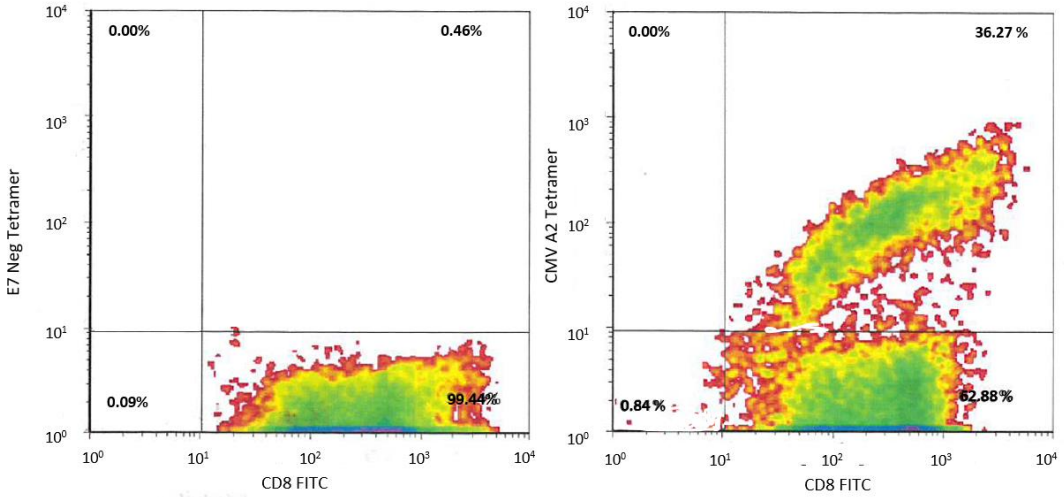

Figure 2.13. Specificity of the anti-CMV pp65 T cells (obtained from Astarte Biologics).

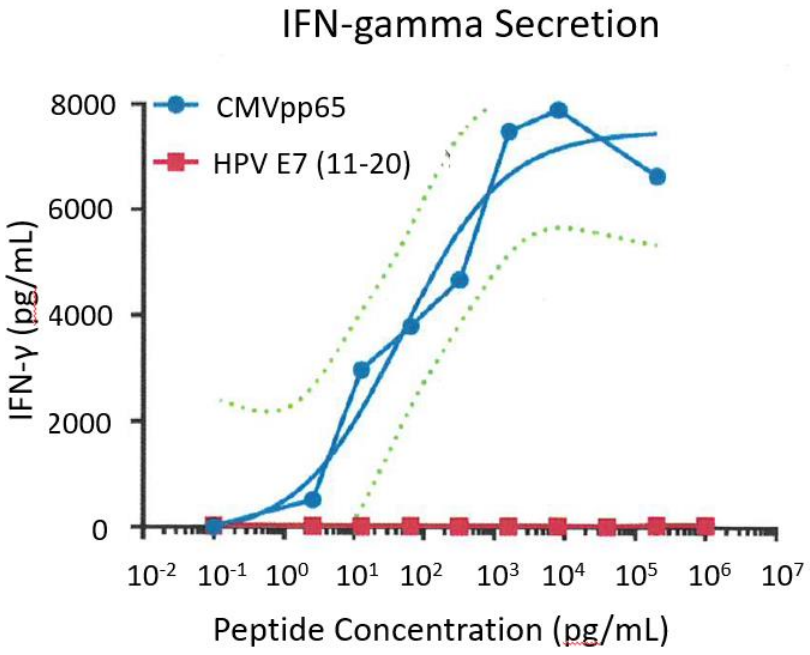

Figure 2.14. CMV pp65 stimulation-induced cytokine secretion in the CD8+ T cells (obtained from Astarte Biologics).

In order to further evaluate the generalizability of the immunoflagging approach, we performed the CMV-pp65/SW620 experiments using peripheral blood mononuclear cells (PBMCs) from a CMV-positive donor, who was representative of the patients targeted for the immunoflagging treatment (Figure 2.15, Table2.1). We cultured the PBMCs in the presence of pp65 peptide and interleukin-2 (IL-2) for 16 days to simulate the anti-pp65 immunity. After this stimulation, we added these PBMCs into the liposome-treated SW620 cells and co-cultured them for 3 days (Figure 2.16a). We found that the presence of peptide indeed elicited significant growth inhibition (Figure 2.16b), albeit less prominent compared with results from the experiments using sorted CD8+ T cells. However, this could also be due to the immune cells attached to the surface, which would drastically increase the measured cell viability values.

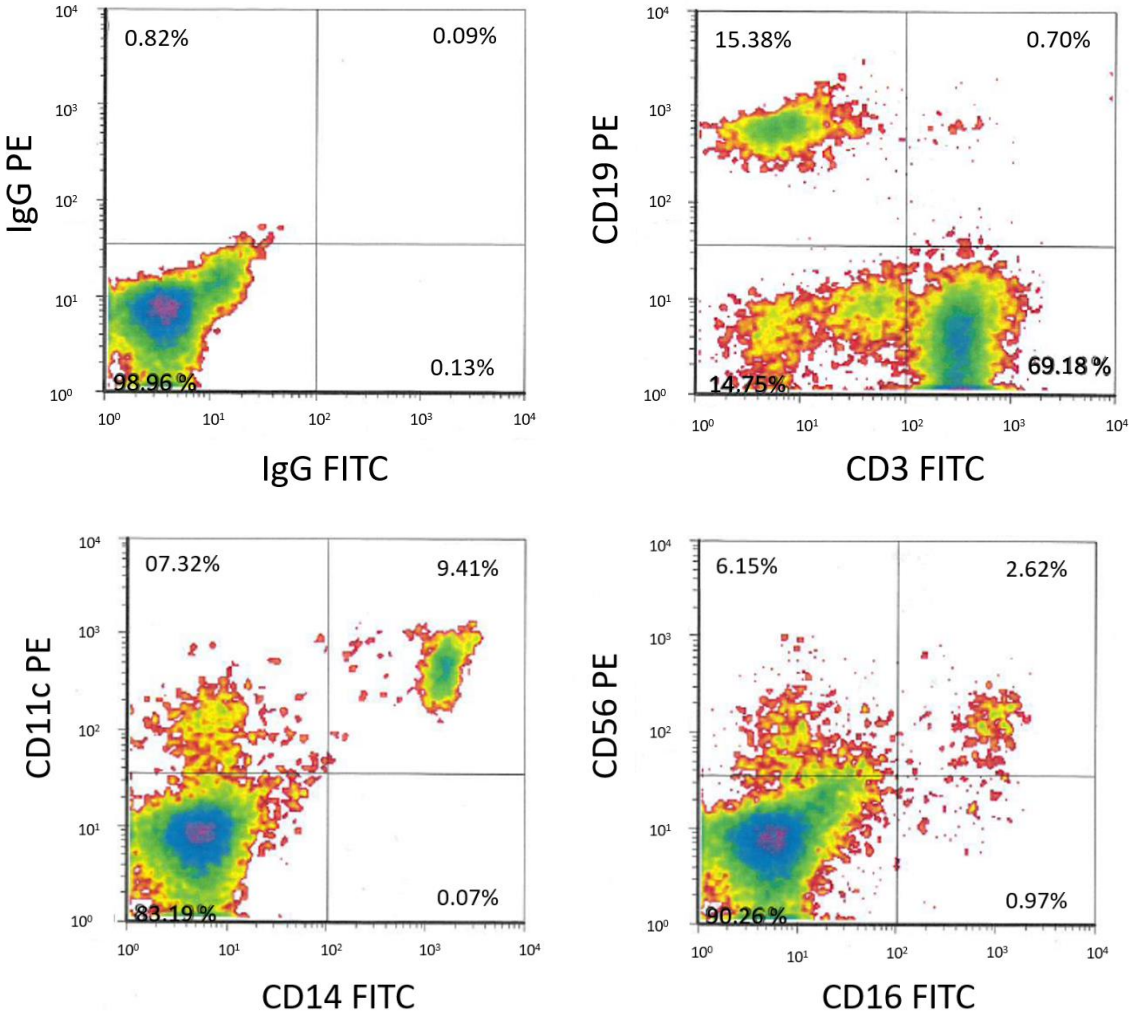

Figure 2.15. Cell population distribution of the PBMC (obtained from Astarte Biologics).

Recall Antigen Response

	Interferon gamma	TNF alpha
Media Control	3	1
Tetanus Toxoid	4334	30
PHA	64963	246
LPS	39860	1469
Cytomegalovirus	13454	73

Table 2.1 The antigen recall experiment using the PBMC. Values are pg/mL of culture medium collected 4 days after stimulation with antigen or mitogen. (obtained from Astarte Biologics).

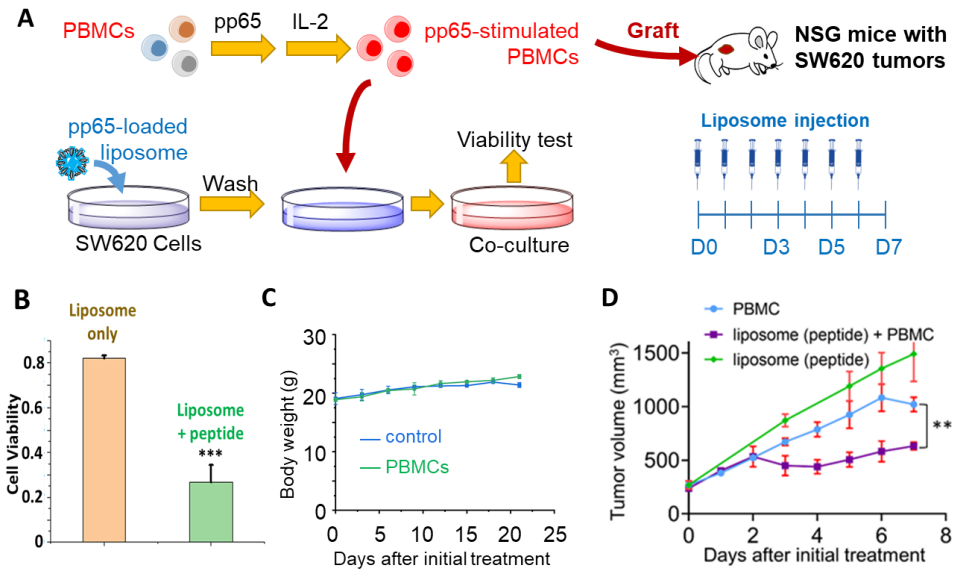

Figure 2.16. (a) Immunoflagging experiment using PBMCs from a CMV-positive donor. The PBMCs were primed using pp65 peptide and IL-2. (b) Treating SW620 cells with pp65 peptide-loaded liposomes and pp65-primed PBMCs led to a decreased cell viability. (c) Body weights of control and PBMC humanized NSG mice showing that no xGvHD emerges within 3 weeks. (d) Tumor growth under different treatment conditions (25 μg liposome-encapsulated CMV peptide was given q.o.d., mean ± SD, **$p < 0.005$)

We sought to test if the immunoflagging approach could function *in vivo*. We engrafted NSG mice with SW620 cells and humanized them with PBMCs isolated from blood samples of an HLA-A*0201 CMV positive donor. Before transferring to the mice, the PBMCs were primed by CMV-pp65 peptide following established protocols.[30] We first confirmed that the PBMC transfer would not induce a xenograft-versus-host disease (xGvHD) within 21 days of the experiment (Figure 2.16c). We then performed intratumoral injection of pp65 peptide-loaded liposomes and followed the tumor growth over time. Mice with concomitant adoptive transfer of PBMCs experienced a slightly slower tumor growth than control mice only without peptide injections, due to the allogeneicity (Figure 2.16d). Treatment with both local injection of the pp65 peptide injection and PBMC transfer led to a clear stabilization of the tumor growth after experiencing a pseudoprogression in the first 2 days (Figure 2.16d). While we only obtained day-7 result, our immunoflagging approach with pp-65 peptide showed promising efficacy compared with the PBMC allogeneic baseline.

2.4 Conclusions

Genome instability is a hallmark of cancer, which often translates to the expression of neoantigens. Immune recognition of these abnormal sequences is the basis of popular cancer immunotherapy strategies, especially those checkpoint blockade therapies such as CTLA-4 and PD-1/PD-L1 antibodies. Recent clinical studies have demonstrated the success of those therapies, but also highlighted their reliance on the

immunogenicity of neoantigens, which often correlates with the total mutational burden (TMB). In the current premise of immunotherapy, cancers with high TMB (melanoma, lung cancer, etc.) promise better therapeutic responses, while cancers with low TMB (MSI-low colorectal cancer, breast cancer, etc.) are not considered as suitable candidates. Although neoantigen vaccination and adoptive cell transfer strategies could potentially circumvent this problem and boost the immunogenicity of low-TMB tumors, there lacks a robust method to identify and prioritize existing neoantigen sequences. In addition, developing such a highly personalized therapy is rather expensive. Currently, adapting immunotherapy to patients with low TMB cancers remains an open challenge.

In this paper, we have demonstrated that intracellular delivery of exogenous immunogenic peptides could flag cancer cells as pathogen-infected cells, which effectively elicits an immune response. Contrary to oncolytic viruses and bacteria, these small peptides are noninfectious, nonpathogenic, but still hold strong immunogenicity due to their sequence homology with (identical to) pathogen fragments[31]. They can be produced at scale and chemically modified to resist humoral clearance. Unlike personal neoantigen vaccines[5], these peptides have been proven to elicit strong immune responses in patients with pre-existing immunity against these peptides. The same peptide can potentially treat all HLA matched patients. Such properties can significantly shorten the turnaround time for therapy delivery and lower the cost.

Our work also validated the feasibility of using tumor mouse models with humanized immune systems. Many previous studies on cancer vaccines employed murine tumor antigens in syngeneic mouse models.[32-34] However, critical differences in the

tumor genetics and immune systems of mice and those of humans have confounded the findings from these studies in mice of uniquely human immune responses.[35] Here, we used severely immunodeficient NSG (*NOD scid gamma)* mice engrafted with human PBMCs to establish the xenograft tumor model.[36-38] While the PBMC-humanized mice have a relatively short life span due to the xenograft-versus-host disease (xGvHD), our results proved that this model can deliver a robust short-term human adaptive immunity for evaluating our immunoflagging strategy.

Indeed, our *in vivo* data did not show complete tumor remission, nor did it provide sustained growth inhibition. This result was likely because the purchased PBMCs were previously frozen and the overall health of those cells were compromised, which would lead to a low priming efficiency and premature T cell exhaustion. Using fresh PBMC samples and further optimizing the antigen stimulation protocol could improve the anti-tumor outcome. In addition, adding adjuvants could help overcome immunosuppressive microenvironments such as those observed in tumors,[39, 40] thereby further enhancing the immune response.

By delivering the antigen directly into the tumor, our immunoflagging approach has the potential to eradicate neoplastic cells with precision, regardless of tumor-specific genetic alterations or the TMB. Moreover, by promoting tumor cell death and neoantigen release, the intratumoral peptide injection may also lead to antigen spreading, thus broadening the antitumor T cell repertoire.[5] Antigen-spreading effects have been observed following vaccine-based anticancer immunotherapy.[41-44] It was also observed

after intratumoral peptide injections.[32, 45] Additionally, it may also synergize with checkpoint blockade in patients without preexisting T cell responses.

2.5 References

1. Ribas, A.; Wolchok, J. D., Cancer immunotherapy using checkpoint blockade. *Science* **2018,** *359* (6382), 1350.

2. Baumeister, S. H.; Freeman, G. J.; Dranoff, G.; Sharpe, A. H., Coinhibitory Pathways in Immunotherapy for Cancer. *Annual Review of Immunology* **2016,** *34* (1), 539-573.

3. Weber, J. S.; D'Angelo, S. P.; Minor, D.; Hodi, F. S.; Gutzmer, R.; Neyns, B.; Hoeller, C.; Khushalani, N. I.; Miller, W. H.; Lao, C. D.; Linette, G. P.; Thomas, L.; Lorigan, P.; Grossmann, K. F.; Hassel, J. C.; Maio, M.; Sznol, M.; Ascierto, P. A.; Mohr, P.; Chmielowski, B.; Bryce, A.; Svane, I. M.; Grob, J.-J.; Krackhardt, A. M.; Horak, C.; Lambert, A.; Yang, A. S.; Larkin, J., Nivolumab versus chemotherapy in patients with advanced melanoma who progressed after anti-CTLA-4 treatment (CheckMate 037): a randomised, controlled, open-label, phase 3 trial. *The Lancet Oncology* **2015,** *16* (4), 375-384.

4. Robert, C.; Schachter, J.; Long, G. V.; Arance, A.; Grob, J. J.; Mortier, L.; Daud, A.; Carlino, M. S.; McNeil, C.; Lotem, M.; Larkin, J.; Lorigan, P.; Neyns, B.; Blank, C. U.; Hamid, O.; Mateus, C.; Shapira-Frommer, R.; Kosh, M.; Zhou, H.; Ibrahim, N.; Ebbinghaus, S.; Ribas, A., Pembrolizumab versus Ipilimumab in Advanced Melanoma. *New England Journal of Medicine* **2015,** *372* (26), 2521-2532.

5. Sahin, U.; Tureci, O., Personalized vaccines for cancer immunotherapy. *Science* **2018,** *359* (6382), 1355-1360.

6. Chalmers, Z. R.; Connelly, C. F.; Fabrizio, D.; Gay, L.; Ali, S. M.; Ennis, R.; Schrock, A.; Campbell, B.; Shlien, A.; Chmielecki, J.; Huang, F.; He, Y.; Sun, J.; Tabori, U.; Kennedy, M.; Lieber, D. S.; Roels, S.; White, J.; Otto, G. A.; Ross, J. S.; Garraway, L.; Miller, V. A.; Stephens, P. J.; Frampton, G. M., Analysis of 100,000 human cancer genomes reveals the landscape of tumor mutational burden. *Genome Medicine* **2017,** *9* (1), 34.

7. Goodman, A. M.; Kato, S.; Bazhenova, L.; Patel, S. P.; Frampton, G. M.; Miller, V.; Stephens, P. J.; Daniels, G. A.; Kurzrock, R., Tumor Mutational Burden as an Independent Predictor of Response to Immunotherapy in Diverse Cancers. *Molecular Cancer Therapeutics* **2017,** *16* (11), 2598.

8. Chesney, J.; Puzanov, I.; Collichio, F.; Singh, P.; Milhem, M. M.; Glaspy, J.; Hamid, O.; Ross, M.; Friedlander, P.; Garbe, C.; Logan, T. F.; Hauschild, A.; Lebbe, C.; Chen, L.; Kim, J. J.; Gansert, J.; Andtbacka, R. H. I.; Kaufman, H. L., Randomized, Open-Label Phase II Study Evaluating the Efficacy and Safety of Talimogene Laherparepvec in Combination With Ipilimumab Versus Ipilimumab Alone in Patients With Advanced, Unresectable Melanoma. *J Clin Oncol* **2018,** *36* (17), 1658-1667.

9. Roberts, N. J.; Zhang, L.; Janku, F.; Collins, A.; Bai, R. Y.; Staedtke, V.; Rusk, A. W.; Tung, D.; Miller, M.; Roix, J.; Khanna, K. V.; Murthy, R.; Benjamin, R. S.; Helgason, T.; Szvalb, A. D.; Bird, J. E.; Roy-Chowdhuri, S.; Zhang, H. H.; Qiao, Y.; Karim, B.; McDaniel, J.; Elpiner, A.; Sahora, A.; Lachowicz, J.; Phillips, B.; Turner, A.; Klein, M. K.; Post, G.; Diaz, L. A., Jr.; Riggins, G. J.; Papadopoulos, N.; Kinzler, K. W.; Vogelstein, B.; Bettegowda, C.; Huso, D. L.; Varterasian, M.; Saha, S.; Zhou, S., Intratumoral injection of Clostridium novyi-NT spores induces antitumor responses. *Sci Transl Med* **2014,** *6* (249), 249ra111.

10. Lang, F. F.; Conrad, C.; Gomez-Manzano, C.; Yung, W. K. A.; Sawaya, R.; Weinberg, J. S.; Prabhu, S. S.; Rao, G.; Fuller, G. N.; Aldape, K. D.; Gumin, J.; Vence, L. M.; Wistuba, I.; Rodriguez-Canales, J.; Villalobos, P. A.; Dirven, C. M. F.; Tejada, S.; Valle, R. D.; Alonso, M. M.; Ewald, B.; Peterkin, J. J.; Tufaro, F.; Fueyo, J., Phase I Study of DNX-2401 (Delta-24-RGD) Oncolytic Adenovirus: Replication and Immunotherapeutic Effects in Recurrent Malignant Glioma. *J Clin Oncol* **2018,** *36* (14), 1419-1427.

11. Ribas, A.; Dummer, R.; Puzanov, I.; VanderWalde, A.; Andtbacka, R. H. I.; Michielin, O.; Olszanski, A. J.; Malvehy, J.; Cebon, J.; Fernandez, E.; Kirkwood, J. M.; Gajewski, T. F.; Chen, L.; Gorski, K. S.; Anderson, A. A.; Diede, S. J.; Lassman, M. E.; Gansert, J.; Hodi, F. S.; Long, G. V., Oncolytic Virotherapy Promotes Intratumoral T Cell Infiltration and Improves Anti-PD-1 Immunotherapy. *Cell* **2017,** *170* (6), 1109-1119 e10.

12. Russell, S. J.; Peng, K. W.; Bell, J. C., Oncolytic virotherapy. *Nat Biotechnol* **2012,** *30* (7), 658-70.

13. Marelli, G.; Howells, A.; Lemoine, N. R.; Wang, Y., Oncolytic Viral Therapy and the Immune System: A Double-Edged Sword Against Cancer. *Front Immunol* **2018,** *9*, 866.

14. Chentoufi, A. A.; Zhang, X.; Lamberth, K.; Dasgupta, G.; Bettahi, I.; Nguyen, A.; Wu, M.; Zhu, X.; Mohebbi, A.; Buus, S.; Wechsler, S. L.; Nesburn, A. B.; BenMohamed, L., HLA-A*0201-Restricted CD8⁺ Cytotoxic T Lymphocyte Epitopes Identified from Herpes Simplex Virus Glycoprotein D. *The Journal of Immunology* **2008,** *180* (1), 426.

15. Terajima, M.; Cruz, J.; Leporati, A. M.; Orphin, L.; Babon, J. A. B.; Co, M. D. T.; Pazoles, P.; Jameson, J.; Ennis, F. A., Influenza A virus matrix protein 1-specific human CD8+ T-cell response induced in trivalent inactivated vaccine recipients. *Journal of virology* **2008,** *82* (18), 9283-9287.

16. Sugaya, N.; Kimura, H.; Hara, S.; Hoshino, Y.; Kojima, S.; Morishima, T.; Tsurumi, T.; Kuzushima, K., Quantitative Analysis of Epstein-Barr Virus (EBV)–Specific CD8+ T Cells in Patients with Chronic Active EBV Infection. *The Journal of Infectious Diseases* **2004,** *190* (5), 985-988.

17. Kondo, E.; Akatsuka, Y.; Kuzushima, K.; Tsujimura, K.; Asakura, S.; Tajima, K.; Kagami, Y.; Kodera, Y.; Tanimoto, M.; Morishima, Y.; Takahashi, T., Identification of novel CTL epitopes of CMV-pp65 presented by a variety of HLA alleles. *Blood* **2004,** *103* (2), 630.

18. Bulbake, U.; Doppalapudi, S.; Kommineni, N.; Khan, W., Liposomal Formulations in Clinical Use: An Updated Review. *Pharmaceutics* **2017,** *9* (2), 12.

19. Blum, J. S.; Wearsch, P. A.; Cresswell, P., Pathways of Antigen Processing. *Annual Review of Immunology* **2013,** *31* (1), 443-473.

20. Liu, W. J.; Liu, X. S.; Zhao, K. N.; Leggatt, G. R.; Frazer, I. H., Papillomavirus Virus-like Particles for the Delivery of Multiple Cytotoxic T Cell Epitopes. *Virology* **2000,** *273* (2), 374-382.

21. Liu, D.-W.; Yang, Y.-C.; Lin, H.-F.; Lin, M.-F.; Cheng, Y.-W.; Chu, C.-C.; Tsao, Y.-P.; Chen, S.-L., Cytotoxic T-Lymphocyte Responses to Human Papillomavirus Type 16 E5 and E7 Proteins and HLA-A*0201-Restricted T-Cell Peptides in Cervical Cancer Patients. *Journal of Virology* **2007,** *81* (6), 2869-2879.

22. Scholtalbers, J.; Boegel, S.; Bukur, T.; Byl, M.; Goerges, S.; Sorn, P.; Loewer, M.; Sahin, U.; Castle, J. C., TCLP: an online cancer cell line catalogue integrating HLA type, predicted neo-epitopes, virus and gene expression. *Genome Medicine* **2015,** *7*, 118.

23. Allen, T. M.; Cullis, P. R., Liposomal drug delivery systems: From concept to clinical applications. *Advanced Drug Delivery Reviews* **2013,** *65* (1), 36-48.

24. Pattni, B. S.; Chupin, V. V.; Torchilin, V. P., New Developments in Liposomal Drug Delivery. *Chemical Reviews* **2015,** *115* (19), 10938-10966.

25. Cavalcanti, R. R. M.; Lira, R. B.; Riske, K. A., Study of the Fusion Mechanism of Fusogenic Cationic Liposomes with Anionic Model Membranes. *Biophysical Journal* **2018,** *114* (3), 606a.

26. Nicoletti, I.; Migliorati, G.; Pagliacci, M. C.; Grignani, F.; Riccardi, C., A rapid and simple method for measuring thymocyte apoptosis by propidium iodide staining and flow cytometry. *Journal of Immunological Methods* **1991,** *139* (2), 271-279.

27. Adams, S.; Robbins, F.-M.; Chen, D.; Wagage, D.; Holbeck, S. L.; Morse, H. C.; Stroncek, D.; Marincola, F. M., HLA class I and II genotype of the NCI-60 cell lines. *Journal of Translational Medicine* **2005,** *3*, 11-11.

28. Solache, A.; Morgan, C. L.; Dodi, A. I.; Morte, C.; Scott, I.; Baboonian, C.; Zal, B.; Goldman, J.; Grundy, J. E.; Madrigal, J. A., Identification of Three HLA-A*0201-Restricted Cytotoxic T Cell Epitopes in the Cytomegalovirus Protein pp65 That Are Conserved Between Eight Strains of the Virus. *The Journal of Immunology* **1999,** *163* (10), 5512.

29. Al Mana, H.; Yassine, H. M.; Younes, N. N.; Al-Mohannadi, A.; Al-Sadeq, D. W.; Alhababi, D.; Nasser, E. A.; Nasrallah, G. K., The Current Status of Cytomegalovirus (CMV) Prevalence in the MENA Region: A Systematic Review. *Pathogens* **2019,** *8* (4), 213.

30. Ruan, G. P.; Ma, L.; Wen, Q.; Luo, W.; Zhou, M. Q.; Wang, X. N., A modified peptide stimulation method for efficient amplification of cytomegalovirus (CMV)-specific CTLs. *Cell Mol Immunol* **2008,** *5* (3), 197-201.

31. Balachandran, V. P.; Luksza, M.; Zhao, J. N.; Makarov, V.; Moral, J. A.; Remark, R.; Herbst, B.; Askan, G.; Bhanot, U.; Senbabaoglu, Y.; Wells, D. K.; Cary, C. I. O.; Grbovic-Huezo, O.; Attiyeh, M.; Medina, B.; Zhang, J.; Loo, J.; Saglimbeni, J.; Abu-Akeel, M.; Zappasodi, R.; Riaz, N.; Smoragiewicz, M.; Kelley, Z. L.; Basturk, O.; Australian Pancreatic Cancer Genome, I.; Garvan Institute of Medical, R.; Prince of Wales, H.; Royal North Shore, H.; University of, G.; St Vincent's, H.; Institute, Q. B. M. R.; University of Melbourne, C. f. C. R.; University of Queensland, I. f. M. B.; Bankstown, H.; Liverpool, H.; Royal Prince Alfred Hospital, C. O. B. L.; Westmead, H.; Fremantle, H.; St John of God, H.; Royal Adelaide, H.; Flinders Medical, C.; Envoi, P.; Princess Alexandria, H.; Austin, H.; Johns Hopkins Medical, I.; Cancer, A. R.-N. C. f. A. R. o.; Gonen, M.; Levine, A. J.; Allen, P. J.; Fearon, D. T.; Merad, M.; Gnjatic, S.; Iacobuzio-Donahue, C. A.; Wolchok, J. D.; DeMatteo, R. P.; Chan, T. A.; Greenbaum, B. D.; Merghoub, T.; Leach, S. D., Identification of unique neoantigen qualities in long-term survivors of pancreatic cancer. *Nature* **2017,** *551* (7681), 512-516.

32. Ishida, E.; Lee, J.; Campbell, J. S.; Chakravarty, P. D.; Katori, Y.; Ogawa, T.; Johnson, L.; Mukhopadhyay, A.; Faquin, W. C.; Lin, D. T.; Wirth, L. J.; Pierce, R. H.; Pai, S. I., Intratumoral delivery of an HPV vaccine elicits a broad anti-tumor immune response that translates into a potent anti-tumor effect in a preclinical murine HPV model. *Cancer Immunology, Immunotherapy* **2019,** *68* (8), 1273-1286.

33. Gubin, M. M.; Zhang, X.; Schuster, H.; Caron, E.; Ward, J. P.; Noguchi, T.; Ivanova, Y.; Hundal, J.; Arthur, C. D.; Krebber, W.-J.; Mulder, G. E.; Toebes, M.; Vesely, M. D.; Lam, S. S. K.; Korman, A. J.; Allison, J. P.; Freeman, G. J.; Sharpe, A. H.; Pearce, E. L.; Schumacher, T. N.; Aebersold, R.; Rammensee, H.-G.; Melief, C. J. M.; Mardis, E. R.; Gillanders, W. E.; Artyomov, M. N.; Schreiber, R. D., Checkpoint blockade cancer immunotherapy targets tumour-specific mutant antigens. *Nature* **2014,** *515* (7528), 577-581.

34. Duan, F.; Duitama, J.; Al Seesi, S.; Ayres, C. M.; Corcelli, S. A.; Pawashe, A. P.; Blanchard, T.; McMahon, D.; Sidney, J.; Sette, A.; Baker, B. M.; Mandoiu, I. I.; Srivastava, P. K., Genomic and bioinformatic profiling of mutational neoepitopes reveals new rules to predict anticancer immunogenicity. *Journal of Experimental Medicine* **2014,** *211* (11), 2231-2248.

35. Allen, T. M.; Brehm, M. A.; Bridges, S.; Ferguson, S.; Kumar, P.; Mirochnitchenko, O.; Palucka, K.; Pelanda, R.; Sanders-Beer, B.; Shultz, L. D.; Su, L.; PrabhuDas, M., Humanized immune system mouse models: progress, challenges and opportunities. *Nature Immunology* **2019,** *20* (7), 770-774.

36. Yong, K. S. M.; Her, Z.; Chen, Q., Humanized Mice as Unique Tools for Human-Specific Studies. *Arch Immunol Ther Exp (Warsz)* **2018,** *66* (4), 245-266.

37. Roth, M. D.; Harui, A., Human tumor infiltrating lymphocytes cooperatively regulate prostate tumor growth in a humanized mouse model. *Journal for ImmunoTherapy of Cancer* **2015,** *3* (1), 12.

38. Sanmamed, M. F.; Rodriguez, I.; Schalper, K. A.; Oñate, C.; Azpilikueta, A.; Rodriguez-Ruiz, M. E.; Morales-Kastresana, A.; Labiano, S.; Pérez-Gracia, J. L.; Martín-Algarra, S.; Alfaro, C.; Mazzolini, G.; Sarno, F.; Hidalgo, M.; Korman, A. J.; Jure-Kunkel, M.; Melero, I., Nivolumab and Urelumab Enhance Antitumor Activity of Human T Lymphocytes Engrafted in Rag2^{−/−}IL2Rγ^{null} Immunodeficient Mice. *Cancer Research* **2015,** *75* (17), 3466.

39. Circelli, L.; Tornesello, M.; Buonaguro, F. M.; Buonaguro, L., Use of adjuvants for immunotherapy. *Hum Vaccin Immunother* **2017,** *13* (8), 1774-1777.

40. Khong, H.; Overwijk, W. W., Adjuvants for peptide-based cancer vaccines. *Journal for ImmunoTherapy of Cancer* **2016,** *4* (1), 56.

41. Disis, M. L.; Goodell, V.; Schiffman, K.; Knutson, K. L., Humoral Epitope-Spreading Following Immunization with a HER-2/neu Peptide Based Vaccine in Cancer Patients. *Journal of Clinical Immunology* **2004,** *24* (5), 571-578.

42. Wierecky, J.; Müller, M. R.; Wirths, S.; Halder-Oehler, E.; Dörfel, D.; Schmidt, S. M.; Häntschel, M.; Brugger, W.; Schröder, S.; Horger, M. S.; Kanz, L.; Brossart, P., Immunologic and Clinical Responses after Vaccinations with Peptide-Pulsed Dendritic Cells in Metastatic Renal Cancer Patients. *Cancer Research* **2006,** *66* (11), 5910.

43. Disis, M. L.; Wallace, D. R.; Gooley, T. A.; Dang, Y.; Slota, M.; Lu, H.; Coveler, A. L.; Childs, J. S.; Higgins, D. M.; Fintak, P. A.; dela Rosa, C.; Tietje, K.; Link, J.; Waisman, J.; Salazar, L. G., Concurrent trastuzumab and HER2/neu-specific vaccination in patients with metastatic breast cancer. *Journal of clinical oncology : official journal of the American Society of Clinical Oncology* **2009,** *27* (28), 4685-4692.

44. Kreiter, S.; Vormehr, M.; van de Roemer, N.; Diken, M.; Löwer, M.; Diekmann, J.; Boegel, S.; Schrörs, B.; Vascotto, F.; Castle, J. C.; Tadmor, A. D.; Schoenberger, S. P.; Huber, C.; Türeci, Ö.; Sahin, U., Mutant MHC class II epitopes drive therapeutic immune responses to cancer. *Nature* **2015,** *520* (7549), 692-696.

45. Nobuoka, D.; Yoshikawa, T.; Takahashi, M.; Iwama, T.; Horie, K.; Shimomura, M.; Suzuki, S.; Sakemura, N.; Nakatsugawa, M.; Sadamori, H.; Yagi, T.; Fujiwara, T.; Nakatsura, T., Intratumoral peptide injection enhances tumor cell antigenicity recognized by cytotoxic T lymphocytes: a potential option for improvement in antigen-specific cancer immunotherapy. *Cancer Immunol Immunother* **2013,** *62* (4), 639-652.

Chapter 3: Degradation of AKT using a cyclic peptide-based PROTAC

3.1 Introduction

AKT, also known as protein kinase B, is a significant signaling node in the PI3K pathway, which is responsible for regulating a plethora of cellular processes such as cell growth, survival, metabolism, apoptosis suppression, and proliferation.[1-7] Hyperactivated AKT signaling is a hallmark in many cancers, where the upregulated AKT activities are often caused by genetic mutations in upstream regulators, such as receptor tyrosine kinases, PI3K, and PTEN.[8-15] Because active AKT directly promotes cell survival and inactive AKT helps orchestrate apoptosis, modulation of AKT signaling has immediate therapeutic implications, as evidenced by the mounting efforts of drug development targeting the AKT pathway and over fifty clinical trials that aim at AKT inhibition. [16-18]

There are three major approaches for targeted AKT inhibition and each method has its own pros and cons. PIP3-analogues can occupy the PIP3 binding cavity in the pleckstrin homology domain, and thereby preventing AKT activation. This strategy is straightforward, but it lacks specificity, because many other proteins also bind with PIP3. Similarly, ATP-competitive active-site inhibitors, such as capivasertib, can block AKT activities, but also often suffers from compromised selectivity due to the conserved ATP-binding pocket structure that is shared among many kinases.[3, 19-20] Allosteric inhibitors, such as MK-2206, can provide high specificity; nevertheless, they have not shown clinical success in later phase trials.[21] To date, modulating AKT activities remains an open challenge, and it calls for more research efforts and new targeting strategies.

As a unique therapeutic modality, proteolysis targeting chimeras (PROTACs) have become an attractive method for inhibiting proteins of interest (POI) due to their heterobifunctional characteristic. Consisting of a ligand for a POI, a linker, and a ligand for E3 ligases, PROTACs hijack the ubiquitination proteasome system and subsequently degrade the POI.[22-23] In contrast to small-molecule inhibitors (SMIs), PROTACs work by promoting protein degradation rather than functional inhibition. Therefore, they pose an advantage as they are catalytic and have an event-driven mode of operation rather than the occupancy-driven pharmacology of SMIs. In many cases, the PROTAC can be used at lower concentrations and can be recycled and degrade more POI molecules.[23-25] PROTACs have proven useful against many challenging and previously deemed "undruggable" protein targets. Some examples include transcription factors that lack binding sites, mutated proteins such as BCR-ABL, and inhibitor-resistant targets such as the androgen receptor.[23-24]

Despite the expanding list of successful PROTACs, very few examples of AKT-specific PROTACs exist,[7, 26] and only one of them has shown durable degradations for up to 96 hours. [7, 27-28] In addition, evidence has shown that AKT signaling is highly heterogeneous among different cell lines.[29-30] The versatile signaling architecture and associated cellular heterogeneity have contributed to some of the failures observed in AKT inhibitor clinical trials.[21] It is expected that AKT degraders may face the same problem and limitations. Therefore, there remains a pressing need to expand the arsenal of AKT degraders and to study the potential resistance mechanisms.

In our recent work, we developed a cyclic peptide cy(GSQTH) that binds to AKT with low nM-level affinity.[31] We hypothesized that this peptide can be adapted to the PROTAC strategy (Figure 3.1). Herein, we conjugated our cyclic peptide to the cereblon E3 ligase ligand (pomalidomide) to produce AKT-specific PROTACs.[32] We demonstrate that these PROTACs were able to degrade AKT and affect its signaling activities.

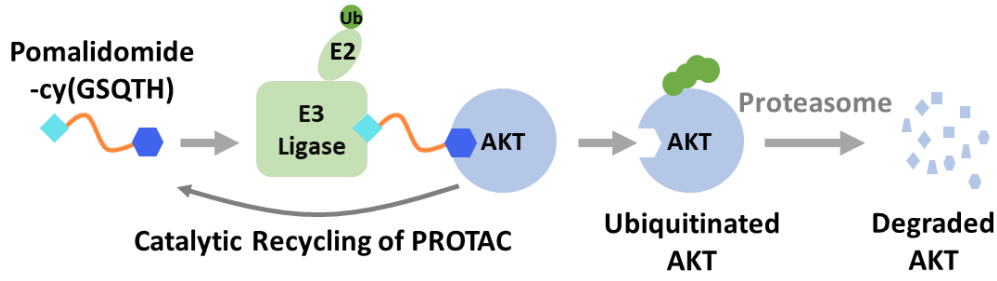

Figure 3.1. Design of the AKT-targeting PROTAC based on the cyclic peptide cy(GSQTH).

3.2 Experimental

Chemicals and reagents

All Fmoc protected amino acids were purchased from Anaspec. Rink amide MBHA resin (0.678 mmol/g) was purchased from Aapptec (Louisville, KY). Resazurin, Pomalidomide-C_3-CO_2H, Pomalidomide-C_6- CO_2H, Pomalidomide-C_9- CO_2H, Pomalidomide-PEG_2- CO_2H, Pomalidomide-PEG_4- CO_2H, Penicillin-Streptomycin (PS), and Copper (I) Iodide were purchased from Sigma Aldrich Inc. (St. Louis, MO). Triisopropylsilane (TIPS) was purchased from TCI (Tokyo, Japan). Trifluoroacetic acid (TFA) was purchased from Oakwood Chemical (Estill, SC). Dimethyl Sulfoxide (DMSO) and HPLC grade Acetonitrile (ACN) were purchased from Fisher Scientific (Waltham, MA). The U87 cell line used in this study was purchased from ATCC (the American Type Culture Collection). Dulbecco's Modified Eagle Medium (DMEM), heat-inactivated Fetal Bovine Serum (FBS), and 0.25% Trypsin (with 2.21mM EDTA) were all purchased from Corning Cellgro (Corning, NY). Bovine Serum Albumin was purchased from bioWORLD (Dublin, OH). L-ascorbic acid was purchased from Chem Impex International l Inc. (Wood Dale, IL). Anti-rabbit IgG/HRP-linked Antibody #7074, GAPDH (14C10) Rabbit mAb #2118, Akt (pan) (C67E7) Rabbit mAb #4691, and Akt (pan) (C67E7) Rabbit mAb (Alexa Fluor® 647 Conjugate) #5186 were all purchased from Cell Signaling Technology, Inc. (Danvers, MA). All Western Blot apparatus and components were purchased from Bio-Rad Laboratories (Hercules,CA). SIS3 HCl inhibitor was purchased from Selleckchem (Houston,TX).

PROTAC synthesis

The peptide sequence, Pra-GSQTH-Az_4 (N to C terminus), was synthesized on Rink Amide MBHA resin using standard Fmoc SPPS on a CSBio CS336S peptide synthesizer (Menlo Park, CA). The peptide's last amino acid remained protected during the following steps. The peptide was then cyclized using a copper-catalyzed click reaction, in which a v/v 20% piperidine in DMF solution containing 2.5 equivalents of CuI and 5.0 equivalents of L-ascorbic acid were mixed with the peptide still on the resin. The cyclization took place at room temperature overnight. The beads were thoroughly washed with 5% w/v sodium diethyldithiocarbamate and 5% v/v DIEA in DMF to remove any excess copper. Afterword, in the same manner of standard Fmoc SPPS steps, the peptide was deprotected and then conjugated with the Pomalidomide-linker-CO_2H component to complete the PROTAC structure. The synthesized PROTACs were cleaved from the resin using a 95% TFA, 2.5% H_2O, 2.5% TIPS solution for 2 hours at room temperature. All PROTACs were then purified on a reversed phase preparative C18 column within a RP-HPLC (using a Dionex UltiMate 3000 UHPLC from Thermo Fisher Scientific). The elution gradient was 0-100% ACN/H_2O (containing 0.1% TFA). Matrix-assisted laser desorption ionization MALDI TOF/TOF (AB Sciex) was used to identify the purest product fractions which were later evaporated, lyophilized, and dissolved in 1X PBS for later use.

Cell Culture

DMEM containing 10% FBS and 1% PS was used for all culture of all cancer cell lines. A Hera Cell incubator (BioSurplus) was set to have 5% CO_2 at a temperature of 37°C for cell culture conditions.

Cell viability after PROTAC treatment

100 µL of 10k U87 cells were seeded per well in at 96-well flat-bottomed plate. A total of 3 plates were used for PROTAC treatment for various time frames. Then 100 µL of DMEM (control), or PROTAC was added to each well to reach a final concentration of 0.01, 0.1, 1, and 10 µM with a total volume of 200 µL. The treatments were left to incubate for 12 or 48 hours. After treatment, the cells were ready for viability testing. 40 µL of 60 µg/mL resazurin solution was added to each well and fluorescence readings were conducted on a plate reader every hour for 4 hours (530 nm emission and 590 nm excitation).

Western blot analysis

1mL of ~200-300k U87 cells were seeded within a 35 mm petri dish and were allowed to settled overnight. The cells were then treated with either 1 mL of DMEM (as control) or with a final concentration of 5 µM PROTAC; a total of four petri dishes were treated. Two petri dishes there then allowed to incubate for 6 and 12 hours. The control and another PROTAC-treated dish was incubated for 24 hours. After treatment, the media was carefully aspirated and the dishes were rinsed once with ice-cold 1X PBS and subsequently aspirated. Then ~90-110 µL of 1X lysis buffer was added to the dish and allowed to incubate over ice for 5 minutes. The dishes were later scraped and the lysates

were collected and centrifuged at 14G for 10 minutes. The supernatant was collected and ready for protein normalization and later Western Blot. The BCA assay and the Western Blot were performed according to standard protocols. The primary rabbit monoclonal antibodies for AKT and for GAPDH, was well as the HRP-linked secondary antibody for Rabbit mAb were diluted 1:1000 in a 5% BSA solution in TBST (containing 1% Tween 20). The Western Blot membranes were first incubated with the primary mAb and then the secondary following standard protocols.

Immunofluorescence Imaging

10k U87 cells were seeded in a 96-well plate and were treated with varying concentrations of C_3 PROTAC (0.1-20 μM) for 6 hours. Three repeats of each treatment were done. After treatment, the cells were gently rinsed 3X with ice-cold 1X PBS and were fixed with ~100 μL of ice-cold MeOH for ~20-30 minutes at -20°C. The cells were again washed 3X with 1X PBS for 5 minutes each. The plate was then blocked with a blocking buffer (1X PBS with 5% normal goat serum) for 1 hour at room temperature. The blocking buffer was aspirated and replaced with a 1:50 dilution of a pan AKT mAb with an Alexa Fluor® 647 conjugate (made in 1X PBS containing 1% BSA). ~80μL of the antibody buffer was added to each well and the plate was left overnight in a 4°C fridge. The following day, the plate was washed 3X for 5 minutes each with 1X PBS. A final 100 μL of 1X PBS was added to the cells which were ready for imaging using a Zeiss 880 confocal microscope.

RNA-seq and data analysis

Around ~200k U87 cells were seeded in a 35 mm petri dish. The cells were treated with 10 μM of the C3-linker PROTAC for 24 hours. The cells were then lysed, and the RNA was extracted following the established protocols of the RNeasy Kit (QIAGEN). Poly-A selective RNA-seq libraries were prepared using the NEB NextUltra II kit (New England Biolabs) and sequenced on an Illumina® NextSeq 500 with 2 X 75 pair-end reads.

The obtained sequencing data was preprocessed using fastp,[1] aligned using STAR,[2] and counted using featureCounts.[3] The normalized expression counts (FPKM) list for each sample were used as the input for principal component analysis. Differentially expressed genes were identified using DESeq2.[4] Gene set enrichment analysis was performed using the GSEA tool and the hallmark gene set.[5-6]

Synergistic experiment

100 μL of 10k U87 cells were seeded per well in at 96-well flat-bottomed plate. The following day, varying concentrations of 50 μL of trametinib and 50 μL of PROTAC were added to each well to give a total volume of 200 μL. The final concentrations of trametinib were 0.5, 1, 5, and 10 μM and the final concentrations of PROTAC were 0.1, 0.5, 1, and 5 μM. The cells were left to incubate at 37C for ~48 hours prior to the same viability testing previously mentioned.

The synergy score of trametinib and PROTAC was calculated with the following equation: $S_{A,B} = I_{A,B} - (I_A + I_B - I_A \times I_B)$

$S_{A,B}$ represents the synergy effect between the drugs A and B (PROTAC and trametinib). The cell killing efficiency of drug A and B is represented by $I_{A,B}$. I_A and I_B represent the

cell killing efficiencies of drug A and drug B in independent doses. The numbers in Figure 3.17 represent the excess activity percentage which were calculated using Bliss scoring.

References for RNA Seq methods

1. Chen, S.; Zhou, Y.; Chen, Y.; Gu, J., fastp: an ultra-fast all-in-one FASTQ preprocessor. *Bioinformatics* **2018,** *34* (17), i884-i890.

2. Dobin, A.; Davis, C. A.; Schlesinger, F.; Drenkow, J.; Zaleski, C.; Jha, S.; Batut, P.; Chaisson, M.; Gingeras, T. R., STAR: ultrafast universal RNA-seq aligner. *Bioinformatics* **2012,** *29* (1), 15-21.

3. Liao, Y.; Smyth, G. K.; Shi, W., featureCounts: an efficient general purpose program for assigning sequence reads to genomic features. *Bioinformatics* **2014,** *30* (7), 923-930.

4. Love, M. I.; Huber, W.; Anders, S., Moderated estimation of fold change and dispersion for RNA-seq data with DESeq2. *Genome Biology* **2014,** *15* (12), 550.

5. Subramanian, A.; Tamayo, P.; Mootha, V. K.; Mukherjee, S.; Ebert, B. L.; Gillette, M. A.; Paulovich, A.; Pomeroy, S. L.; Golub, T. R.; Lander, E. S.; Mesirov, J. P., Gene set enrichment analysis: A knowledge-based approach for interpreting genome-wide expression profiles. *Proceedings of the National Academy of Sciences* **2005,** *102* (43), 15545.

6. Liberzon, A.; Birger, C.; Thorvaldsdóttir, H.; Ghandi, M.; Mesirov, Jill P.; Tamayo, P., The Molecular Signatures Database Hallmark Gene Set Collection. *Cell Systems* **2015,** *1* (6), 417-425.

3.3 Results and Discussion

It is well known that the distance between the POI ligand and the E3 ligase ligand plays a critical role in the degradation efficiency of PROTACs, and that the optimal distance varies among different POIs. Therefore, we used five different linkers to construct the AKT-specific PROTAC: a 3-carbon chain (C_3), a 6-carbon chain (C_6), and a 9-carbon chain (C_9) linker, and the other two were PEG_2 and PEG_4 (Figures 3.2-3.6, 3.7a). All PROTACs showed solubility in aqueous solutions, which allowed for ease of handling for cell testing.

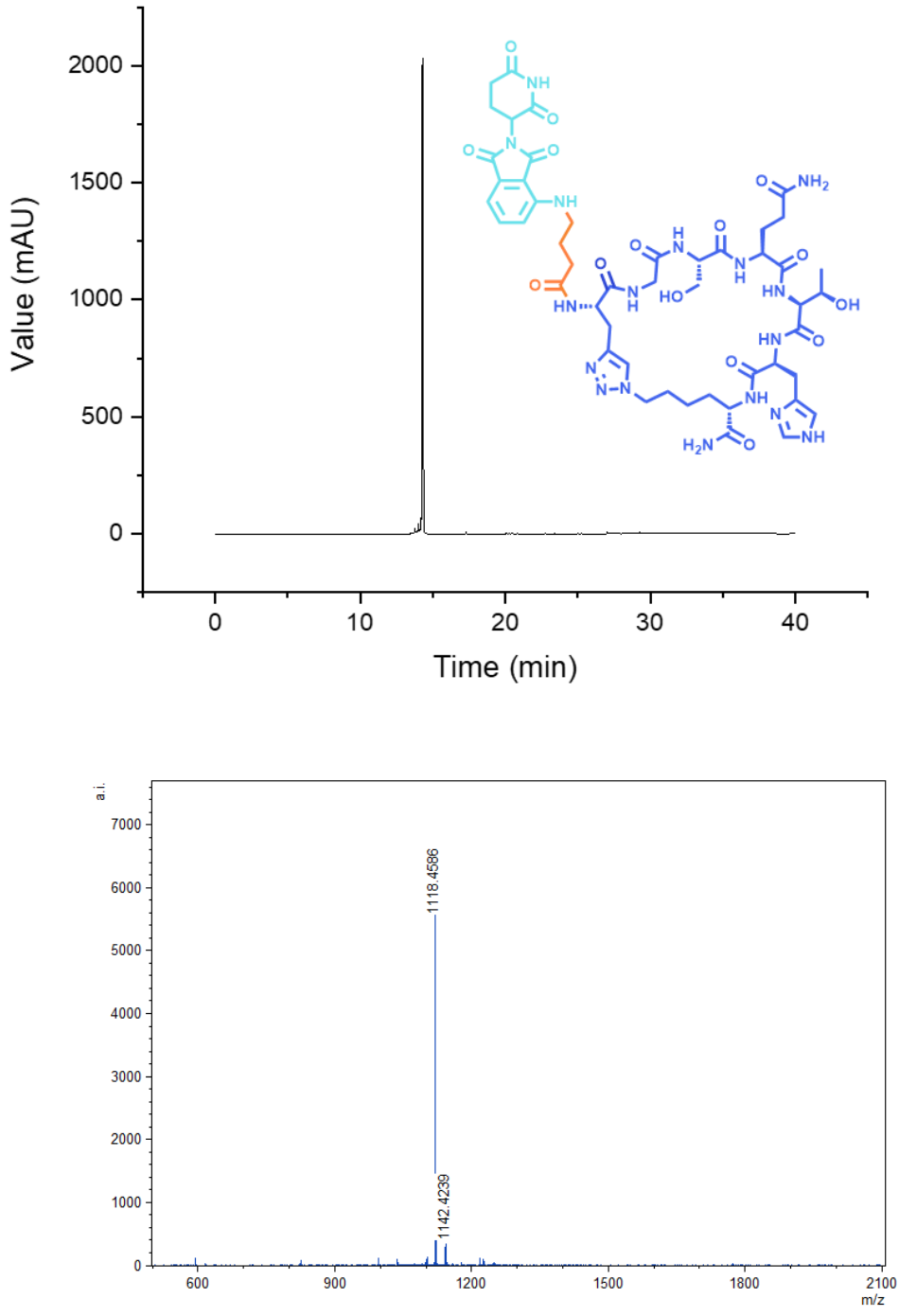

Figure 3.2. Analytical HPLC chromatogram (absorption 280 nm) and a MALDI-TOF mass spectrum of the C_3 PROTAC. Calculated $[M+H]^+$: 1118.14, found 1118.4586.

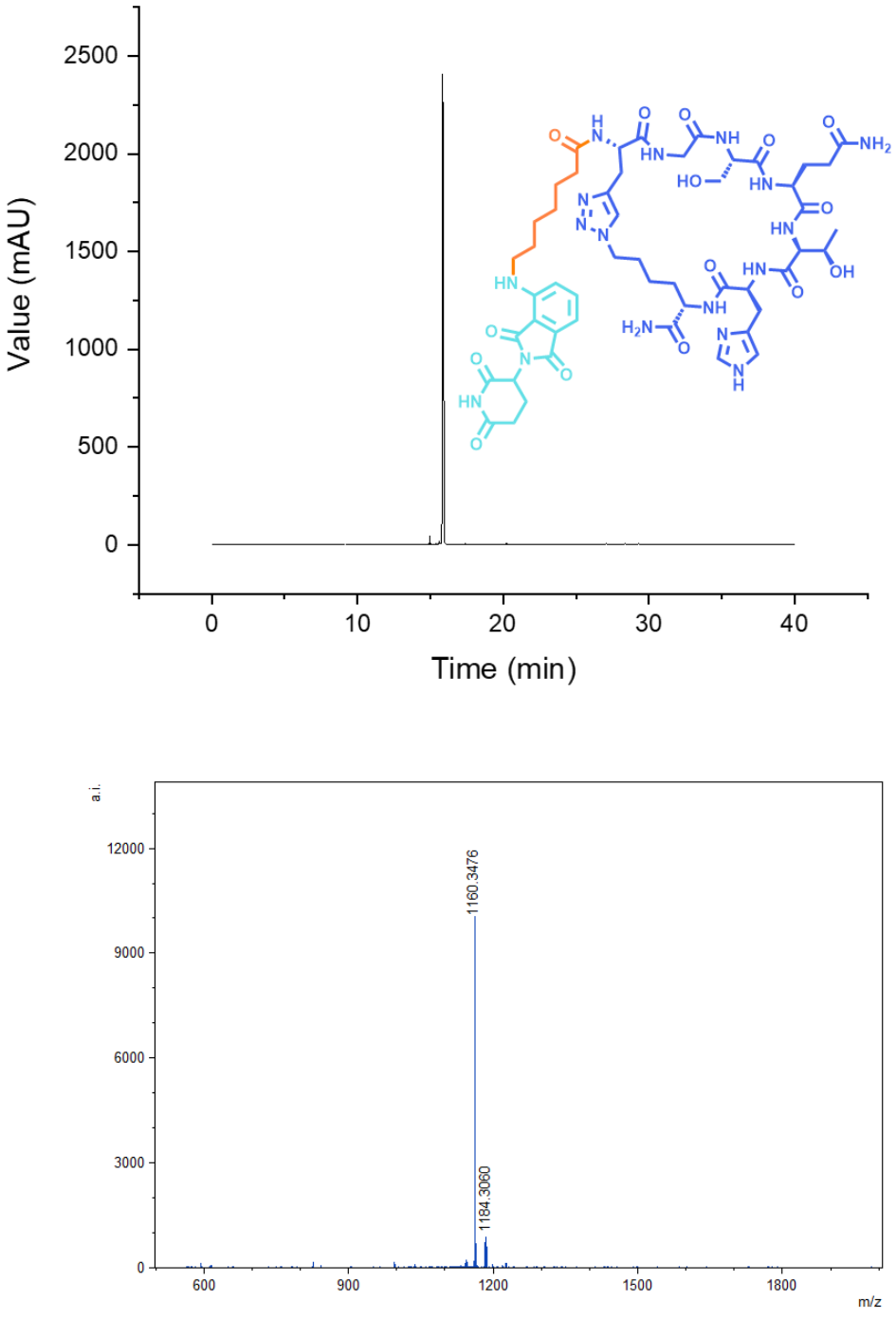

Figure 3.3. Analytical HPLC chromatogram (absorption 280 nm) and a MALDI-TOF mass spectrum of the C_6 PROTAC. Calculated $[M+H]^+$: 1160.22, found 1160.3476.

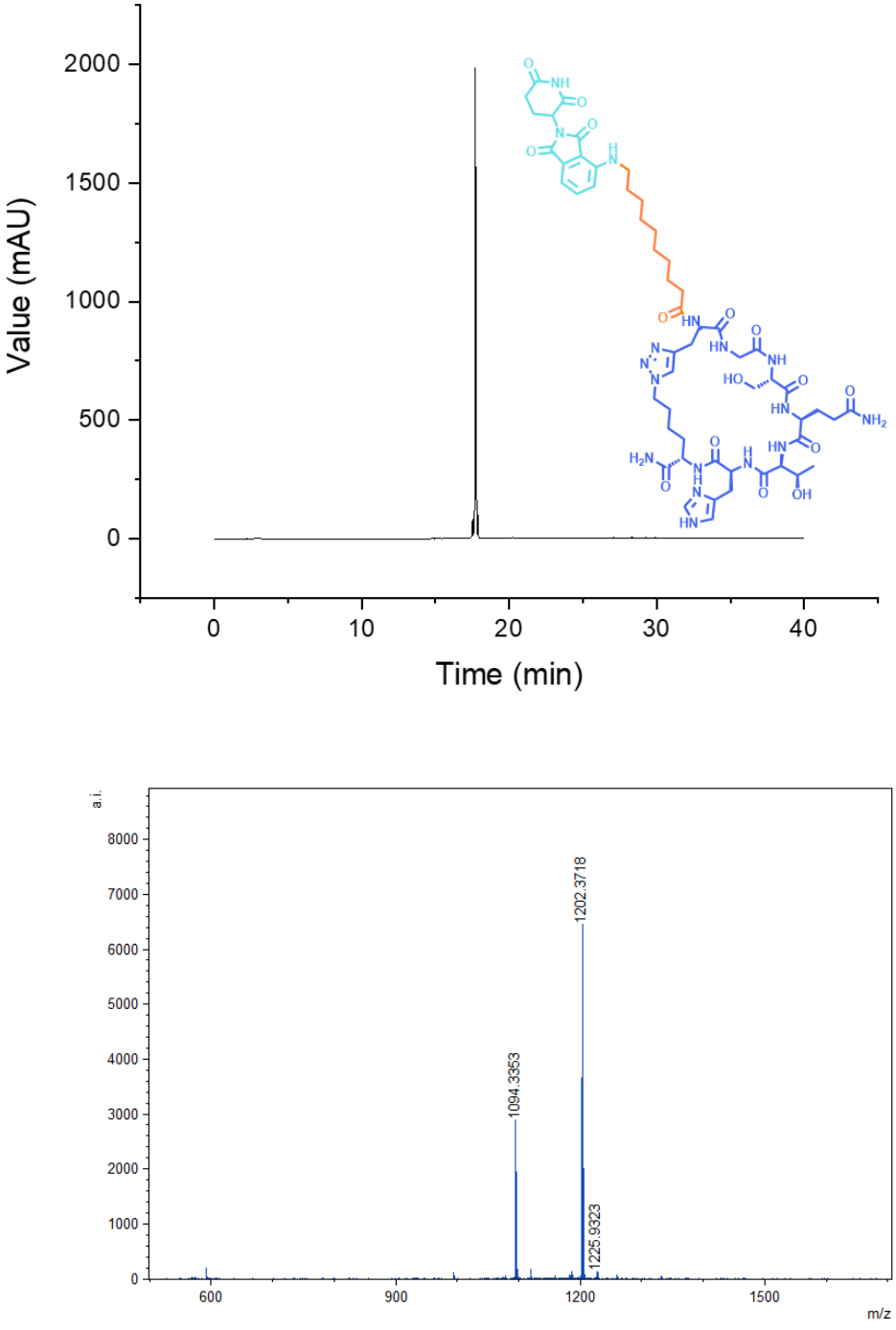

Figure 3.4. Analytical HPLC chromatogram (absorption 280 nm) and a MALDI-TOF mass spectrum of the C_9 PROTAC. Calculated $[M+H]^+$:1202.30, found 1202.3718.

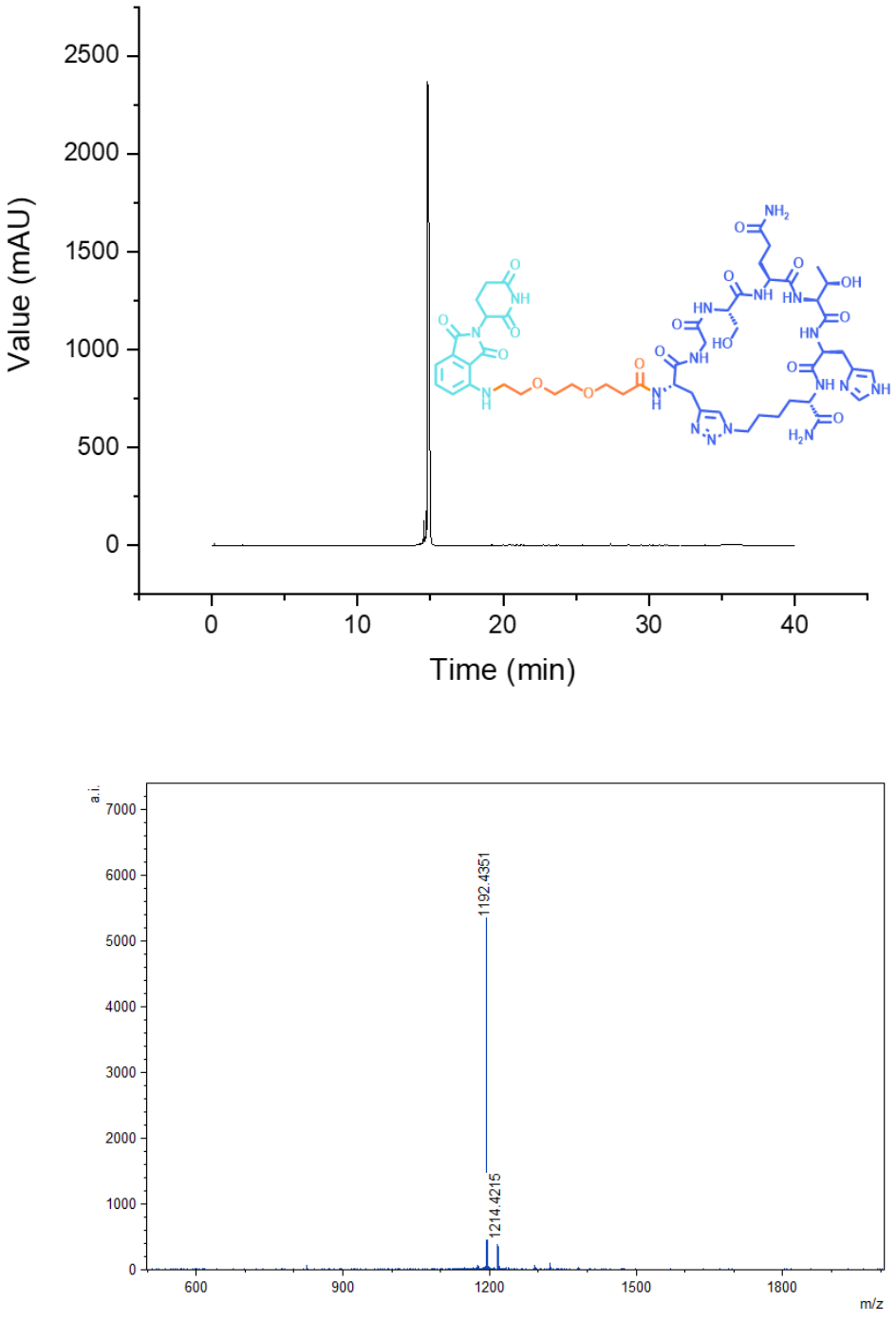

Figure 3.5. Analytical HPLC chromatogram (absorption 280 nm) and a MALDI-TOF mass spectrum of the PEG_2 PROTAC. Calculated $[M+H]^+$: 1192.22, found 1192.4351.

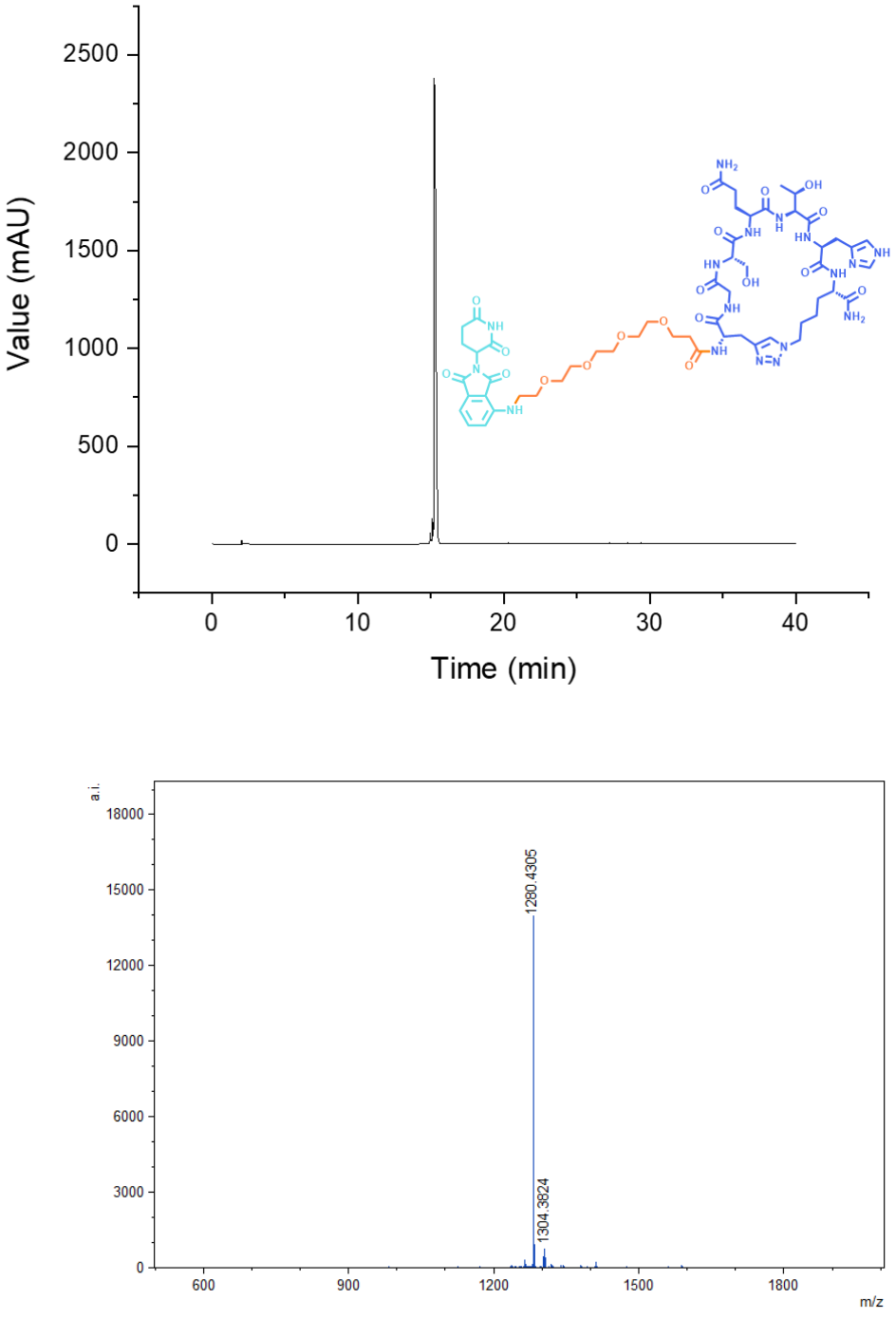

Figure 3.6. Analytical HPLC chromatogram (absorption 280 nm) and a MALDI-TOF mass spectrum of the PEG_4 PROTAC. Calculated $[M+H]^+$: 1280.32, found 1280.43.

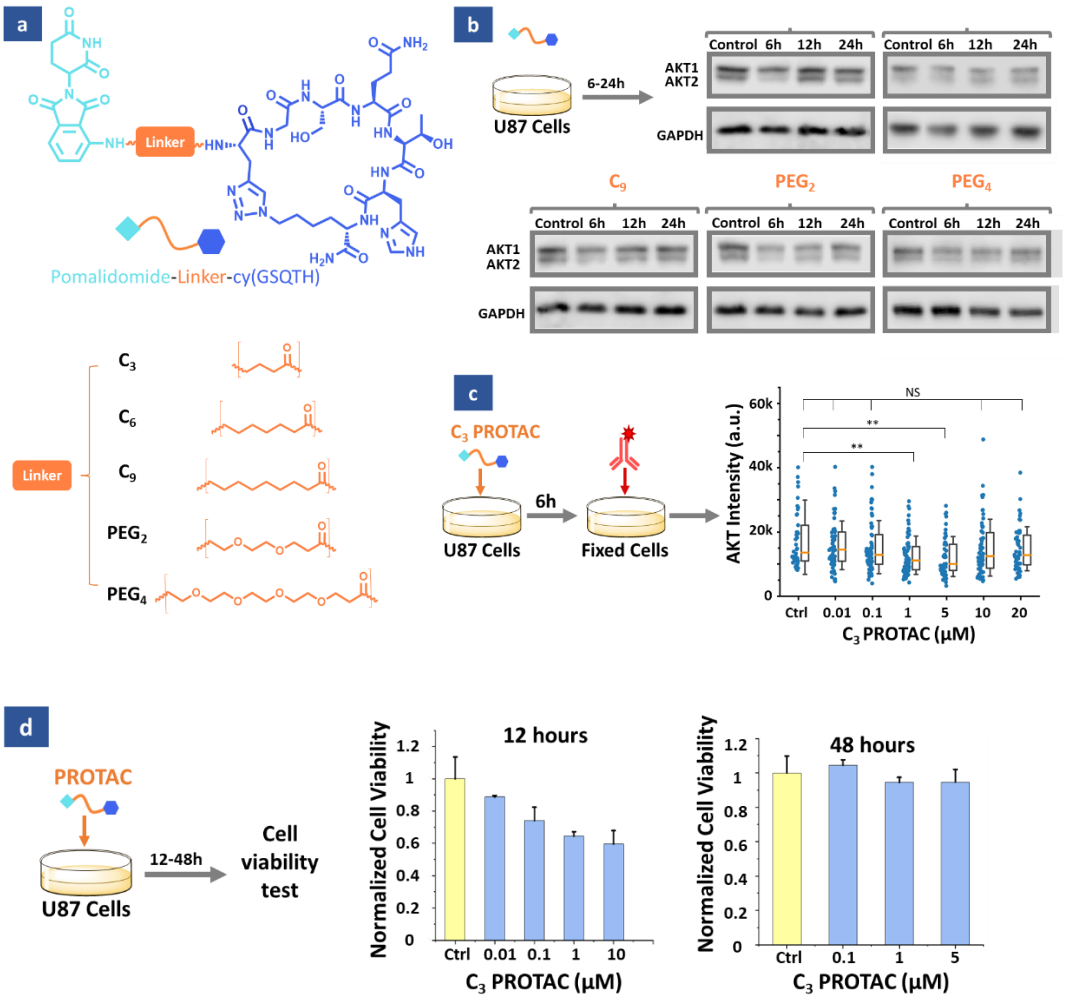

Figure 3.7. (a) The structure of the PROTAC. Five different linkers were employed. (b) Western blot analysis of AKT expression levels in U87 cells after the treatment with 5 μM of PROTACs. GAPDH was used as the internal control. (c) Single-cell immunofluorescence quantitation of AKT expression levels in U87 cells treated with the C3 PROTAC for 6 hours. The boxes denote the middle two quartiles, the whiskers represent the standard deviations, and the orange lines show the median values of the distributions. Mann-Whitney test was used for statistical analysis. NS: not significant. **: $p < 0.01$. (d) U87 cell viability after 12 and 48 hours of the C3 PROTAC treatment.

We chose U87 cells as the model system to test these PROTACs. U87 is a human glioblastoma cell line that harbors a loss-of-function PTEN mutation.[33] Consequently, these cells present a hyperactivated PI3K-AKT signaling pathway that drives cell proliferation.[34] This feature makes it a suitable platform for testing the AKT degradation efficacies of our PROTACs. We treated U87 cells with 5 μM of each PROTAC for 6, 12, and 24 hours, and performed western blot analysis to assess the AKT protein levels in each sample. We found that C_3 and PEG_2 PROTACs were able to cause AKT degradation after 6 hours of treatment (Figure 3.7b). Similarly, C_6, C_9, and PEG_4 PROTACs also led to lowered AKT levels, albeit less prominent. This result was consistent with the fact that the linker structures can drastically affect PROTAC activities. Interestingly, we discovered that after 12 hours of PROTAC treatment, the AKT levels started to recover. Because our previous experience suggested that cy(GSQTH) was stable inside cells, such transient degradation kinetics suggested that the cells might have quickly adapted to the PROTAC perturbation, perhaps through increasing AKT expression levels to compensate for the degraded AKT. Of course, such a speculation warranted further investigation. Because the C_3 PROTAC showed the most significant AKT degradation efficacy followed by the most prominent recovery, we chose it for our subsequent studies.

To validate the AKT degradation observed in the western blot results, we performed immunofluorescence analysis. We incubated U87 cells with varying concentrations of the C_3 PROTAC for 6 hours, fixed the cells, and used a pan-AKT antibody to label AKT in these cells. We used confocal microscopy methods to quantify

the AKT levels in each sample at single-cell resolution. As shown in Figure 3.7c, U87 cells exhibit significant heterogeneity in AKT expression levels, with many outliers expressing a high amount of AKT. At low concentrations (0.01 – 5 μM), increasing PROTAC treatment led to decreasing AKT levels, while at higher concentrations (10, 20 μM), the PROTAC treatment lost its effect. This unique concentration dependence is consistent with the expected "hook effect" of PROTACs, where higher PROTAC concentrations decrease the possibility of forming the Target-PROTAC-E3 ligase ternary complex. This result further agreed with the anticipated PROTAC mechanism of action.

We then tested how the C_3 PROTAC affected cell viability. We incubated U87 cells with different concentrations of PROTAC and used the resazurin assay to assess cell viability. As seen in Figure 3.7d, there was a steady decrease in the viability as the concentration of PROTAC increased after treatment for 12 hours. However, upon treatment with the PROTAC for 48 hours, we saw no significant decrease compared to the first viability test. This result was consistent with the western blot result in Figure 3.7b and further highlighted the transient effect of the PROTAC.

Intrigued by the results above, we sought to further delineate the effects of AKT degradation in these cells. We treated U87 cells with 5 μM of C_3 PROTAC, extracted RNAs from the cells at 0, 6, and 24 hours, and performed transcriptome analysis by RNA-seq (Figure 3.8a). We prepared three biological repeats for each condition, which averaged 31 million reads per sample (Figures 3.9-3.11, Table 3.1). We used the fastp, STAR, and featureCounts methods to perform the read preprocessing and alignment.[35-37] After trimming, the sample datasets displayed Q30 mean quality scores around 90%, and

about 93% of the reads were successfully aligned. Among the aligned reads, about 82% of them were aligned to mRNA transcripts (Table 3.1). These results ensured that the obtained RNA-seq datasets were suitable for further analysis.

To examine the overall variance among the nine samples, we performed principal component analysis (PCA) using the annotated transcriptome dataset as the input. As shown in Figure 3.8b, PC1 captured around 60% of the total variance, and it differentiated the 6h PROTAC samples from the control and the 24h samples. On the other hand, the control and the 24h samples differentially aligned along PC2, which captured 20% of the total variance. It is worth noting that the 6h PROTAC samples displayed negligible contribution to PC1, and that all three replicates were closely clustered. Taken together, these results suggested that the 6h samples were significantly different from the rest. This finding echoed our western blot result above, where the most significant AKT degradation was observed at 6 hours.

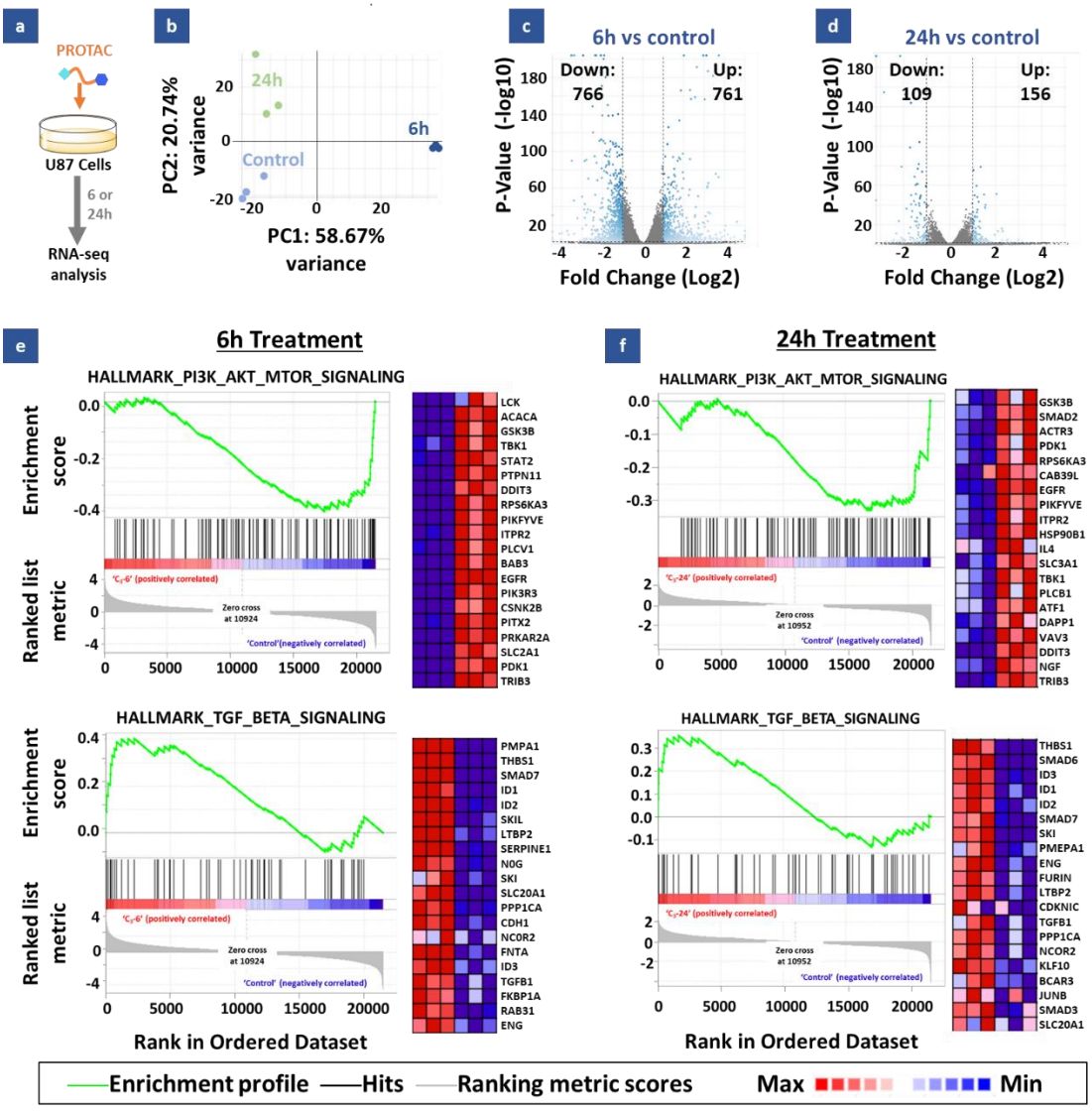

Figure 3.8. RNA-seq analysis of U87 cells treated with the C3 PROTAC. (a) Illustration of the experimental procedure. (b) Principal component analysis result of the RNA-seq datasets. (c-d) Volcano plot showing the overall landscape of differentially expressed genes as the result of 6h (c) and 24h (d) PROTAC treatment. Cutoff criteria: $p < 0.01$, fold change > 2. (e-f) Enrichment plots (left) and the top 20 contributing genes (right) of the PI3K-AKT-mTOR and TGF-β signaling pathways as the result of 6h (e) and 24h (f) PROTAC treatment.

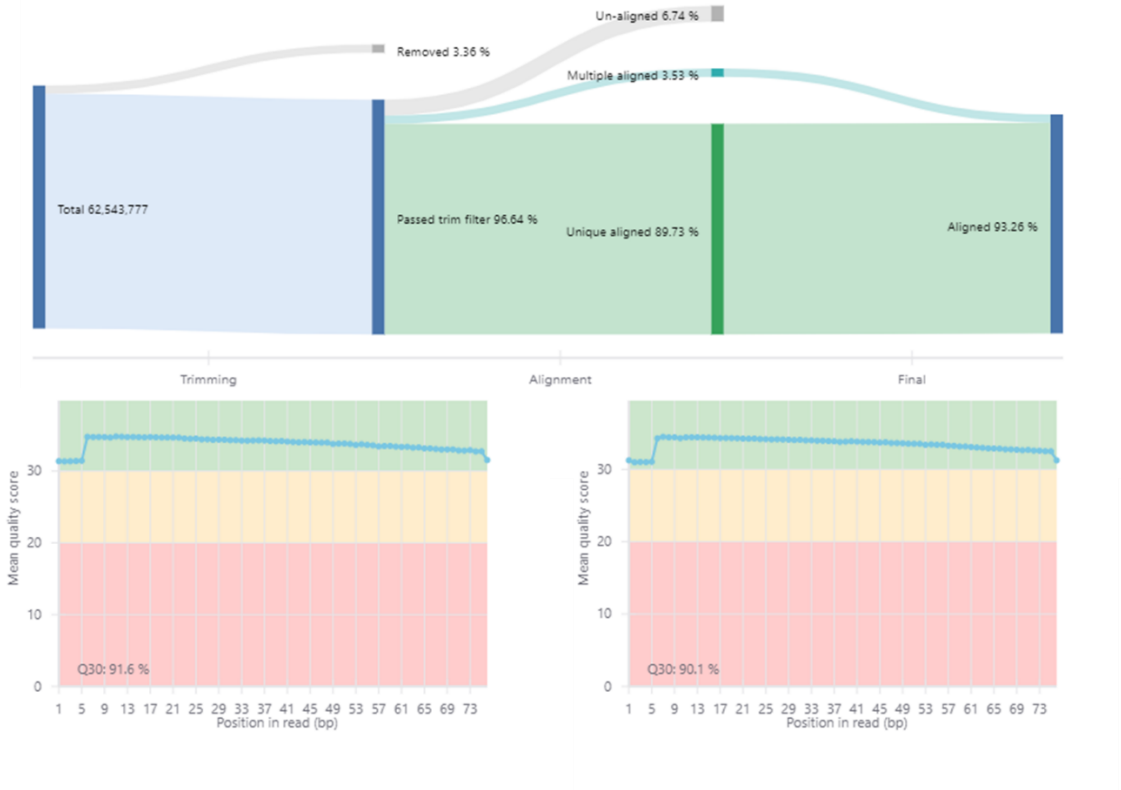

Figure 3.9-1. Quality of the RNA-seq reads for the control sample #1.

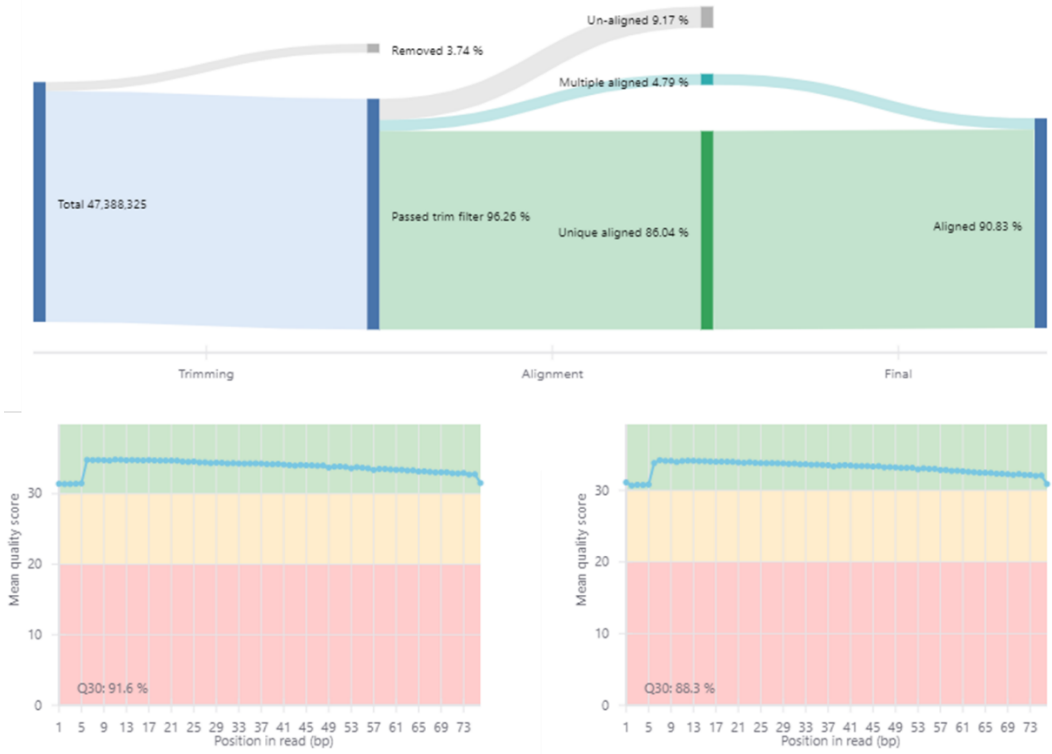

Figure 3.9-2. Quality of the RNA-seq reads for the control sample #2.

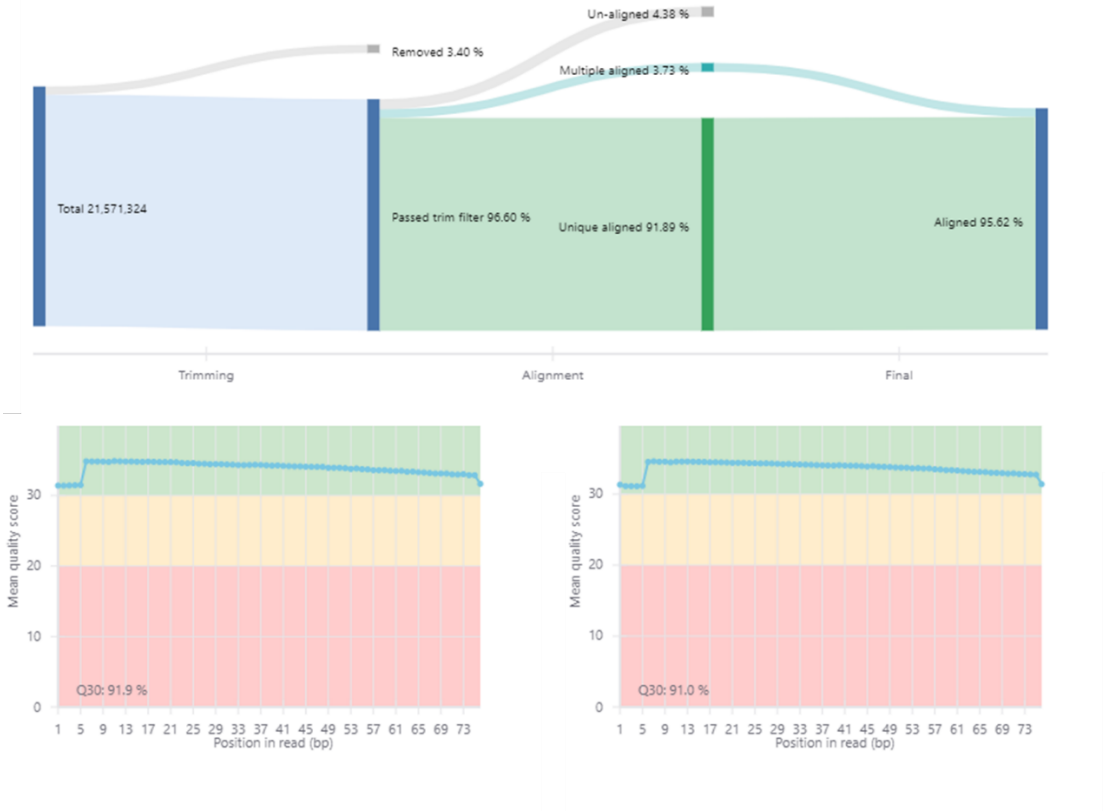

Figure 3.9-3. Quality of the RNA-seq reads for the control sample #3.

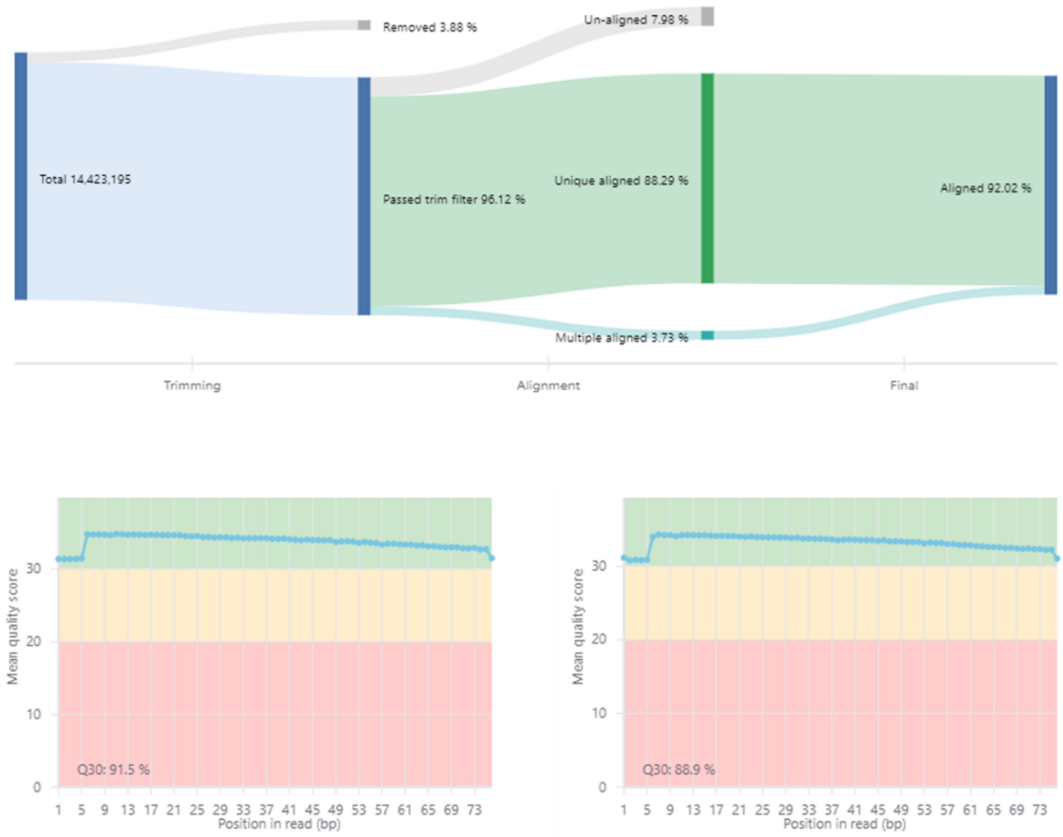

Figure 3.10-1. Quality of the RNA-seq reads for the 6-hr PROTAC treated sample #1.

Figure 3.10-2. Quality of the RNA-seq reads for the 6-hr PROTAC treated sample #2.

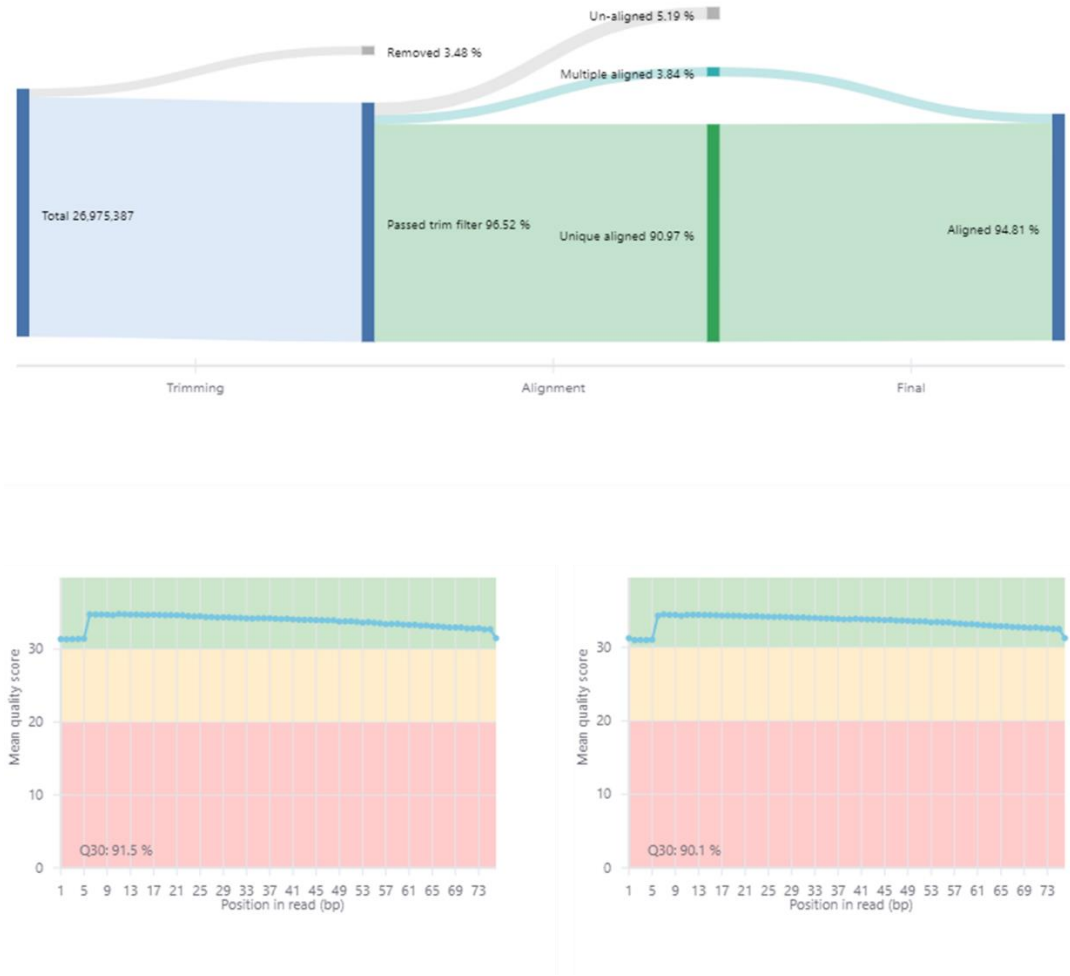

Figure 3.10-3. Quality of the RNA-seq reads for the 6-hr PROTAC treated sample #3.

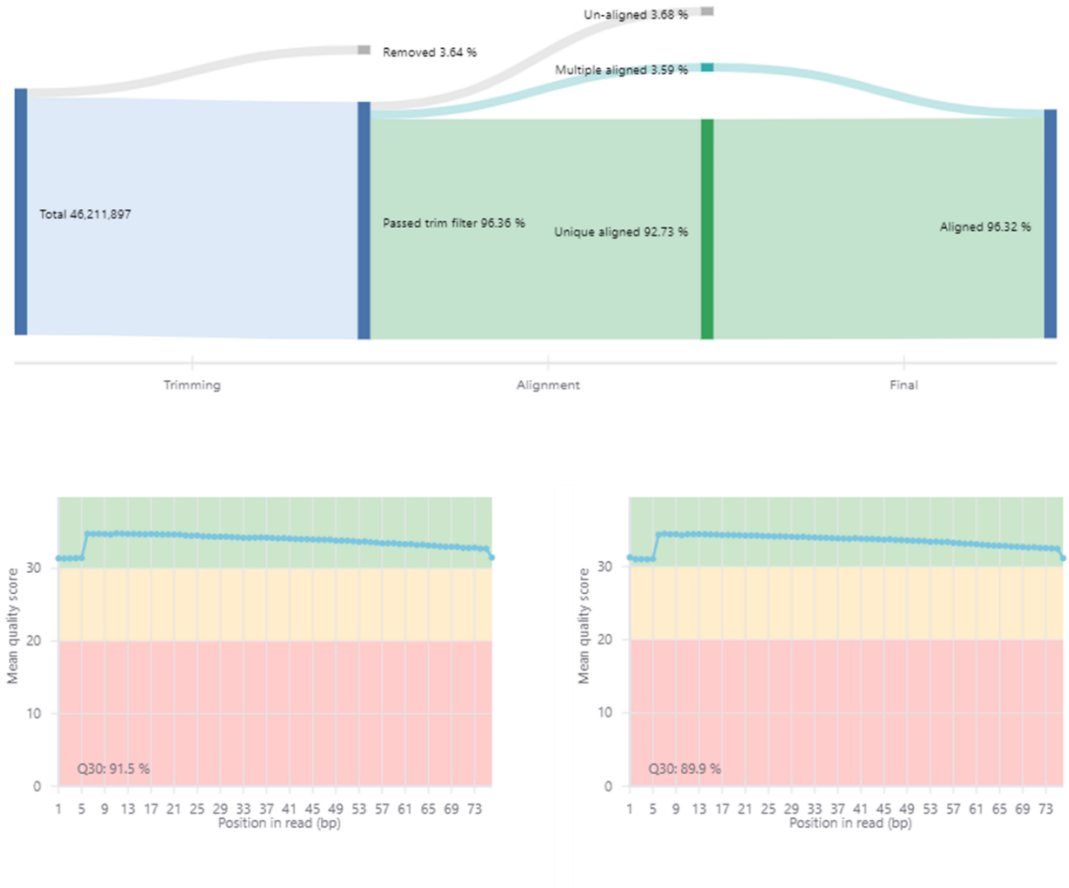

Figure 3.11-1. Quality of the RNA-seq reads for the 24-hr PROTAC treated sample #1.

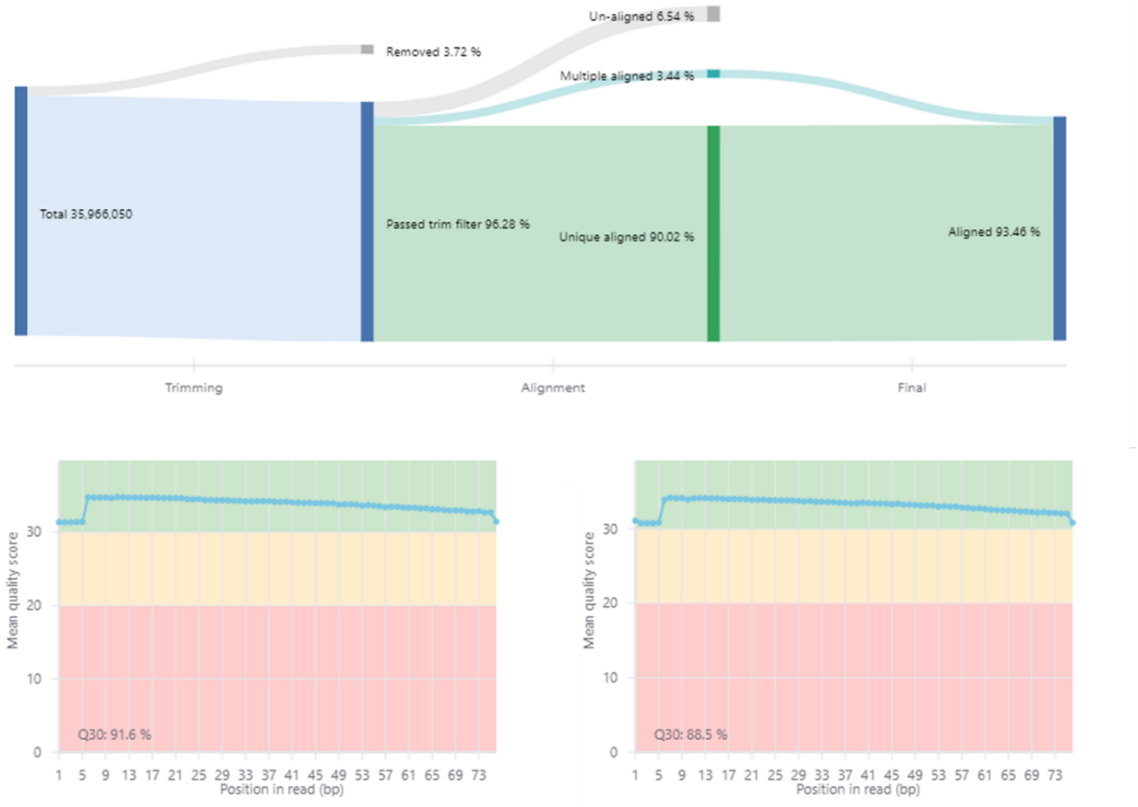

Figure 3.11-2. Quality of the RNA-seq reads for the 24-hr PROTAC treated sample #2.

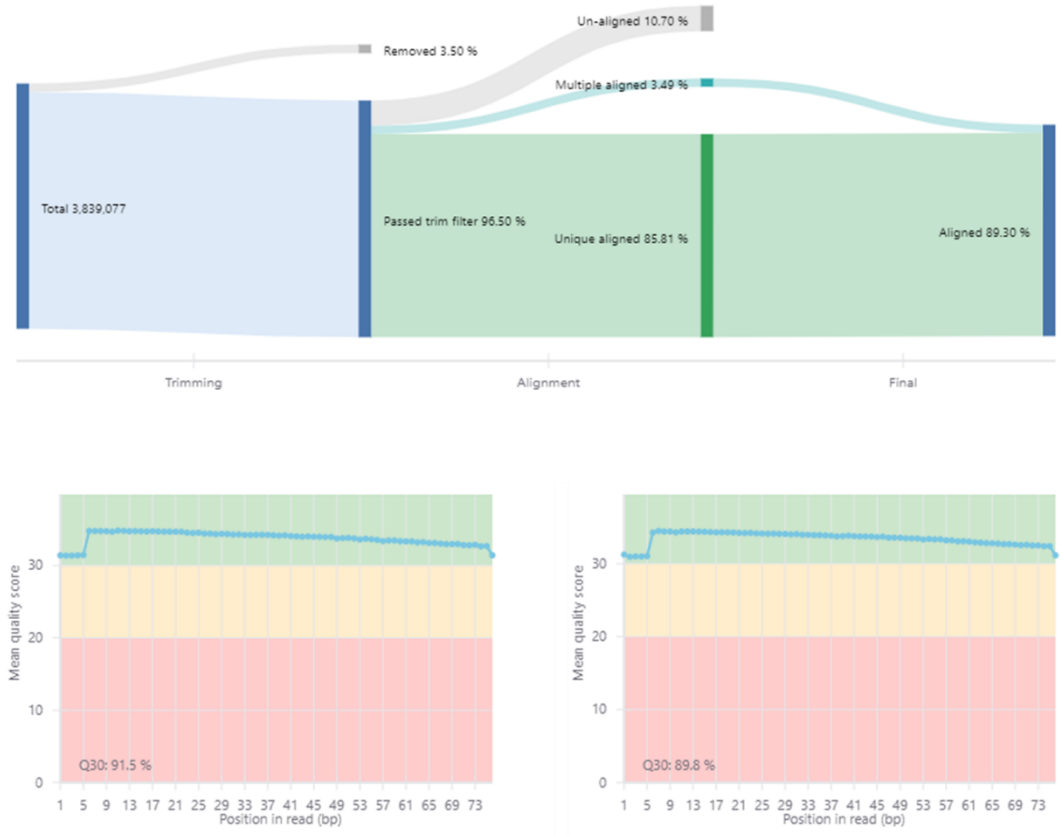

Figure 3.11-3. Quality of the RNA-seq reads for the 24-hr PROTAC treated sample #3.

Sample	Raw reads	Aligned %	Q30-1 %	Q30-2 %	mRNA %
Control #1	62543777	93.26	91.6	90.1	82.74
Control #2	47388325	90.83	91.6	88.3	82.77
Control #3	21571324	95.62	91.9	91	82.97
6-hr PROTAC #1	14423195	92.02	91.5	88.9	82.44
6-hr PROTAC #2	22280481	94.17	91.2	89.2	82.39
6-hr PROTAC #3	26975387	94.81	91.5	90.1	83.01
24-hr PROTAC #1	46211897	96.32	91.5	89.9	80.15
24-hr PROTAC #2	35966050	93.46	91.6	88.5	79.86
24-hr PROTAC #3	3839077	89.3	91.5	89.8	80.36

Table 3.1. Quality of the RNA-seq reads

Next, we scrutinized the differentially expressed genes between the samples using DESeq2.[38] Because the 6-hr samples were significantly different from the rest of the samples, we first compared the 6-hr samples to the rest. Using the criteria of $p < 0.01$ and > 2-fold changes, we found that 666 genes were upregulated and 647 genes were downregulated as the result of 6-hr PROTAC treatment (Figure 3.12). These gene expression differences were reproducible within each sample set (Figure 3.13), and they dovetailed the overall sample variances captured in the PCA analysis above.

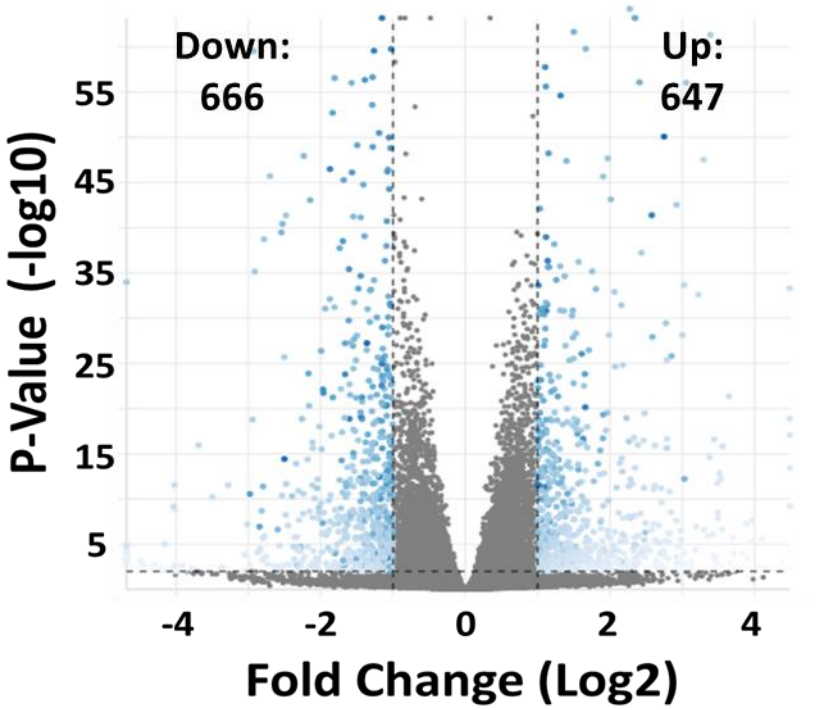

Figure 3.12. Volcano plot showing the overall landscape of the differentially expressed genes in the C3 6h treatment sample versus the control and the 24 h treatment samples. (Cutoff criteria: $p < 0.01$, fold change > 2)

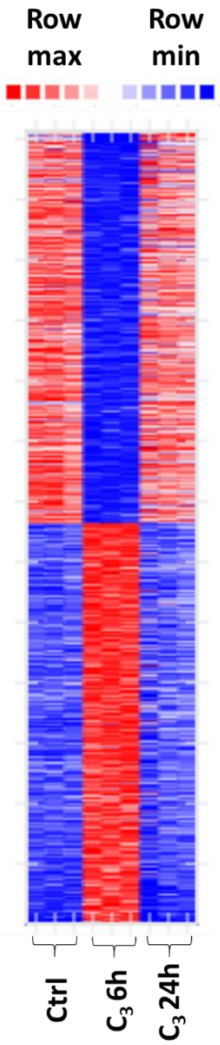

Figure 3.13. Heatmap showing the differentially expressed genes among the samples.

We then sought to compare the PROTAC-treated samples to the control. Evidently, PROTAC treatment had profound consequences on the transcriptome. In the 6h samples, 766 genes were significantly downregulated, and 761 genes were significantly upregulated compared with the control (Figure 3.8c). At 24 hours, these effects became less prominent, with 109 genes remain downregulated and 156 genes upregulated (Figure 3d). Such a time-dependent response was consistent with our observations that the PROTAC was more effective at 6 hours versus 24 hours (Figure 3.7b). More importantly, we discovered that AKT1 and AKT2 expression levels were significantly upregulated in 24h samples (Figure 3.14), which validated our previous hypothesis that the cells produced more AKT transcripts to compensate for the degraded AKT.

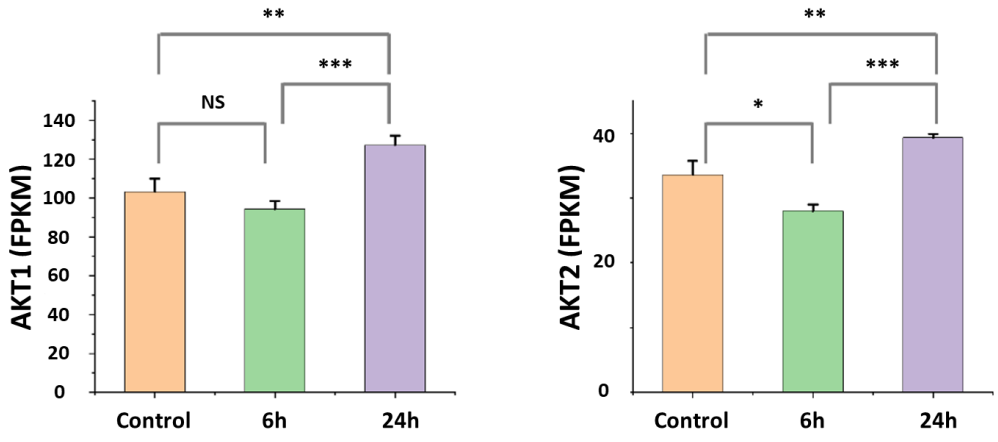

Figure 3.14. AKT1 and AKT2 mRNA levels in the samples. Student's t-test was performed to assess the statistical significance. NS: not significant. *: $p < 0.05$. **: $p < 0.01$. ***: $p < 0.001$.

To identify critically involved pathways in response to AKT degradation, we performed gene set enrichment analysis (GSEA) on the differential expression results using the hallmark gene sets.[39-40] We first compared the 6-hr PROTAC treatment sample versus the control. Nine gene sets were significantly ($p < 0.01$, $q < 0.25$) enriched in the control sample, and the mTORC1 signaling and PI3K-AKT signaling gene sets were among the top enriched ones (Figure 3.8e, Figure 3.15, Table 3.2, 3.3). Because mTORC1 is directly downstream of AKT, this result is consistent with our proposed mechanism of action, where the PROTAC caused AKT degradation and, in turn, decreased AKT signaling activities. Similarly, the unfolded protein response, glycolysis, and hypoxia gene sets were also enriched. Because these processes are known to be regulated by the AKT-mTOR signaling axis, it was expected that critical proteins in these processes would become downregulated upon AKT degradation.

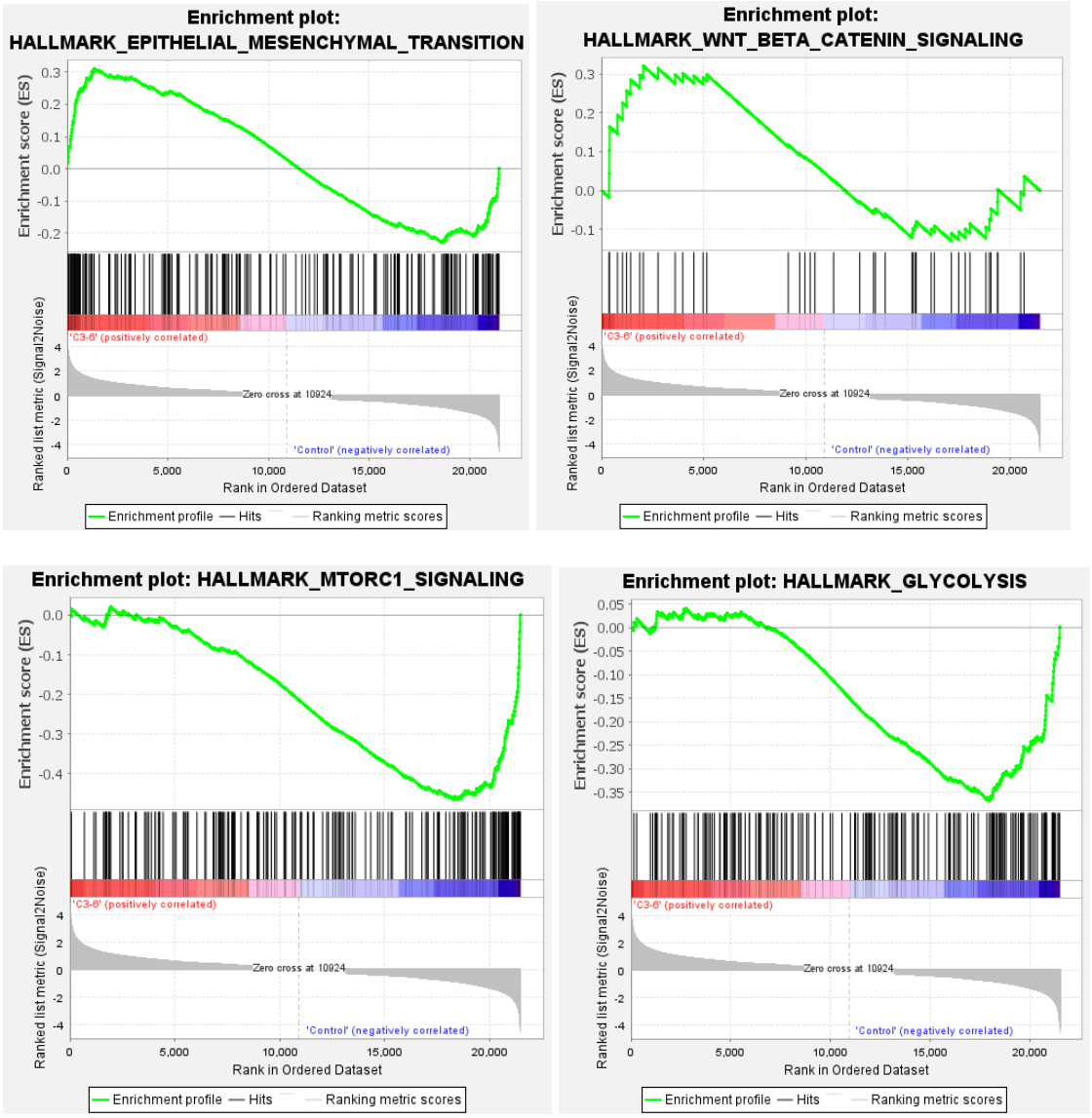

Figure 3.15. Additional enrichment plots of the C3 6h treatment versus the Control.

PATHWAY	SIZE	ES	NES	NOM p-value	FDR q-value	RANK at MAX
HALLMARK_EPITHELIAL_MEYSENCHEMCAL_TRANSITION	193	0.31	1.80	0.000	0.148	1341
HALLMARK_TGF_BETA_SIGNALING	54	0.40	1.80	0.000	0.098	2206
HALLMARK_WNT_BETA_CATENIN_SIGNALING	42	0.32	1.64	0.000	0.131	2049

Table 3.2. Gene sets enriched in the C3 6h sample vs the Control

PATHWAY	SIZE	ES	NES	NOM p-value	FDR q-value	RANK at MAX
HALLMARK_UNFOLDED_PROTEIN_RESPONSE	107	-0.28	-2.14	0.000	0.048	2299
HALLMARK_MTORC1_SIGNALING	195	-0.46	-1.95	0.000	0.048	2986
HALLMARK_GLYCOLYSIS	196	-0.37	-1.73	0.000	0.087	3540
HALLMARK_HYPOXIA	190	-0.49	-1.68	0.000	0.077	3021
HALLMARK_PI3K_AKT_MTOR_SIGNALING	102	-0.41	-1.67	0.000	0.071	4059
HALLMARK_IL6_JAK_STAT3_SIGNALING	77	-0.47	-1.61	0.000	0.085	3003
HALLMARK_ANDROGEN_RESPONSE	94	-0.43	-1.61	0.000	0.080	2815
HALLMARK_CHOLESTEROL_HOMEOSTASIS	72	-0.54	-1.59	0.000	0.076	911
HALLMARK_UV_RESPONSE_UP	150	-0.27	-1.54	0.000	0.077	2024

Table 3.3. Gene sets enriched in the Control vs. the C3 6h sample

In the 6-hr PROTAC treated sample, the EMT, TGF-β signaling, and WNT signaling gene sets were enriched. TGF-β is upstream of AKT, and its signaling can also bypass AKT and directly promote cell survival through SMAD-activated transcription.[41] Similarly, WNT signaling exhibits substantial crosstalk with the AKT signaling pathway, and they converge at the β-catenin-activated transcription process.[42-43] Therefore, it is plausible that cells might use the TGF-β and/or WNT signaling pathways to compensate for the loss of AKT signaling activities and adapt to the PROTAC-induced stress.

Comparing the 24h samples to the control samples, we found that 20 gene sets were enriched in the control sample this time. Surprisingly, the mTORC1 signaling and PI3K-AKT signaling gene sets remained enriched (Figures 3.8f, 3.16) despite our western blot results showing that AKT levels recovered at 24 hours. In addition, a panel of signaling pathways and biological processes were enriched in the control samples, including the KRAS signaling, the P53 pathway, the ROS pathway, and the apoptosis process (Table 3.4). These results proved that even though the cells adapted to the AKT degradation at 24 hours, significant changes to the overall cellular status and signaling landscape remained effective. On the other hand, the TGF-β pathway gene sets remained enriched in the 24-hr samples, and the WNT pathway was not enriched (Figure 3.8f, Table 3.5). This result suggested that the TGF-β pathway was involved throughout the time course. Taken together, these results indicated that TGF-β signaling played a more critical role in the cells adapting to AKT degradation.

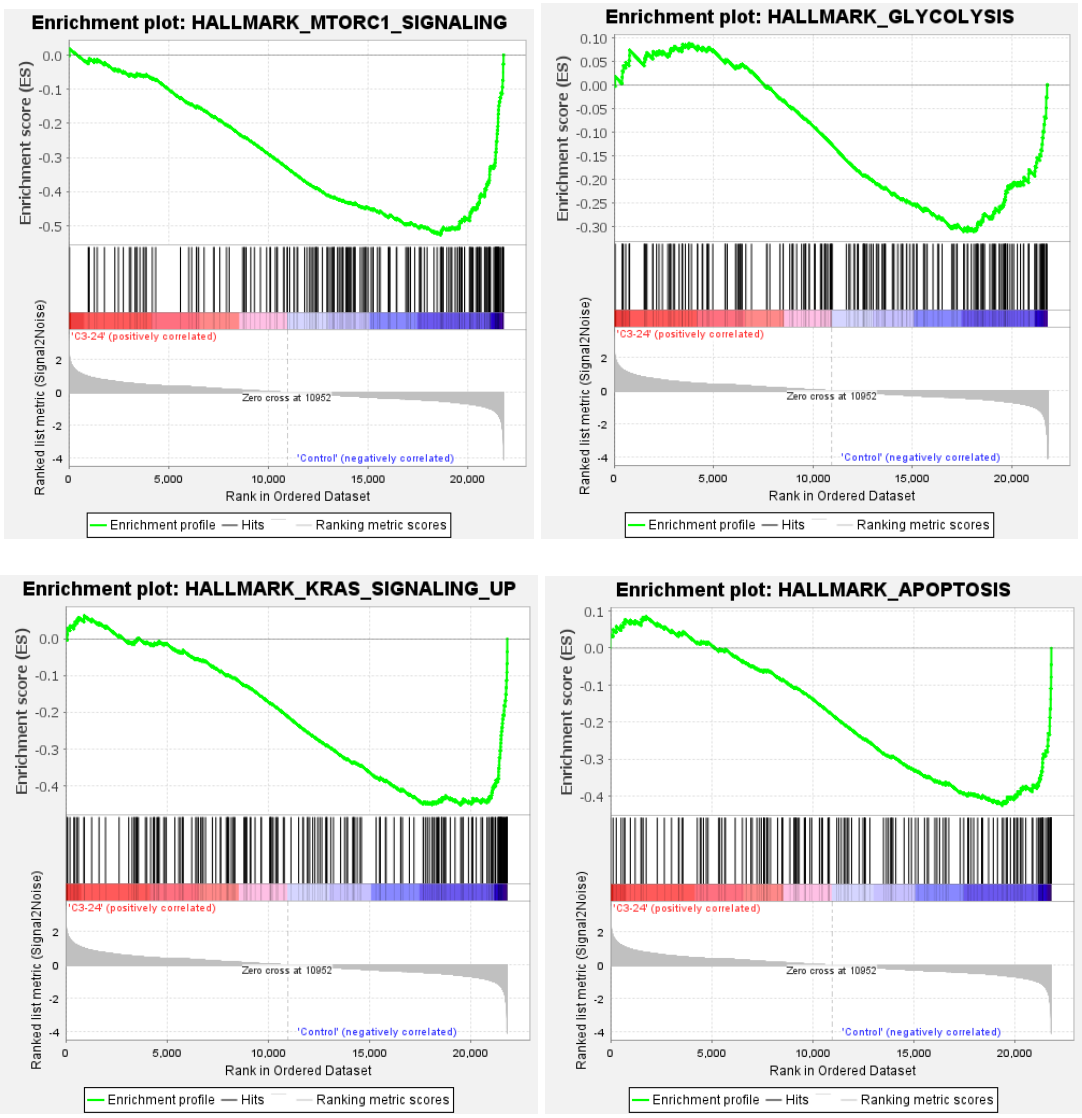

Figure 3.16. Additional enrichment plot of the C3 24h treatment versus the Control.

PATHWAY	SIZE	ES	NES	NOM p-value	FDR q-value	RANK at MAX
HALLMARK_EPITHELIA_MESENCHYMAL_TRANSITION	194	-0.34	-1.73	0.000	0.057	1790
HALLMARK_APOPTOSIS	155	-0.42	-1.68	0.000	0.080	2428
HALLMARK_UV_RESPONSE_UP	151	-0.31	-1.68	0.000	0.072	2030
HALLMARK_IL6_JAK_STAT3_SIGNALING	74	-0.50	-1.62	0.000	0.136	742
HALLMARK_TNFA_SOGNALING_VIA_NFKB	193	-0.49	-1.62	0.000	0.120	2158
HALLMARK_KRAS_SIGNALING_UP	190	-0.45	-1.61	0.000	0.109	2300
HALLMARK_INFLAMMATORY_RESPONSE	191	-0.52	-1.59	0.000	0.102	2737
HALLMARK_ANDROGEN_RESPONSE	94	-0.48	-1.58	0.000	0.096	2942
HALLMARK_PI3K_AKT_MTOR_SIGNALING	103	-0.33	-1.58	0.000	0.092	4857
HALLMARK_HYPOXIA	189	-0.41	-1.58	0.000	0.088	2163
HALLMARK_GLYCOLYSIS	194	-0.31	-1.55	0.000	0.099	4228
HALLMARK_UV_RESPONSE_DN	136	-0.38	-1.53	0.000	0.100	4878
HALLMARK_UNFOLDED_PROTEIN_RESPONSE	107	-0.53	-1.47	0.000	0.101	3642
HALLMARK_P53_PATHWAY	190	-0.25	-1.45	0.000	0.106	2500
HALLMARK_INTERFERON_GAMMA_RESPONSE	193	-0.36	-1.45	0.000	0.103	2701
HALLMARK_MTORC1_SIGNALING	195	-0.53	-1.44	0.000	0.100	3169
HALLMARK_REACTIVE_OXYGEN_SPECIES_PATHWAY	47	-0.40	-1.41	0.000	0.117	4107
HALLMARK_COMLEMENT	193	-0.39	-1.39	0.000	0.124	3435
HALLMARK_PROTEIN_SECRETION	94	-0.56	-1.39	0.000	0.120	5441
HALLMARK_HEME_METABOLISM	187	-0.27	-1.37	0.000	0.126	3066

Table 3.4. Gene sets enriched in the Control vs the C3 24h sample

PATHWAY	SIZE	ES	NES	NOM p-value	FDR q-value	RANK at MAX
HALLMARK_TGF_BETA_SIGNALING	54	0.36	1.71	0.000	0.079	1651

Table 3.5. Gene sets enriched in the C3 24h sample vs the Control

Built upon the RNA-seq results, we hypothesized that inhibiting the TGF-β pathway could synergize with AKT degradation and inhibit cell proliferation. To test this hypothesis, we treated U87 cells with the C_3 PROTAC (5 μM), SIS3 HCl (TGF-β/Smad3 inhibitor, 1 μM),[44] and a combination of the two (Figure 3.17a). As shown in Figure 3.17b, the combination synergistically inhibited cell proliferation. To quantitatively evaluate this synergy, we treated the cells with various concentration combinations of the two drugs and calculated the synergy score using the BLISS definition of independence. As shown in Figure 3.17c, a strong synergy between the two drugs existed across a wide range of concentrations. This result supported our hypothesis that the cells adapted to AKT degradation by activating the TGF-β pathway. It further proved that inhibiting the TGF-β pathway could improve the therapeutic effects of AKT degradation.

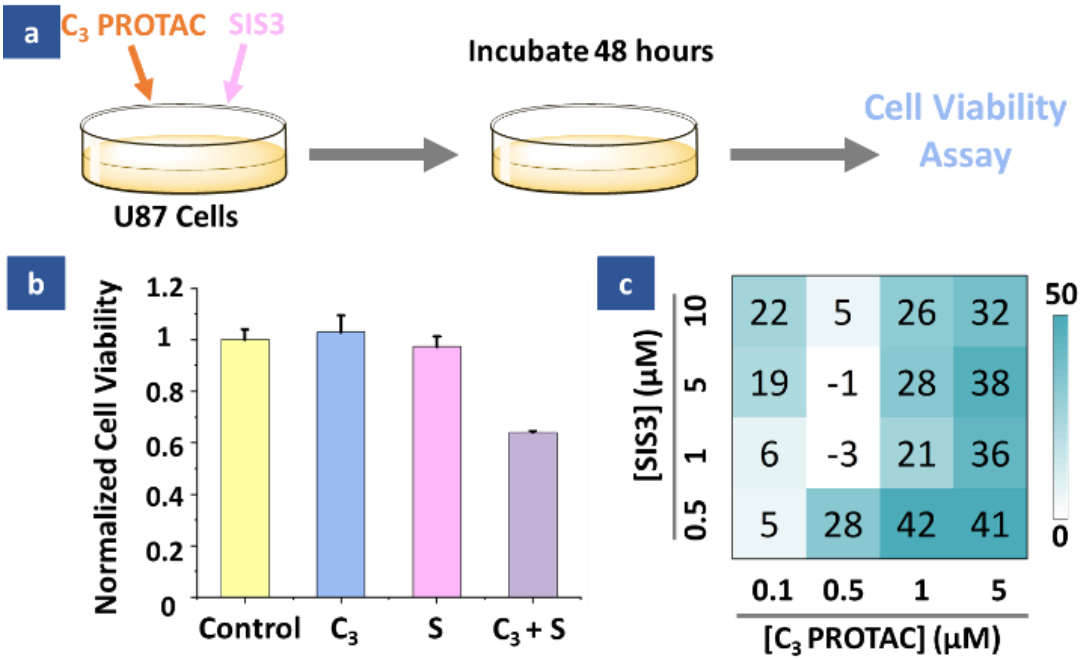

Figure 3.17. (a) Workflow of the synergy experiment. (b) Synergistic effects observed when U87 were treated with 5 μM of the C_3 PROTAC (C_3) and 1 μM of SIS3 (S). (c) Synergy scores calculated using the BLISS method.

3.4 Conclusion

In conclusion, we developed AKT-targeting PROTACs by conjugating an AKT-binding cyclic peptide to pomalidomide through a series of linkers. Using U87 cells as a model system, we demonstrated that our PROTACs were able to degrade AKT. We also discovered that the cells could quickly adapt to AKT degradation by activating the TGF-β pathway as well as increasing the AKT transcript levels. We found that inhibiting the TGF-β pathway could synergize with AKT degradation to inhibit cell proliferation.

3.5 References

1. Manning, B. D.; Cantley, L. C., AKT/PKB Signaling: Navigating Downstream. *Cell* **2007,** *129* (7), 1261-1274.

2. Manning, B. D.; Toker, A., AKT/PKB Signaling: Navigating the Network. *Cell* **2017,** *169* (3), 381-405.

3. Landel, I.; Quambusch, L.; Depta, L.; Rauh, D., Spotlight on AKT: Current Therapeutic Challenges. *ACS Med Chem Lett* **2020,** *11* (3), 225-227.

4. Mundi, P. S.; Sachdev, J.; McCourt, C.; Kalinsky, K., AKT in cancer: new molecular insights and advances in drug development. *Br J Clin Pharmacol* **2016,** *82* (4), 943-956.

5. Gao, Y.; Moten, A.; Lin, H. K., Akt: a new activation mechanism. *Cell Res* **2014,** *24* (7), 785-6.

6. Bellacosa A, K. C., Di Cristofano A, Testa JR. . Activation of AKT kinases in cancer: implications for therapeutic targeting. *Adv Cancer Res.* **2005,** *94*.

7. You, I.; Erickson, E. C.; Donovan, K. A.; Eleuteri, N. A.; Fischer, E. S.; Gray, N. S.; Toker, A., Discovery of an AKT Degrader with Prolonged Inhibition of Downstream Signaling. *Cell Chem Biol* **2020,** *27* (1), 66-73 e7.

8. Manning, B. D., Balancing Akt with S6K: implications for both metabolic diseases and tumorigenesis. *The Journal of cell biology* **2004,** *167* (3), 399-403.

9. Bossi, P.; Resteghini, C.; Paielli, N.; Licitra, L.; Pilotti, S.; Perrone, F., Prognostic and predictive value of EGFR in head and neck squamous cell carcinoma. *Oncotarget* **2016,** *7* (45), 74362-74379.

10. da Cunha Santos, G.; Shepherd, F. A.; Tsao, M. S., EGFR Mutations and Lung Cancer. *Annual Review of Pathology: Mechanisms of Disease* **2011,** *6* (1), 49-69.

11. Misale, S.; Yaeger, R.; Hobor, S.; Scala, E.; Janakiraman, M.; Liska, D.; Valtorta, E.; Schiavo, R.; Buscarino, M.; Siravegna, G.; Bencardino, K.; Cercek, A.; Chen, C.-T.; Veronese, S.; Zanon, C.; Sartore-Bianchi, A.; Gambacorta, M.; Gallicchio, M.; Vakiani, E.; Boscaro, V.; Medico, E.; Weiser, M.; Siena, S.; Di Nicolantonio, F.; Solit, D.; Bardelli, A., Emergence of KRAS mutations and acquired resistance to anti-EGFR therapy in colorectal cancer. *Nature* **2012,** *486* (7404), 532-536.

12. Mayer, I. A.; Arteaga, C. L., The PI3K/AKT Pathway as a Target for Cancer Treatment. *Annual Review of Medicine* **2016,** *67* (1), 11-28.

13. Karakas, B.; Bachman, K. E.; Park, B. H., Mutation of the PIK3CA oncogene in human cancers. *British journal of cancer* **2006,** *94* (4), 455-459.

14. Wang, S. I.; Puc, J.; Li, J.; Bruce, J. N.; Cairns, P.; Sidransky, D.; Parsons, R., Somatic Mutations of PTEN in Glioblastoma Multiforme. *Cancer Research* **1997,** *57* (19), 4183.

15. Jamaspishvili, T.; Berman, D. M.; Ross, A. E.; Scher, H. I.; De Marzo, A. M.; Squire, J. A.; Lotan, T. L., Clinical implications of PTEN loss in prostate cancer. *Nature Reviews Urology* **2018,** *15*, 222.

16. Dienstmann, R.; Rodon, J.; Serra, V.; Tabernero, J., Picking the Point of Inhibition: A Comparative Review of PI3K/AKT/mTOR Pathway Inhibitors. *Molecular Cancer Therapeutics* **2014,** *13* (5), 1021.

17. Nitulescu, G. M.; Margina, D.; Juzenas, P.; Peng, Q.; Olaru, O. T.; Saloustros, E.; Fenga, C.; Spandidos, D. A.; Libra, M.; Tsatsakis, A. M., Akt inhibitors in cancer treatment: The long journey from drug discovery to clinical use (Review). *International journal of oncology* **2015,** *48* (3), 869-885.

18. Jansen, V. M.; Mayer, I. A.; Arteaga, C. L., Is There a Future for AKT Inhibitors in the Treatment of Cancer? *Clinical Cancer Research* **2016,** *22* (11), 2599.

19. Banerji, U. D., Emma Jane; Perez-Fidalgo, Jose Alejandro; Batist, Gerald; Bedard, Philippe L.; You, Benoit; Westin, Shannon Neville; Kabos, Peter; Davies, Barry; Elvin, Paul; Lawrence, Peter; Yates, James W T; Ambrose, Helen; Rugman, Paul; Foxley, Andrew; Salim, Shaista; Casson, Ed; Lindemann, Justin P O; Schellens, Jan H.

M., A pharmacokinetically (PK) and pharmacodynamically (PD) driven phase I trial of the pan-AKT inhibitor AZD5363 with expansion cohorts in PIK3CA mutant breast and gynecological cancers. *J Clin Oncol* **2015,** *33* (2500).

20. Janku, F.; Yap, T. A.; Meric-Bernstam, F., Targeting the PI3K pathway in cancer: are we making headway? *Nat Rev Clin Oncol* **2018,** *15* (5), 273-291.

21. Xing, Y.; Lin, N. U.; Maurer, M. A.; Chen, H.; Mahvash, A.; Sahin, A.; Akcakanat, A.; Li, Y.; Abramson, V.; Litton, J.; Chavez-MacGregor, M.; Valero, V.; Piha-Paul, S. A.; Hong, D.; Do, K.-A.; Tarco, E.; Riall, D.; Eterovic, A. K.; Wulf, G. M.; Cantley, L. C.; Mills, G. B.; Doyle, L. A.; Winer, E.; Hortobagyi, G. N.; Gonzalez-Angulo, A. M.; Meric-Bernstam, F., Phase II trial of AKT inhibitor MK-2206 in patients with advanced breast cancer who have tumors with PIK3CA or AKT mutations, and/or PTEN loss/PTEN mutation. *Breast Cancer Research* **2019,** *21* (1), 78.

22. Dale, B.; Cheng, M.; Park, K. S.; Kaniskan, H. U.; Xiong, Y.; Jin, J., Advancing targeted protein degradation for cancer therapy. *Nat Rev Cancer* **2021**.

23. Khan, S.; He, Y.; Zhang, X.; Yuan, Y.; Pu, S.; Kong, Q.; Zheng, G.; Zhou, D., PROteolysis TArgeting Chimeras (PROTACs) as emerging anticancer therapeutics. *Oncogene* **2020,** *39* (26), 4909-4924.

24. Konstantinidou, M.; Li, J.; Zhang, B.; Wang, Z.; Shaabani, S.; Ter Brake, F.; Essa, K.; Domling, A., PROTACs- a game-changing technology. *Expert Opin Drug Discov* **2019,** *14* (12), 1255-1268.

25. Nalawansha, D. A.; Crews, C. M., PROTACs: An Emerging Therapeutic Modality in Precision Medicine. *Cell Chem Biol* **2020,** *27* (8), 998-1014.

26. Henning, R. K.; Varghese, J. O.; Das, S.; Nag, A.; Tang, G.; Tang, K.; Sutherland, A. M.; Heath, J. R., Degradation of Akt using protein-catalyzed capture agents. *Journal of Peptide Science* **2016,** *22* (4), 196-200.

27. Guo, Y.; Jin, Y.; Qu, B.; Zhang, Y.; Che, J.; Dong, X., An updated patent review of Akt inhibitors (2016-present). *Expert Opin Ther Pat* **2021**, 1-13.

28. Zeng, S.; Huang, W.; Zheng, X.; Liyan, C.; Zhang, Z.; Wang, J.; Shen, Z., Proteolysis targeting chimera (PROTAC) in drug discovery paradigm: Recent progress and future challenges. *Eur J Med Chem* **2021,** *210*, 112981.

29. Manzella, G.; Schreck, L. D.; Breunis, W. B.; Molenaar, J.; Merks, H.; Barr, F. G.; Sun, W.; Römmele, M.; Zhang, L.; Tchinda, J.; Ngo, Q. A.; Bode, P.; Delattre, O.; Surdez, D.; Rekhi, B.; Niggli, F. K.; Schäfer, B. W.; Wachtel, M., Phenotypic profiling

with a living biobank of primary rhabdomyosarcoma unravels disease heterogeneity and AKT sensitivity. *Nature Communications* **2020,** *11* (1), 4629.

30. Grabiner, B. C.; Nardi, V.; Birsoy, K.; Possemato, R.; Shen, K.; Sinha, S.; Jordan, A.; Beck, A. H.; Sabatini, D. M., A Diverse Array of Cancer-Associated MTOR Mutations Are Hyperactivating and Can Predict Rapamycin Sensitivity. *Cancer Discovery* **2014,** *4* (5), 554.

31. Shao, S.; Li, Z.; Cheng, H.; Wang, S.; Perkins, N. G.; Sarkar, P.; Wei, W.; Xue, M., A Chemical Approach for Profiling Intracellular AKT Signaling Dynamics from Single Cells. *Journal of the American Chemical Society* **2018,** *140* (42), 13586-13589.

32. Schneider, M.; Radoux, C. J.; Hercules, A.; Ochoa, D.; Dunham, I.; Zalmas, L.-P.; Hessler, G.; Ruf, S.; Shanmugasundaram, V.; Hann, M. M.; Thomas, P. J.; Queisser, M. A.; Benowitz, A. B.; Brown, K.; Leach, A. R., The PROTACtable genome. *Nature Reviews Drug Discovery* **2021**.

33. Furnari, F. B.; Lin, H.; Huang, H. J. S.; Cavenee, W. K., Growth suppression of glioma cells by PTEN requires a functional phosphatase catalytic domain. *Proceedings of the National Academy of Sciences* **1997,** *94* (23), 12479.

34. Guo, D.; Prins, R. M.; Dang, J.; Kuga, D.; Iwanami, A.; Soto, H.; Lin, K. Y.; Huang, T. T.; Akhavan, D.; Hock, M. B.; Zhu, S.; Kofman, A. A.; Bensinger, S. J.; Yong, W. H.; Vinters, H. V.; Horvath, S.; Watson, A. D.; Kuhn, J. G.; Robins, H. I.; Mehta, M. P.; Wen, P. Y.; DeAngelis, L. M.; Prados, M. D.; Mellinghoff, I. K.; Cloughesy, T. F.; Mischel, P. S., EGFR Signaling Through an Akt-SREBP-1–Dependent, Rapamycin-Resistant Pathway Sensitizes Glioblastomas to Antilipogenic Therapy. *Science Signaling* **2009,** *2* (101), ra82.

35. Dobin, A.; Davis, C. A.; Schlesinger, F.; Drenkow, J.; Zaleski, C.; Jha, S.; Batut, P.; Chaisson, M.; Gingeras, T. R., STAR: ultrafast universal RNA-seq aligner. *Bioinformatics* **2012,** *29* (1), 15-21.

36. Chen, S.; Zhou, Y.; Chen, Y.; Gu, J., fastp: an ultra-fast all-in-one FASTQ preprocessor. *Bioinformatics* **2018,** *34* (17), i884-i890.

37. Liao, Y.; Smyth, G. K.; Shi, W., featureCounts: an efficient general purpose program for assigning sequence reads to genomic features. *Bioinformatics* **2014,** *30* (7), 923-930.

38. Love, M. I.; Huber, W.; Anders, S., Moderated estimation of fold change and dispersion for RNA-seq data with DESeq2. *Genome Biology* **2014,** *15* (12), 550.

39. Subramanian, A.; Tamayo, P.; Mootha, V. K.; Mukherjee, S.; Ebert, B. L.; Gillette, M. A.; Paulovich, A.; Pomeroy, S. L.; Golub, T. R.; Lander, E. S.; Mesirov, J. P., Gene set enrichment analysis: A knowledge-based approach for interpreting genome-wide expression profiles. *Proceedings of the National Academy of Sciences* **2005,** *102* (43), 15545.

40. Liberzon, A.; Birger, C.; Thorvaldsdóttir, H.; Ghandi, M.; Mesirov, Jill P.; Tamayo, P., The Molecular Signatures Database Hallmark Gene Set Collection. *Cell Systems* **2015,** *1* (6), 417-425.

41. Zhang, L.; Zhou, F.; ten Dijke, P., Signaling interplay between transforming growth factor-β receptor and PI3K/AKT pathways in cancer. *Trends in Biochemical Sciences* **2013,** *38* (12), 612-620.

42. Zhan, T.; Rindtorff, N.; Boutros, M., Wnt signaling in cancer. *Oncogene* **2017,** *36* (11), 1461-1473.

43. Prossomariti, A.; Piazzi, G.; Alquati, C.; Ricciardiello, L., Are Wnt/β-Catenin and PI3K/AKT/mTORC1 Distinct Pathways in Colorectal Cancer? *Cellular and Molecular Gastroenterology and Hepatology* **2020,** *10* (3), 491-506.

44. Jinnin, M.; Ihn, H.; Tamaki, K., Characterization of SIS3, a Novel Specific Inhibitor of Smad3, and Its Effect on Transforming Growth Factor-β1-Induced Extracellular Matrix Expression. *Molecular Pharmacology* **2006,** *69* (2), 597.

Chapter 4: Perturbation of cell migration using a cyclic peptide and inhibitors

4.1 Introduction

Glioblastoma is considered one of the most aggressive cancer types. To date, there is no therapeutic success against glioblastoma, which is partly due to its extreme invasiveness.[1] Glioblastomas are highly heterogeneous, and there remains a lack of understanding about the specific differences between cells present within the same glioblastoma tumor.[2] In general, there is little clinical success in targeting cancer cell migration, invasion, or metastasis due to the complicated mechanisms which cancer cells utilize to adapt and survive. It has been reasoned that cancer cells can reprogram their metabolism in order to adapt to microenvironmental changes and aid in migration.[3] For example, cancer cells can adapt to an oxygen-rich/poor environment by preferentially utilizing glycolysis (known as the Warburg effect) to uptake more glucose in comparison to healthy cells. It has been reported that glycolysis plays a significant role in cell migration. [3-4] This is certainly the case for glioblastomas since glucose is a major metabolite for aiding in malignancy and progression.[5] Glutamine addiction has also been discovered to show influence on cell motility and invasion in some cancers as it provides the basis for ATP production in the TCA cycle.[3, 6] A connection between elevated glucose uptake and increased glutamine metabolism has been suggested, thus possibly promoting the ability of cells to migrate.[3] In response to mTOR-targeted therapy, glioblastomas appear to compensate for this stress by elevating glutamine uptake.[6] A final example (of many) which aids in cell migration/metastasis is the degradation of extracellular matrix through the activation of matrix metalloproteinases (MMP) by cancer

cells.[3] Glioblastomas are known to have a very hypoxic environment, which leads to the upregulation of MMP2 expression, thus aiding in tumor invasion. [7] From these findings, we have a very generalized idea of the connection between cell migration methods and metabolism. The details of what/how critical metabolites generally affect the overall population of cancer cells is currently underexplored.

A possible method to aid in stopping cell migration is the use of metabolic inhibitors. STF 31, a glucose transporter1 (GLUT 1) specific inhibitor, prevents glucose uptake and has shown antitumor effects. It has also been shown to work synergistically with chemotherapeutic agents.[8] V-9302, an antagonist of the alanine-serine-cysteine transporter 2 (ASCT 2), prevents the uptake of glutamine and has shown antitumor efficacy as well. [9] Our own group has also designed a cyclic peptide which is able to bind to proMMP2 at the nM level and ultimately prevent MMP2 activation.[10] These examples of small molecules certainly show promise in negatively affecting cancer cell migration/progression. However, having a clear understanding of how such inhibitors globally affect tumors at the single-cell level remains an open challenge, certainly in the case of glioblastoma cells.

In this study, we attempt to assess the heterogeneity of cell mobility in U87 glioblastoma cells. The goal is to determine how single-cell mobility is affected by critical metabolites (such as glutamine, glutamic acid, and glucose). By monitoring the migration of cells at the single-cell level via imaging, we were able to identify which metabolites played a significant role in U87 cell migration; this was done through software calculation of the speed of single cells. In addition, we scrutinized how MMP2

inhibition and metabolic inhibition can also affect cell movement. It was apparent that the overall movement of the cells was certainly limited by the introduction of the inhibitors. Lastly, we explored the potential of combining our peptide-based inhibitor and other metabolic inhibitors in slowing down cell migration. Interestingly, each inhibitor negatively affected the cell movement, but a combination of the inhibitors had the opposite effect. There is currently a very surface-level understanding of cacner cell mobility behavior and patterns. However, our study highlights the importance of evaluating the heterogeneity between single cells and their migration patterns in response to their environmental changes.

4.2 Experimental

The human glioblastoma U87 cell line was purchased from ATCC (the American Type Culture Collection). Dulbecco's Modified Eagle Medium (DMEM), heat-inactivated Fetal Bovine Serum (FBS), and 0.25% Trypsin (with 2.21mM EDTA) were all purchased from Corning Cellgro (Corning, NY). Poly-D Lysine, Basal Medium Eagle (BME) (from GIBCO), Dimethyl Sulfoxide (DMSO) and HPLC grade Acetonitrile (ACN) were purchased from Thermo Fisher Scientific (Waltham,MA). L-ascorbic acid was purchased from Chem Impex International l Inc. (Wood Dale, IL). The Fmoc protected amino acids were purchased from Anaspec. Rink amide MBHA resin (0.67 mmol/g) was purchased from Aapptec (Louisville, KY). L-glutamine, L-glutamic acid, sodium pyruvate, resazurin, Penicillin-Streptomycin (PS), and Copper (I) Iodide were purchased from Sigma Aldrich Inc. (St. Louis, MO). Triisopropylsilane (TIPS) was purchased from TCI

(Tokyo, Japan). Trifluoroacetic acid (TFA) was purchased from Oakwood Chemical (Estill, SC). STF 31 was purchased from TOCRIS a biotechne brand (Minneapolis, MN). V-9302 was purchased from Selleck Chemicals (Selleck Drain, MI).

Peptide Synthesis

The peptide sequence, cy(WPHPY) (N to C terminus), was synthesized on Rink Amide MBHA resin using standard Fmoc SPPS on a CSBio CS336S peptide synthesizer (Menlo Park, CA). The peptide's last amino acid retained the Fmoc protecting group during the next steps. A copper-catalyzed click reaction was done to cyclize the peptide. 2.5 equivalents of CuI and 5.0 equivalents of L-ascorbic acid were dissolved in a solution of DMY containing 20% 2,6 lutidine. This solution was added to the peptide resin and mixed at RT overnight. Then a 5% w/v sodium diethyldithiocarbamate and 5% v/v DIEA in DMF solution was used to wash the resin in order to remove any excess copper. The resin was then deprotected using 20% piperidine in DMF 3 times for 5 minutes each. The resin was then rinsed three times each with DMF, methanol, and DCM in order. The resin was dried, and the peptide was cleaved from the resin using a 95% TFA, 2.5% H2O, 2.5% TIPS solution for 2 hours at RT. The peptide was then purified using a reversed-phase preparative C18 column within an RP-HPLC (using a Dionex UltiMate 3000 UHPLC from Thermo Fisher Scientific). The elution gradient was 0-100% ACN/H2O (containing 0.1% TFA). Matrix-assisted laser desorption ionization MALDI TOF/TOF (AB Sciex) was used to identify the purest product fractions, which were later evaporated and lyophilized.

Cell culture

DMEM containing 10% FBS and 1% PS was used for the general culture of U87 cells. The cells were incubated in a Hera Cell incubator (BioSurplus) set to have 5% CO_2 at a temperature of 37°C. BME with 1% PS was used for further cell treatment. To evaluate which nutrients affect cell migration, U87 cells were treated with the following: lone BME was used as a control, BME with D-Glucose (4,500 mg/L), BME with sodium pyruvate (110 mg/L), BME with L-glutamine (584 mg/mL), BME with L-glutamic acid (584 mg/L), BME with D-Glucose and L-glutamine, BME with D-Glucose and L-glutamic acid, and BME with D-Glucose and sodium pyruvate (same concentrations). The ingredient concentrations are based on the concentrations found in traditional DMEM.

Cell treatment under nutrient-poor conditions and Imaging

All petri dishes/96-well plates were pre-treated with a 50 µg/mL solution of PolyDLysine for 1 hour at RT. Afterwards, the dish was washed 3 times with sterile water and allowed to air dry for 2 hours. For imaging experiments, ~100-200k cells in DMEM were seeded within a 35mm petri dish and allowed to settle overnight. The next day, the media was replaced with BME media containing one or more of the extra ingredients mentioned above. The dish was immediately placed under the microscope in the incubator and imaged using an EzScope 101

Live Cell Imaging System (Blue-Ray Biotech Corp., Taiwan) for 12 hours. The obtained images were then processed using the ImageJ FIJI software with the Trackmate plugin.[11]

Cell treatment with Inhibitors and Imaging

In a similar manner as above, 50-80k cells were seeded in a pre-treated 35 mm petri dish this time in DMEM containing 10% FBS and 1%PS. The next day the following inhibitors were added to meet the final concentrations to the cells: 0.1 μM cy(WPHPY), 1 μM STF 31, 10 μM V-9302, 0.1 μM cy(WPHPY) + 1 μM STF 31, or 0.1 μM cy(WPHPY) + 10 μM V-9302. The cells were then incubated and imaged for 12 hours. The images were again processed with Trackmate.

4.3 Results and Discussion

To evaluate which critical metabolites affect the heterogeneity of cell mobility, we cultured the cells in multiple dishes containing BME, a very basic and nutrient-poor media. We then added various nutrients to the separate dishes. The nutrients we chose to add to BME were D-Glucose, L-Glutamic Acid, L-Glutamine, and Sodium Pyruvate. We also combined D-Glucose with the other three ingredients as well. The cells were then incubated and imaged for 12 hours (Figure 4.1a). The obtained images were then processed using ImageJ tracking software, which provided analysis of single cells. The results obtained were the maximum, mean, standard, minimum, and median speeds of each individual cell distributed over a dataset. As shown in Figure 4.1b, there are high-speed and low-speed populations that were identified in each treatment. Interestingly, the metabolites affected the distribution of the two populations differently. Glucose and glutamine had the largest effect in driving cell mobility as there is a larger high-speed population compared with the low-speed population. This is consistent with the

characteristic of U87 cells, which are highly dependent on glutamine and glucose in their metabolic processes. What was more interesting was that combining glucose and glutamine would increase the low-speed population, but not the high-speed population; despite how the overall speed was increased in comparison to the other metabolite combinations. This result emphasizes overall complexity that exists within the cell migration process and provides motivation to further investigate the single-cell migration dynamics. The other metabolites (glutamic acid and sodium pyruvate) also showed more low-speed populations than high-speed populations. When looking at the mean and standard deviation speeds (Figures 4.1c-d), they are consistent with the results obtained from the maximum speed of the cells under each treatment. However, the minimum and median speeds do not show much difference (Figures 4.1e-f). A comparison of the change in the distrubtion of a representative single cell's migration behavior (under the control condition or the glucose/glutamine condition) is illustrated and summarized in Figure 4.2. When comparing the control to the the glucose/glutamine treatment, it was observed that the median speed remained unchanged, while the mean and standard deviation speeds were significantly increased. This change in parameters led to the distribution of the cell's movement to become positively skewed. In addition, the overall maximum speed of the cell was increased and the minimum speed was unchanged. Taken together, these results indicate that glucose and glutamine increased the cellular heterogeneity in cell mobility by increasing the percentage of cells that achieve high speed.

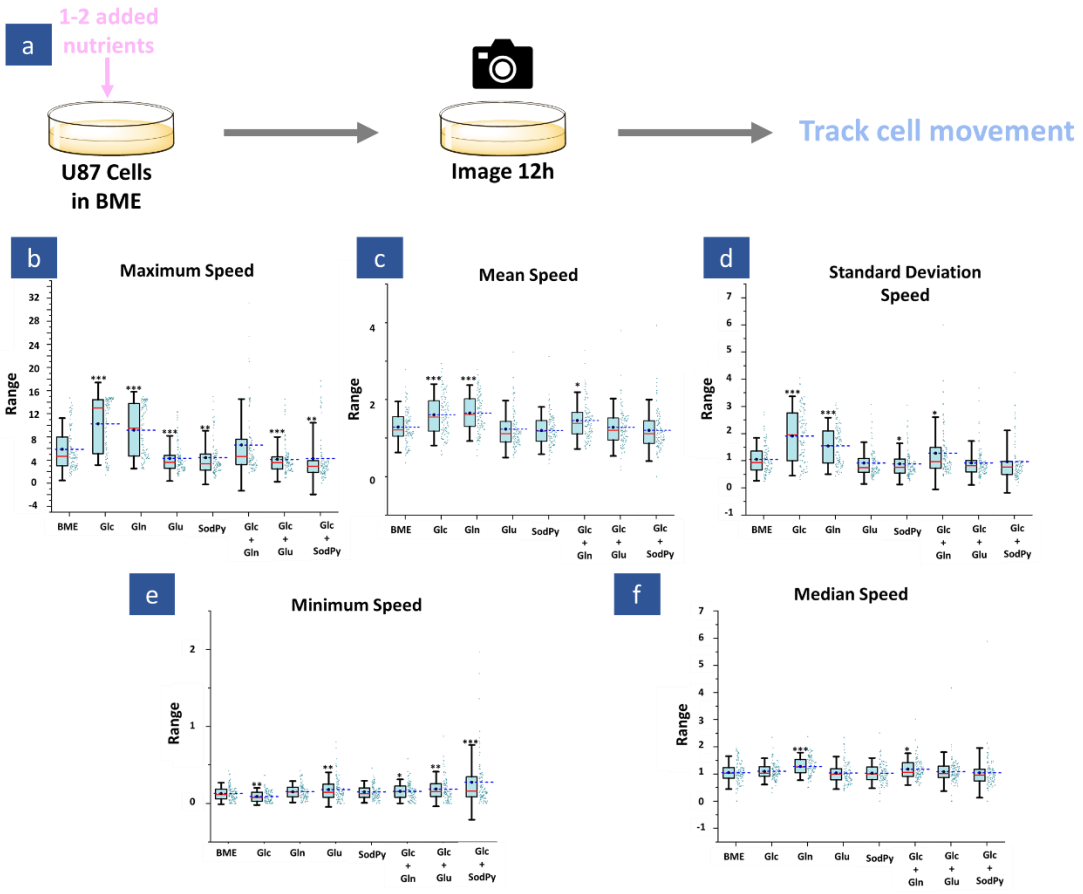

Figure 4.1. (a) Experimental flow for treating U87 cells and imaging. (b) Maximum speed distribution of single cells from each treatment. (c) Mean speed distributions from each treatment. (d)The standard deviation speed distributions. (e) The minimum speed distributions. (f) The median speed distributions. The blue dotted line in each bar represents the mean of each data set and the red line represents the median. Student's t-test was performed to assess the statistical significance. *: $p < 0.05$. **: $p < 0.01$. ***: $p < 0.001$. Abbreviations: Glc = glucose, Gln = glutamine, SodPy = sodium pyruvate

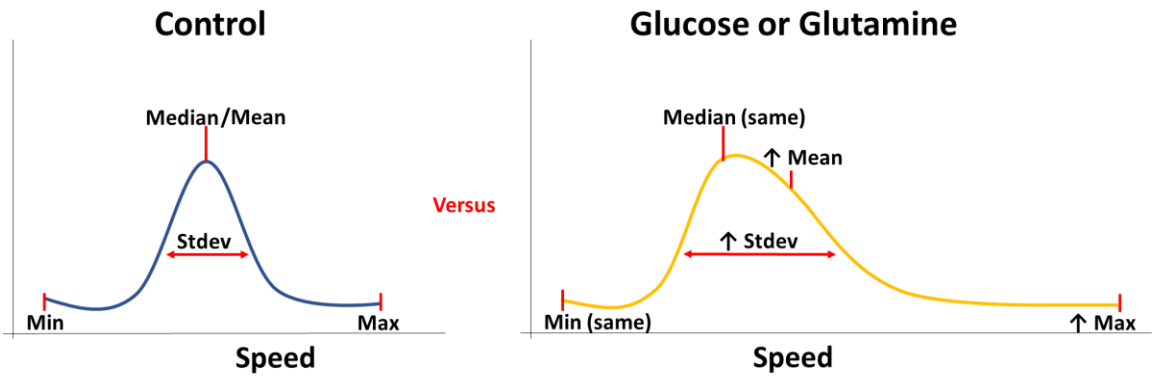

Figure 4.2. An example illustration of the differences observed between one representative single cell from the control treatment in versus the treatment of the cell with either glucose or glutamine. From the data, it was observed that the metabolite-treated cells has a positively skewed distribution. It is shown that the mean, standard deviation (stdev), and maximum speeds are increased (↑) due to the treatment from these two essential metabolites, while the median and minimum speeds remained similar.

We then sought to investigate how the introduction of inhibitors would affect the distribution of cell movement at the single-cell level. A similar procedure was done as previously mentioned (Figure 4.3a); however, this time the U87 cells were cultured in full DMEM which contained one or two inhibitors. We introduced our cyclic peptide, cy(WPHPY), which is an inhibitor of MMP2 activation. An interesting result obtained from our lab's previous study showed that even after treating a WM-115 cancer cell line with cy(WPHPY) at the low micromolar level, some cells were still able to migrate through in a trans-well assay experiment.[10] Intrigued by this past result, we sought to determine whether the the speed/migration pattern of all cells can be negatively affected by cy(WPHPY) or the inhibition by this peptide only affects a portion of cells while others retain their speed/mobility. These ideas pushed us to further investigate how inhibitors can impact cell movement at the single-cell level. Thus we decided to include the treatment of the U87 cells with two other inhibitors involved in metabolic uptake: STF 31 (which prevents glucose uptake) and V-9302 (which prevents glutamine uptake). As shown in Figure 4.3b-c, the maximum speed decreased when treated with individual inhibitors, and there is also a smaller standard deviation. The minimum speeds also seem to be slightly affected depending on the treatment, as shown in Figure 4.3d. However, this time the median and the mean remained unchanged and were consistent with each other (Figure 4.3e-f). As illustrated in our example in Figure 4.4, the inhibitors' effects on the response of single cells certainly narrowed the overall distribution. The difference between the results of Figures 4.1 and 4.2 show there or no two high/low speed populations of cells. Therefore, the majority of the single cells were negatively affected

by these lone inhibitors. However, the observance of outliers again highlight the existence of heterogeneity between cells as they can still migrate. The differences in the overall results concerning the lone inhibitor treatment suggest that MMP2 inhibition and decreasing glucose uptake play a much more critical role in cellular movement compared to glutamine inhibition. These results seem consistent with those in Figure 4.1. We also observed that there is lowered displacement of the cells depending on the treatment (Figure 4.3g), which is also consistent with our observations on the speeds of the cells.

From these results, we were curious about whether combining multiple inhibitors could also increase the negative effect on cellular movement. It was expected that the knockdown of critical metabolite uptake in conjunction with MMP2 inhibition would provide a synergistic effect. However, as seen in Figure 4.3, it appears that combining cy(WPHPY) with either STF 31 or V-9302 did not further decrease cellular movement. Interestingly, either combination appeared to increase the general speed of the individual cells. This may suggest antagonistic effects may be occurring when combining these inhibitors. This unexpected result also emphasizes the overall complexity of cellular movement and implies the need for more studies focused on single-cell level research concerning migration patterns.

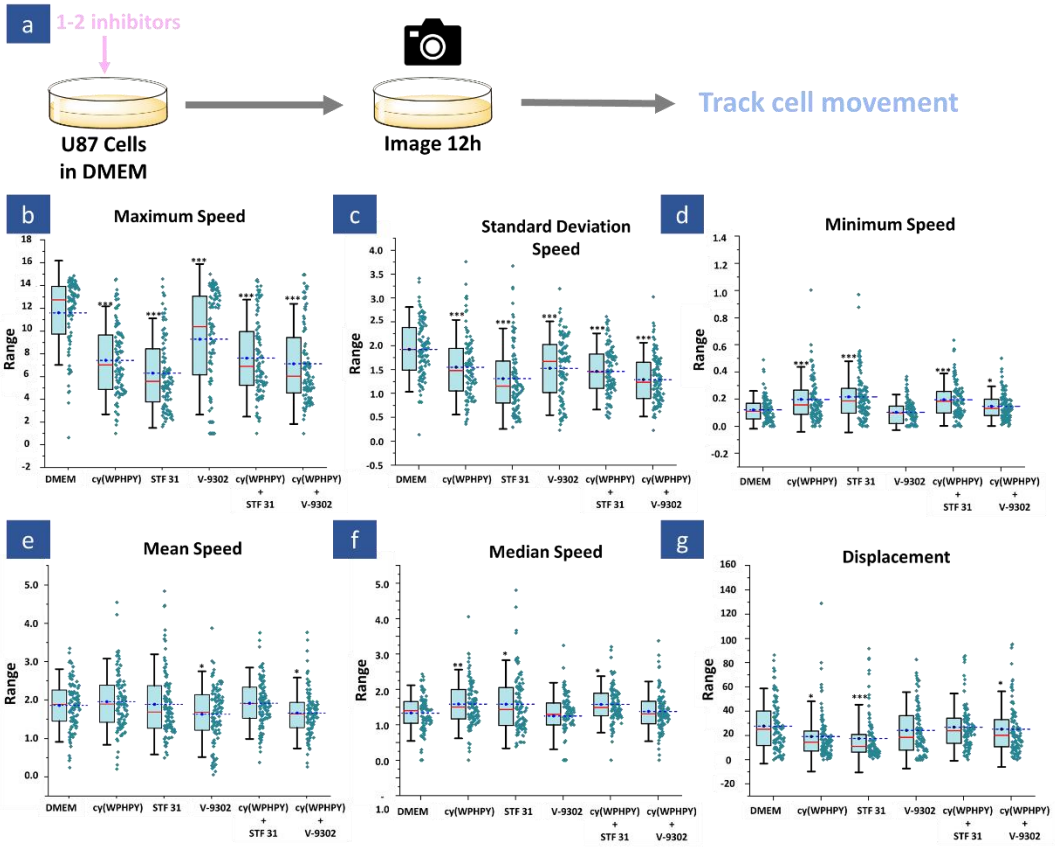

Figure 4.3. (a) Experimental flow for treating U87 cells and imaging. (b) Maximum speed distribution of single cells from each treatment. (c) Standard deviation speed distributions from each treatment. (d)The minimum speed distributions. (e) The mean speed distributions. (f) The median speed distributions. (g) The displacement distributions. The blue dotted line in each bar represents the mean of each data set and the red line represents the median. Student's t-test was performed to assess the statistical significance. *: $p < 0.05$. **: $p < 0.01$. ***: $p < 0.001$

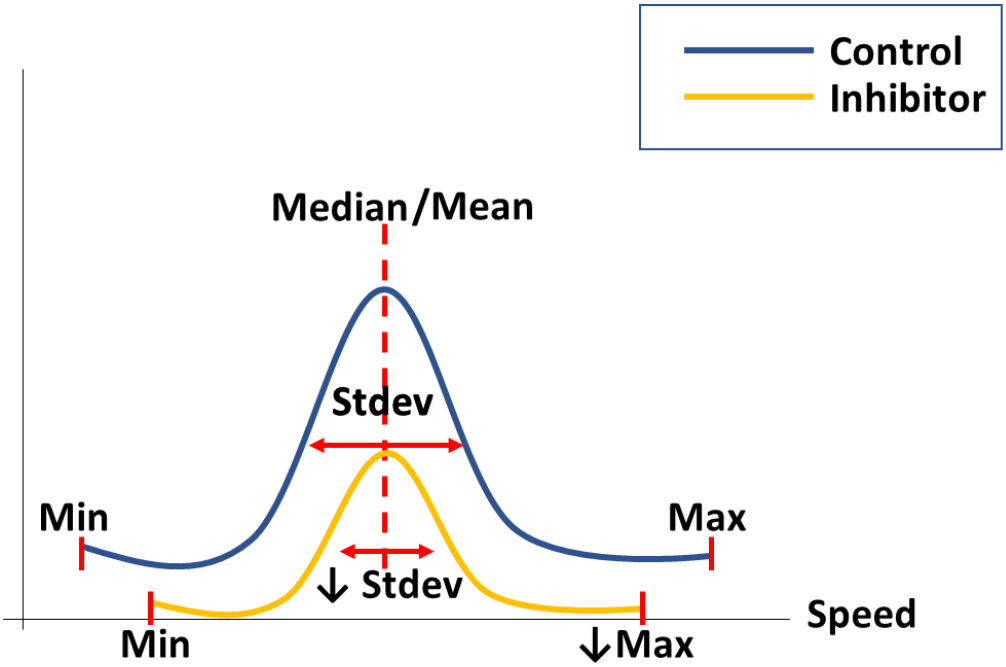

Figure 4.4. An example illustration of the differences observed between one representative single cell from the control treatment in versus the treatment of the cell with an inhibitor. It is shown that the mean/median remained unchanged while the max and standard deviation have decreased (↓).

4.4 Conclusion

In this study, we evaluated how critical metabolites affected the cellular heterogeneity in terms of their overall migration patterns. It was concluded that glucose and glutamine played a much more critical role in cell mobility. These metabolites aided single cells in achieving significantly higher speeds in comparison to the other metabolites. We also found that metabolic and MMP2 inhibition did significantly affect single-cell mobility as well. Interestingly, the combination of inhibitors did not negatively affect the cell movement, which may allow the assumption for antagonistic effects of the inhibitors or the cells are adapting to combination treatment. Further study on these possible effects or concentration gradients of these inhibitors are needed to answer these unexpected results. It is apparent that the overall heterogeneity of cell migration patterns certainly relies on specific nutrients and proteins. Inhibiting these nutrients and proteins ultimately promotes motility inhibition. Overall, this was an exploratory study on how single-cells respond in the presence/lack of metabolites or inhibitors, and how those responses are evaluated based on their movement. Our investigation presents a call to action for further investigation on obtaining a clearer understanding of cell mobility heterogeneity at the single-cell level. Our study also introduces how finding explanations behind single-cell behavior in response to migration inhibition has direct therapeutic implications.

4.5 References

1. Diao, W.; Tong, X.; Yang, C.; Zhang, F.; Bao, C.; Chen, H.; Liu, L.; Li, M.; Ye, F.; Fan, Q.; Wang, J.; Ou-Yang, Z. C., Behaviors of Glioblastoma Cells in in Vitro Microenvironments. *Sci Rep* **2019,** *9* (1), 85.

2. Stieber D, G. A., Evers L, Lenkiewicz E, Brons NH, Nicot N, Oudin A, Bougnaud S, Hertel F, Bjerkvig R, Vallar L, Barrett MT, Niclou SP. , Glioblastomas are composed of genetically divergent clones with distinct tumourigenic potential and variable stem cell-associated phenotypes. *Acta Neuropathol.* **2014,** *2*, 203-219.

3. Zanotelli, M. R.; Zhang, J.; Reinhart-King, C. A., Mechanoresponsive metabolism in cancer cell migration and metastasis. *Cell Metab* **2021,** *33* (7), 1307-1321.

4. Mosier, J. A.; Schwager, S. C.; Boyajian, D. A.; Reinhart-King, C. A., Cancer cell metabolic plasticity in migration and metastasis. *Clin Exp Metastasis* **2021,** *38* (4), 343-359.

5. Bao, Z.; Chen, K.; Krepel, S.; Tang, P.; Gong, W.; Zhang, M.; Liang, W.; Trivett, A.; Zhou, M.; Wang, J. M., High Glucose Promotes Human Glioblastoma Cell Growth by Increasing the Expression and Function of Chemoattractant and Growth Factor Receptors. *Transl Oncol* **2019,** *12* (9), 1155-1163.

6. Tanaka, K.; Sasayama, T.; Irino, Y.; Takata, K.; Nagashima, H.; Satoh, N.; Kyotani, K.; Mizowaki, T.; Imahori, T.; Ejima, Y.; Masui, K.; Gini, B.; Yang, H.; Hosoda, K.; Sasaki, R.; Mischel, P. S.; Kohmura, E., Compensatory glutamine metabolism promotes glioblastoma resistance to mTOR inhibitor treatment. *J Clin Invest* **2015,** *125* (4), 1591-602.

7. Fujiwara S, N. K., Harada H, Nagato S, Furukawa K, Teraoka M, Seno T, Oka K, Iwata S, Ohnishi T., Silencing hypoxia-inducible factor-1· inhibits cell migration and invasion under hypoxic environment in malignant gliomas. *Int J Oncol* **2007,** *4*, 793-802.

8. Matsumoto, T.; Jimi, S.; Migita, K.; Takamatsu, Y.; Hara, S., Inhibition of glucose transporter 1 induces apoptosis and sensitizes multiple myeloma cells to conventional chemotherapeutic agents. *Leuk Res* **2016,** *41*, 103-10.

9. Schulte, M. L.; Fu, A.; Zhao, P.; Li, J.; Geng, L.; Smith, S. T.; Kondo, J.; Coffey, R. J.; Johnson, M. O.; Rathmell, J. C.; Sharick, J. T.; Skala, M. C.; Smith, J. A.; Berlin, J.; Washington, M. K.; Nickels, M. L.; Manning, H. C., Pharmacological blockade of

ASCT2-dependent glutamine transport leads to antitumor efficacy in preclinical models. *Nat Med* **2018,** *24* (2), 194-202.

10. Sarkar, P.; Li, Z.; Ren, W.; Wang, S.; Shao, S.; Sun, J.; Ren, X.; Perkins, N. G.; Guo, Z.; Chang, C.-E. A.; Song, J.; Xue, M., Inhibiting Matrix Metalloproteinase-2 Activation by Perturbing Protein–Protein Interactions Using a Cyclic Peptide. *Journal of Medicinal Chemistry* **2020,** *63* (13), 6979-6990.

11. Tinevez, J.Y.; Perry, N; Schindelin, J.; Hoopes, G.M.; Reynolds, G.D.; Laplantine, E.; Bednarek, S.Y.; Shorte S.L.; Eliceiri, K.W. TrackMate: An open and extensible platform for single-particle tracking. *Methods*. **2017**. 115, 80-90.

Chapter 5: Concluding Remarks and Future Directions

Within these three studies, we have investigated how peptides can be utilized in either overcoming or investigating the challenges posed by tumor heterogeneity. In our first study, we answered concerns of intertumoral and intratumoral heterogeneity with regards to the prescence/lack of neoantigens. Our introduction of a pathogen-derived immunogenic peptide to cancer cells was able to effectively elicit an immune response. This study proved that potentially any cancer type can be treated with this method regardless of the TMB status. To further enhance the efficacy of such treatment, one can incorporate adjuvants and other combination treatments in future studies. Some limitations of course exist with this method, such as our method cannot target cancers that have the loss of a functioning MHC Class I pathway. Despites such challenges, this study can potentially shift the paradigm of immunotherapy by introducing another strategy for anti-tumor immunity.

Our second study showcases how a peptide-based drug can address the complexities of cellular heterogeneity in response to drug treatment. A novel PROTAC design in which we incorporated apeptide specific for AKT was indeed able to help degrade AKT. Of course, we did not observe complete degradation and cell death, but due to the flexibility of the PROTAC design, testing other linkers to improve efficacy is possible. Despite such limitations, these results prompted us to further investigate the reasons behind this resistance. The investigation highlighted the importance of understanding the mechanisms cancer cells may use to survive against treatment.

The final project certainly had therapeutic implications, but it served more as an exploratory project. We aimed further understand how small molecule inhibitors and our own peptide inhibitor can affect the heterogeneity of cell migration behavior at the single-cell level. There is a current generalized understanding of heterogeneity existing in regards to cell movement, investigations on the hetereogeneity between single cells as they migrate in response to slight environmental changes to be lacking. Thus, our study showcases how the introduction of a lone peptide inhibitor or in combination yields varied results in terms of single cell movement patterns; this presents that migration is indeed highly complex and requires more in-depth study.

It is apparent that in each study, more investigation can be useful to fully understand the mechanisms and efficacy of the peptide treatments. The introduction of combinatorial methods such as co-treatment with other known inhibitors, adjuvants, etc. would likely improve our methods. Observing if these therapies can be successfully translated into *in vivo* models would also very important in investigate. Of course, each study utilized different methods to answer our hypotheses. However, further experimentation in which one could to incorporate those methods into all three studies would be very useful. For example, introducing RNA sequencing in the first and last study would provide much more insight on cellular mechanisms in response to peptide drug treatment.

Overall, each study has proven the potential of peptides as valuable drugs against cancer cells of any type. Our own peptides show potential in being applicable in both the clinical setting and in understanding cellular mechanisms/behavior. Despite the

complexities of tumor heterogeneity, the utilization of peptides can play a significant role in tackling the different areas in which tumors survive.